SpADAM, an embryonic sea urchin ADAM related to vertebrate meltrins, is expressed primarily in mesenchyme, and functions in skeleton formation.

by

Matthew Rise
B.Sc., Whitworth College, 1988
M.Sc., Boston College, 1990

A Dissertation Submitted in Partial Fulfillment of the
Requirements for the Degree of

DOCTOR OF PHILOSOPHY

in the Department of Biology

We accept this dissertation as conforming to the required standard

Dr. R.D. Burke, Supervisor (Dept. of Biology and Biochemistry/Microbiology)

Dr. L.R. Page, Department Member (Dept. of Biology)

Dr. B.F. Koop, Department Member (Dept. of Biology)

Dr. A.W. Gibson, Additional Member (Malaspina University-College)

Dr. J. Ausio, Outside Member (Dept. of Biochemistry and Microbiology)

Dr. B.P. Brandhorst, External Examiner
(Dept. of Molecular Biology/Biochemistry, Simon Fraser University)

Supervisor: Dr. R.D. Burke

ABSTRACT

The ADAM (A Disintegrin And Metalloproteinase) family of multidomain cell surface proteins has been shown to function in receptor-ligand processing, cell adhesion, cell fusion, and intracellular signaling. Several events in sea urchin embryogenesis involve proteolytic, adhesive, and fusogenic activities that could potentially be mediated by ADAMs. Here we describe an ADAM expressed during sea urchin development. Overlapping cDNA clones were used to identify a 3069 bp open reading frame. The deduced SpADAM protein is 1023 amino acids long and includes a signal peptide, a pro-domain, a metalloproteinase domain with a Zn-binding motif, a disintegrin domain, a cysteine-rich domain containing a putative fusion peptide, a transmembrane domain, and a proline-rich cytoplasmic domain. Phylogenetic analyses reveal that SpADAM is most closely related to mammalian ADAMs 12 and 19, and *Xenopus* ADAM 13. Southern blots indicate that SpADAM is a single copy gene and an alternatively spliced variant is identified. We have made a polyclonal antibody to a bacterially expressed fragment of the extracellular domain that recognizes 95 kDa and 72 kDa proteins. RNA *in situ* hybridizations and immunolocalizations show that SpADAM expression is dynamic throughout embryonic and larval development. In mesenchyme blastulae, SpADAM expression is highest in the vegetal plate, suggesting a potential role in ingression of primary mesenchyme cells. During gastrulation, the highest levels

of SpADAM expression are seen in secondary mesenchyme cells (SMCs) as they release from the lengthening archenteron. Since SMCs are capable of homotypic fusion during this time, and SpADAM contains a putative fusogenic peptide, SpADAM could be involved in SMC-SMC fusion. In plutei, SpADAM is expressed in skeletogenic mesenchyme, muscle cells, pigment cells, and the preoral neural ectoderm. Primary mesenchyme cells express SpADAM weakly at ingression, and expression strengthens after syncytia are formed and skeletal elements are being secreted. Micromeres cultured in media containing anti-SpADAM antibodies or Fab fragments aggregate normally and form spicules that are significantly longer than those in control cultures. We propose that SpADAM functions in skeletal morphogenesis, possibly in the removal of skeletal matrix. SpADAM has some of the properties of the types of molecules hypothesized to regulate skeleton morphogenesis through ectoderm signaling. SpADAM structure, expression, and function suggest that the group of meltrins including SpADAM, ADAM 12, ADAM 13, and ADAM 19, are structurally and functionally conserved in deuterostomes.

Examiners:

Dr. R.D. Burke, Supervisor (Dept. of Biology and Biochemistry/Microbiology)

Dr. L.R. Page, Department Member (Dept. of Biology)

Dr. B.F. Koop, Department Member (Dept. of Biology)

Dr. A.W. Gibson, Additional Member (Malaspina University-College)

Dr. J. Austin, Outside Member (Dept. of Biochemistry and Microbiology)

Dr. B.P. Brandhorst, External Examiner
(Dept. of Molecular Biology/Biochemistry, Simon Fraser University)

Table of Contents

Abstract		ii
Table of Contents		v
List of Figures		vii
List of Tables		ix
List of Abbreviations		x
Acknowledgements		xiii
Dedication		xiv
Chapter 1	**Introduction**	1
1.1	ADAMS and Development	1
1.1.1	ADAMs and the Development of Muscle, Bone, and Nervous Tissue	3
1.2	Sea Urchin Embryogenesis	6
1.2.1	Nonuniform Distribution of Maternal Factors in the Sea Urchin Egg	6
1.2.2	Cleavage and Cell Fate Specification	7
1.2.3	Hatching	13
1.2.4	Primary Mesenchyme Ontogeny	14
1.2.5	Secondary Mesenchyme Ontogeny	17
1.2.6	Larval Nervous System	18
1.3	Objectives	
Chapter 2	**Materials and Methods**	20
2.1	Embryo Culture	20
2.2	Homology RT-PCR	20
2.3	Screening Lambda and Arrayed cDNA Libraries	23
2.4	*In Situ* RNA Hybridization	26
2.5	RT-PCR	26
2.6	Northern Blot	27
2.7	Antibody Production	28
2.8	Immunoblots	29
2.9	Immunoprecipitation	29
2.10	Whole Mount Immunofluorescence	30
2.11	Affinity Purification of Anti-SpADAM Antibodies	30
2.12	Genomic Southern Blot	31
2.13	Purification of Anti-SpADAM IgG and Isolation of Anti-SpADAM Fab Fragments	31
2.14	Micromere Isolation and Culture	32
2.15	Spicule Measurement	32
2.16	Deduced Amino Acid Sequence Comparisons	33

Chapter 3 Results 34

3.1	Identification of SpADAM	34
3.2	SpADAM Similarities	35
3.3	SpADAM is a Single Copy Gene.	48
3.4	RT-PCR	48
3.5	Northern Blot	55
3.6	*In Situ* RNA Hybridization	58
3.7	Immunoblots and Immunoprecipitations	58
3.8	SpADAM Immunolocalization	63
3.9	SpADAM and Skeletogenesis	77

Chapter 4 Discussion 89

4.1	SpADAM is Most Closely Related to ADAMs 12, 13, and 19.	89
4.2	SpADAM Protein Occurs in Various Forms.	90
4.3	SpADAM Functions in Skeleton Formation.	92
4.4	Hypothetical Role for SpADAM in SMC Ingression and Formation	94
4.5	Hypothetical Role for SpADAM in SMC-SMC Adhesion and Fusion	97
4.6	SpADAM Localization in Cleavage Stage Embryos	106
4.7	SpADAM in Muscle Cells	107
4.8	SpADAM and the Larval Nervous System	108

Conclusions 110

References 112

List of Figures

Figure 1.	Normal development and fate map of the *S. purpuratus* embryo.	9
Figure 2.	Primers used to clone, subclone, and sequence SpADAM.	21
Figure 3.	Arrayed library membrane and clone identification scheme.	24
Figure 4.	Clone map showing SpADAM domain structure and hydrophilicity profile.	36
Figure 5.	Alignment of deduced amino acid sequences of SpADAM and human ADAM 12	38
Figure 6.	SpADAM cDNA sequence with deduced amino acid translation.	40
Figure 7.	Phylogenetic analysis of all ADAMs for which complete cDNA sequence is available.	49
Figure 8.	Genomic Southern Blot.	51
Figure 9.	RT-PCR.	53
Figure 10.	Northern Blot.	56
Figure 11.	Whole mount *in situ* hybridization of glutaraldehyde-fixed early embryos using 425 bp sense and antisense digoxygenin-labeled SpADAM riboprobes.	59
Figure 12.	Whole mount *in situ* hybridization of glutaraldehyde-fixed late larvae using 425 bp sense and antisense digoxygenin-labeled SpADAM riboprobes.	61
Figure 13.	SpADAM protein expression assessed by immunoblot and immunoprecipitation.	64
Figure 14.	Confocal laser scanning images of cleavage stage embryos, prepared for immunofluorescence with anti-SpADAM or pre-immune serum.	66

Figure 15. Confocal laser scanning images of mesenchyme blastula to late gastrula stage embryos prepared for immuno-fluorescence with anti-SpADAM or pre-immune serum. 69

Figure 16. Confocal laser scanning images of 4-arm plutei (72 h) prepared for immunofluorescence with affinity-purified anti-SpADAM antibodies, anti-SpADAM serum, or pre-immune serum. 71

Figure 17. Confocal laser scanning images of 7 day larvae prepared for immunofluorescence with anti-SpADAM serum, pre-immune serum, or anti-serotonin. 74

Figure 18. Results of experiment in which micromeres were cultured in the presence of anti-SpADAM serum in ASW, or ASW alone. 78

Figure 19. Frequency histograms of spicule lengths from micromeres cultured in the presence of anti-SpADAM serum in ASW, or ASW alone. 80

Figure 20. Results of experiment in which micromeres were cultured in the presence of anti-SpADAM serum in ASW, heat-killed anti-SpADAM serum in ASW, or ASW alone. 82

Figure 21. Frequency histograms of spicule lengths from micromeres cultured in the presence of anti-SpADAM serum in ASW, heat-killed anti-SpADAM serum in ASW, or ASW alone. 84

Figure 22. Results of experiment in which micromeres were cultured in the presence of purified anti-SpADAM IgG in ASW, normal rabbit IgG in ASW, anti-SpADAM Fab fragments in ASW, or heat-killed anti-SpADAM Fab fragments in ASW. 86

Figure 23. Aligned Kyte-Doolittle hydrophilicity profiles of 3 ADAMs with potential fusion peptides. 100

Figure 24. Model of hypothetical SpADAM-integrin involvement in SMC-SMC adhesion and fusion. 103

List of Tables

Table 1. Regional sequence similarities of SpADAM and other ADAMs of known functions. 45

List of Abbreviations

α, alpha

ADAM, a disintegrin and metalloproteinase domain

AEBSF, 4-(2-Aminoethyl)benzenesulfonyl Fluoride

an_1, first animal tier of blastomeres in fifth cleavage sea urchin embryo

an_2, second animal tier of blastomeres in fifth cleavage sea urchin embryo

ASW, artificial sea water

A-V, animal-vegetal

β, beta

bp, base pairs

cDNA, complementary deoxyribonucleic acid

°C, degrees Celsius

dH_2O, deionized water

dNTPs, deoxyribonucleoside triphosphates

ECM, extracellular matrix

EGF, epidermal growth factor

γ, gamma

h, hour

HE, hatching enzyme

H_2O, water

IgG, immunoglobulin G

kb, kilobases

kDa, kilodalton

λ, Lambda phage

MB, mesenchyme blastula

min, minute

µg, microgram

mg, milligram

µJoule, microjoule

µl, microlitre

ml, millilitre

μM, micromolar

mM, millimolar

MMLV-RT, Moloney murine leukemia virus reverse transcriptase

mRNA, messenger ribonucleic acid

NCBI, National Centre for Biotechnology Information

ng, nanogram

N-linked, asparagine-linked

N-terminal, amino terminal

^{32}P, radioactive isotope of phosphorus

PAGE, polyacrylamide gel electrophoresis

PBS, phosphate-buffered saline

PCR, polymerase chain reaction

PMC, primary mesenchyme cell

RGD, arginine – glycine - aspartate

RNA, ribonucleic acid

RNase, ribonuclease

RT, reverse transcription

RT-PCR, reverse transcription – polymerase chain reaction

s, seconds

SDS, sodium dodecyl sulphate

SDS-PAGE, sodium dodecyl sulphate – polyacrylamide gel electrophoresis

SEM, standard error of the mean

SMC, secondary mesenchyme cell

SP, signal peptide

SpADAM, *Strongylocentrotus purpuratus* a disintegrin and metalloproteinase

SSC, sodium chloride – sodium citrate solution (Sambrook et al., 1989)

SSPE, sodium chloride – sodium dihydrogen orthophosphate – EDTA solution (Sambrook et al., 1989)

SVMP, snake venom metalloproteinase

TA, thymine – adenine

TACE, tumour necrosis factor-alpha converting enzyme

TBS, Tris-buffered saline (Sambrook et al., 1989)

TBST, Tris-buffered saline + 0.1% Tween 20

TGF-α, transforming growth factor-alpha

TM, transmembrane

TNF-α, tumour necrosis factor-alpha

U, units

UTR, untranslated region

UV, ultraviolet

veg$_1$, first vegetal tier of blastomeres in sixth cleavage sea urchin embryo

veg$_2$, second vegetal tier of blastomeres in sixth cleavage sea urchin embryo

3′, 3 prime

5′, 5 prime

Acknowledgements

I owe thanks to many people for helping this project to blossom into the thesis you now hold. My wife, Marlies, spent countless nights waiting while I hunched over the confocal assuring her I just needed another half hour. Thank you, Mar, for your patience, love, and support. I owe gratitude to several people in the Burke lab: Robert, for being interminably steeped in the scientific method, and for being the quintessential editor; Diana, for her molecular sixth sense, and for always being willing to help when her knowledge and experience were needed; Chris, for training me with the Lambda library; Greg, for friendship and for protocols (i.e. IP); Dan and Ross, for camaraderie. I would also like to thank my committee for stimulating conversations and other forms of professional guidance over the years. Dr. L.R. Page and Alex Eaves supplied late larvae for *in situ* hybridizations and immunolocalizations. Ute Rink, working for Dr. B.F. Koop, performed much of the sequencing of SpADAM clones. In addition to providing the highest quality sequence attainable on those machines, Ute gave smiles and real conversation, and I miss her. Thanks are due to Tom Gore and Heather Down for computer and imaging assistance. This list would not be complete without acknowledging CR15, the New Zealand White rabbit that endured months of exposure to SpADAM polypeptide, and then gave its life for this project. Lastly, I would like to thank my family for their love and encouragement over the course of this project.

Dedication

S.D.G.

CHAPTER 1

INTRODUCTION

Embryogenesis encompasses the morphological and physiological changes that occur from fertilization of the egg through formation of a juvenile. Changes in embryonic structure involve complex cellular behaviours, including extracellular matrix (ECM) secretion and degradation, epithelial-mesenchymal transformation, migration, intercellular adhesion and fusion, and skeleton formation. The molecular mechanisms underlying these activities are incompletely known. ADAMs (proteins containing A Disintegrin And Metalloproteinase domain), a family of cell-surface molecules thought to serve as integrin ligands, are expressed in vertebrate and invertebrate embryos. In addition to adhesive domains, ADAMs also contain domains with potential proteolytic, fusogenic, and intracellular signaling activities, suggesting they might be involved in the complex morphogenic events occurring in embryos. The objective of this research project was to identify an embryonic sea urchin ADAM, and determine its expression and function.

1.1 ADAMs and Development

ADAMs contain the following domains from amino to carboxy terminus: signal peptide, pro-domain, metalloproteinase, disintegrin, cysteine-rich (with putative fusogenic peptide), EGF-like, transmembrane, and cytoplasmic domains (Yagami-Hiromasa et al., 1995; Gilpin et al., 1998). Proteolytic

processing may expose different N-terminal functional domains, resulting in different activities for a given ADAM (Miller, 1995; Yagami-Hiromasa et al., 1995). ADAM extracellular domains are very similar in amino acid sequence to snake venom metalloproteinases (SVMPs), soluble proteins containing metalloproteinase and disintegrin domains (Zhou et al., 1995; Wolfsberg and White, 1996). The disintegrin domains of SVMPs, like ECM proteins such as collagen and fibrinogen, contain RGD sequences. The SVMP disintegrin domain binds to a platelet-surface fibrinogen receptor (an integrin), preventing platelet aggregation. Simultaneously, the SVMP metalloproteinase domain erodes the victim's endothelial basement membranes, exacerbating the ensuing haemorrhage (Liu and Huang, 1997).

ADAMs are expressed in a diverse group of animals where they appear to have a range of functions. ADAMs have been described in mammals (Wolfsberg et al., 1995; Yagami-Hiromasa et al., 1995; Wolfsberg and White, 1996), *Caenorhabditis elegans* (Podbilewicz, 1996), *Xenopus laevis* (Alfandari et al., 1997; Cai et al., 1998), and *Drosophila* (Pan and Rubin, 1997; Sotillos et al., 1997). ADAMs play important roles in early development (Primakoff and Myles, 2000). The zinc-dependent metalloproteinase domains of some ADAMs have been shown to process protein extracellular domains (Pan and Rubin, 1997; Black et al., 1997; Peschon et al., 1998). For example, kuzbanian, a *Drosophila* ADAM, proteolytically modifies Notch (Pan and Rubin, 1997), while mammalian ADAM 17 (TACE) mediates tumour necrosis factor-α (TNF-α) and

transforming growth factor α (TGF-α) ectodomain shedding (Black et al., 1997; Peschon et al., 1998). The disintegrin domain of ADAM 2 (fertilin β) acts in sperm-egg adhesion (Myles et al., 1994; Evans et al., 1995; Cho et al., 2000). A hydrophobic peptide in the cysteine-rich domain of ADAM 12 (meltrin α) is thought to be involved in myoblast fusion (Yagami-Hiromasa et al., 1995). In addition, the cytoplasmic domains of some ADAMs contain proline-rich motifs characteristic of proteins that participate in signal transduction pathways (Wolfsberg and White, 1996; Weskamp et al., 1996; Howard et al., 1999).

In this thesis, an embryonic sea urchin ADAM (SpADAM) is identified and characterized, its embryonic and larval expression patterns are determined, and its function in spiculogenesis is evaluated. In amino acid sequence and expression pattern, SpADAM is similar to mammalian ADAM 12 and ADAM 19 (meltrin β), and *Xenopus* ADAM 13.

1.1.1 ADAMs and the Development of Muscle, Bone, and Nervous Tissues

Vertebrate ADAM 12, ADAM 13, and ADAM 19, are well characterized ADAMs that are expressed in early development, initially by mesenchyme. Mouse ADAM 12 and *Xenopus* ADAM 13 are expressed in myoblasts (Yagami-Hiromasa et al., 1995; Alfandari et al., 1997). ADAM 12 is involved in the fusion of myoblasts into multinucleate myotubes during the normal development of mammalian skeletal muscle (Yagami-Hiromasa et al., 1995; Gilpin et al., 1998). Mouse myoblasts transfected with ADAM 12 constructs lacking the

metalloproteinase domain fuse more readily than those transfected with full-length ADAM 12 (Yagami-Hiromasa et al., 1995). *In vivo*, the proteolysis of ADAM 12 may expose a fusogenic peptide, facilitating the joining of adjacent myoblast plasma membranes. When tumour cells expressing a soluble form of ADAM 12 (ADAM 12-S) were injected into nude mice, resulting tumours contained ectopic muscle cells of host origin (Gilpin et al., 1998). The mechanisms by which the membrane bound and secreted forms of ADAM 12 act in myogenesis are not known.

Both the disintegrin and cysteine-rich domains of ADAM 12 have been shown to mediate cell-cell adhesion (Yagami-Hiromasa et al., 1995; Iba et al., 2000). In cell attachment assays comparing the adhesion of tumour cells to laminin and recombinant ADAM 12 disintegrin or cysteine-rich domains, high levels of cell adhesion were observed with laminin and ADAM 12 cysteine-rich domain, and low levels with ADAM 12 disintegrin domain (Iba et al., 1999). While the disintegrin domain likely interacts with an unidentified integrin receptor, the cysteine-rich domain of human ADAM 12 appears to act in cell-cell adhesion via syndecan receptors (Iba et al., 1999, 2000). Syndecans are heparan sulfate glycosaminoglycans capable of binding growth factors, ECM components, proteases and their inhibitors, as well as cell adhesion molecules (Iba et al., 2000). A model has been proposed in which the cysteine-rich domain of human ADAM 12 binds to a cell surface syndecan, triggering β1 integrin-dependent cell spreading (Iba et al., 2000).

In addition to their involvement in the development of skeletal muscle, meltrins are also thought to play roles in the formation of bone and nervous tissues. ADAM 12 and ADAM 19 are expressed by osteoblasts and osteoclasts: cells involved in the formation of the vertebrate skeleton (Inoue et al., 1998; Abe et al., 1999). The neuroectoderm and some cranial neural crest cells in *Xenopus* embryos express ADAM 13 (Alfandari et al., 1997). Mouse ADAM 19 is strongly expressed in neural crest-derived ganglia and ventral horns of the spinal cord during neurogenesis (Kurisaki et al., 1998) and is capable of proteolytically processing Neuregulin (Shirakabe et al., 2001), a growth factor involved in the differentiation of neural crest-derived neurons and glial cells (Meyer and Birchmeier, 1995; Meyer et al., 1997; Cameron et al., 2001; Meintanis et al., 2001).

Several events in sea urchin embryogenesis could involve the adhesive, fusogenic, and proteolytic activities of ADAMs. These events include primary mesenchyme cell (PMC) and secondary mesenchyme cell (SMC) ingression and migration, PMC-PMC and SMC-SMC adhesion and fusion, skeleton formation, myoblast adhesion and fusion, and neurogenesis. The molecular mechanisms of these processes remain poorly understood. During early embryogenesis, SpADAM is expressed in skeletogenic mesenchyme (PMCs), SMC derivatives such as pigment cells, blastocoelar cells, and muscle cells, and also in neural ectoderm. Functional studies indicate that SpADAM plays a role in skeletal

morphogenesis, suggesting a high degree of structural and functional conservation in this group of ADAMs.

The deuterostome phyla (i.e. Echinodermata, Chordata) diverged from the protostome phyla (i.e. Mollusca, Annelida, Arthropoda) in the Proterozoic eon, approximately 1.2 billion years ago (Wray et al., 1996; Knoll and Carroll, 1999). Molecular and morphological evidence indicates that deuterostomes are monophyletic (Peterson et al., 2000). Therefore, a thorough understanding of sea urchin embryogenesis might shed light on archetypal molecular and morphogenic events leading to the formation of analogous progenitor deuterostome systems such as skeletal and nervous systems.

1.2 Sea Urchin Embryogenesis

1.2.1 Nonuniform Distribution of Maternal Factors in the Sea Urchin Egg

During oogenesis, sea urchin eggs are imparted with an animal-vegetal (A-V) polarity that is morphologically visible in only certain species. In *Paracentrotus lividus* ova, for example, this polarity is apparent as a belt of pigment granules near the vegetal pole (Boveri, 1901; Czihak, 1971). This mosaic distribution of pigment granules along the A-V axis reflects the polar distribution of maternal transcription factor activities involved in early cell fate specification events (Davidson et al., 1998; Angerer and Angerer, 2000). When sea urchin eggs are split equatorially (perpendicular to the A-V axis), and the

resulting merogones are fertilized, animal halves develop into ciliated epithelial balls (dauerblastulae), while vegetal halves develop into small, but complete, larvae. However, when sea urchin eggs are split meridionally (parallel to the A-V axis), and fertilized, both halves develop into small larvae (Hörstadius, 1928, 1939; Maruyama et al., 1985; Gilbert, 1997). These experiments point to the existence of a maternal determinant, restricted to the vegetal portion of the unfertilized sea urchin egg, that functions in the specification of endoderm and mesoderm.

1.2.2 Cleavage and Cell Fate Specification

Sea urchin embryos, like those of mollusks and nematodes, undergo stereotypic cleavage, resulting in the differentiated parts of every individual always arising from the same lineage of founder cells in the early embryo (Davidson, 1990). Autonomous specification depends on inheritance of regionally sequestered maternal factors, whereas conditional specification is mediated by cell-cell interactions (Davidson, 1991; Slack, 1991). The sea urchin, like most animals, utilizes autonomous and conditional specification (Davidson et al., 1998). In embryos that undergo variant cleavage, such as amphibians, teleost fish, and mammals, all cell lineages are believed to be conditionally specified. Conditional cell fate specification, set by a cell's relative position within the embryo, is mediated by diffusible ligands or cell surface ligands on adjacent cells (Davidson, 1989, 1990).

Sea urchins exhibit radial, holoblastic cleavage. Cleavage furrows are oriented either parallel or perpendicular to the A-V axis and extend through the entire egg (Gilbert, 1997). The first two cleavage planes are meridional (pass through animal and vegetal poles) and perpendicular to one another. The 4-cell embryo retains the A-V polarity of the egg (Fig. 1). When 2-cell or 4-cell embryos are dissociated into individual cells, each blastomere develops into a small larva (Driesch, 1892; Hörstadius and Wolsky, 1936; Gilbert, 1997).

The third cleavage plane is equatorial, forming four animal and four vegetal blastomeres (Fig. 1). When an 8-cell sea urchin embryo is split along a meridional cleavage plane, preserving the distribution of maternal factors along the A-V axis, both halves develop into small plutei (Hörstadius, 1928, 1939). However, when an 8-cell embryo is split along the equatorial cleavage plane, the animal half develops into a dauerblastula and the vegetal half develops into a small pluteus (Hörstadius, 1928, 1939). These experiments demonstrated the A-V polarity of the unfertilized sea urchin egg, with animalizing factors specifying blastomeres to ectoderm fate, and vegetalizing factors initiating the specification events resulting in the formation of mesoderm and endoderm.

The fourth cleavage in sea urchin embryos is unequal. The animal quartet of the 8-cell embryo divide meridionally, forming eight mesomeres of identical size. The vegetal quartet divide equatorially and unequally, forming four macromeres and four micromeres. The micromeres, due to their position at

Figure 1. Normal development and fate map of the *S. purpuratus* embryo (adapted from Hörstadius, 1939; Davidson, 1990; Davidson et al., 1998). (A-F) Normal cleavage divisions from fertilized egg through 60-cell morula (2-cell stage omitted). Lineages are presented as different colours in 16-cell (D), 32-cell (E), 60-cell (F), hatched (early) blastula (G), mesenchyme (late) blastula (H), late gastrula (I), prism (J), and pluteus larva (K in ventral view, L in lateral view). *Black*: large micromeres. The large micromeres differentiate into primary mesenchyme cells (PMCs) and ingress into the blastocoel (H), where they form skeleton (I-L). *Orange*: veg_2 blastomeres, including the vegetal plate (vp) mesoderm, which gives rise to secondary mesenchyme cells (SMCs) and parts of the endoderm. *Green*: veg_1 blastomeres, including parts of the endoderm (intestine) and aboral ectoderm. *Purple*: an_2 blastomeres, including parts of the oral ectoderm, ciliated band (cb), and aboral ectoderm. *Blue*: an_1 blastomeres, including parts of the oral ectoderm, ciliated band and aboral ectoderm. smμ, small micromeres; e, esophagus; sto, stomach; int, intestine; stomo, stomodeum; m, mouth.

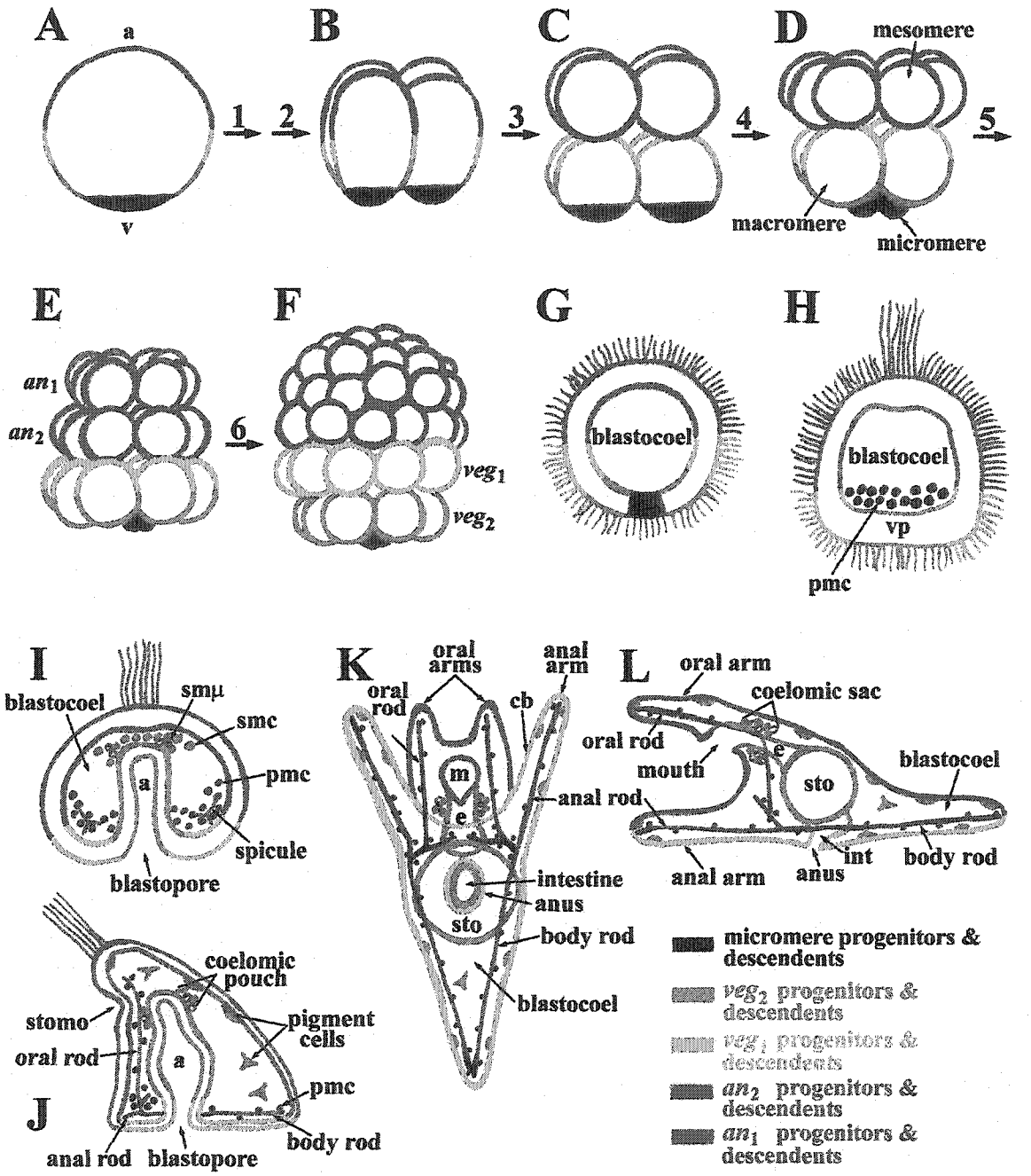
A
a
v
1
2
B
3
C
4
D
mesomere
5
macromere
micromere
E
an1
an2
6
F
veg1
veg2
G
blastocoel
H
blastocoel
vp
pmc
I
blastocoel
smμ
smc
pmc
a
spicule
blastopore
coelomic pouch
stomo
pigment cells
oral rod
a
pmc
J
anal rod
blastopore
body rod
K
oral arms
anal arm
oral rod
cb
m
e
anal rod
intestine
anus
sto
body rod
blastocoel
L
oral arm
coelomic sac
oral rod
e
mouth
sto
blastocoel
anal arm
anus
int
body rod
micromere progenitors & descendents
veg2 progenitors & descendents
veg1 progenitors & descendents
an2 progenitors & descendents
an1 progenitors & descendents

the vegetal pole, inherit the hypothetical maternal determinant that autonomously specifies them to a skeletogenic fate (Fig. 1; Davidson, 1990). Fourth cleavage micromeres are determined to the skeletogenic mesenchyme fate. When isolated and cultured, micromeres behave much like they would *in vivo*. They divide several times, migrate, fuse into a syncytium, and form spicules (Okazaki, 1975).

The autonomously specified micromeres of the 16-cell embryo are the only blastomeres at this stage that are irreversibly committed to a specific fate. When micromeres are transplanted to the animal pole of a recipient 16-cell embryo, an ectopic vegetal plate forms (Hörstadius, 1935; Ransick and Davidson, 1993, 1995). Primary mesenchyme cells (PMCs), derived from the transplanted micromeres, ingressed and formed skeletons. Vegetal plates formed at the animal and vegetal poles and buckled, forming two archenterons (Hörstadius, 1935; Ransick and Davidson, 1993, 1995). These results indicate there is a micromere-derived signal for the specification of the vegetal plate mesendoderm lineage.

The fifth cleavage planes differ for each type of blastomere. Mesomeres divide equatorially, yielding two octet tiers: an_1 at the animal pole, and an_2 below it. The macromeres divide meridionally yielding an octet, while the micromeres divide eccentrically yielding a quartet of small micromeres at the vegetal pole and a quartet of large micromeres above it. The four large micromeres are committed to a skeletogenic mesenchyme fate, and the four

small micromeres contribute to the coelomic epithelium (Davidson et al., 1998; Angerer and Angerer, 2000). In the sixth cleavage, an_1 and an_2 tiers divide equatorially. The sixth cleavage daughters of the an_1 and an_2 tiers are referred to as the animal cap of the 60-cell embryo (Fig. 1). The sixth cleavage sees the macromere daughters dividing equatorially to form veg_1 and veg_2 tiers (Fig. 1), the large micromeres dividing to form an octet, and the small micromeres remaining a quartet. The 60-cell sea urchin embryo is composed of five territories that will express specific sets of genes (Davidson et al., 1998). These lineages are the small micromeres, the skeletogenic mesenchyme, the vegetal plate, the oral ectoderm, and the aboral ectoderm.

Davidson (1989, 1990) proposed that the hypothetical vegetal maternal determinant must be a positively acting regulatory factor that turns on a PMC-specific set of genes. He also hypothesized the existence of globally distributed inactive regulatory factors in the egg which, following invariant cleavages, would be separated into the blastomere tiers of the 60 cell embryo (Fig. 1). In the Davidson hypothesis, all tiers arranged along the primordial A-V axis, except the vegetal-most tier, contain the same complement of inactive regulatory factors. Once the vegetal-most tier (fourth cleavage micromeres and their descendents) has been specified, these blastomeres produce an inductive ligand. A hypothetical receptor on blastomeres in the adjacent tier (veg_2), binds the ligand, and transduces a signal that activates one of the regulatory factors. Translocation of an activated transcription factor into veg_2 nuclei would result in

the expression of a histospecific battery of genes, specifying these cells to the vegetal plate mesendoderm territory. Veg_2 cells or their progeny would then conditionally specify the next tier of blastomeres using a different inductive ligand-receptor combination. If all mesomere and macromere progeny contain the same inactive regulatory factors, then any of these blastomeres could be specified to the vegetal plate mesendoderm lineage simply by contact with a micromere. This theory explains how micromeres can induce a vegetal plate to form when placed in contact with veg_2 blastomeres (in the unperturbed embryo), the vegetal-most surface of the 60-cell animal cap (Hörstadius, 1939), or the animal-most surface of the 60-cell animal cap (Ransick and Davidson, 1993).

1.2.3 *Hatching*

Blastomeres develop cilia on their apical surfaces prior to hatching (Fig. 1). The beating of these cilia causes the late blastula to spin inside the fertilization envelope (Czihak, 1971). The *P. lividus* hatching enzyme gene (HE), coding for a collagenase-like secreted metalloprotienase, is transcribed in animal blastomeres for a 5-10 hour period before hatching (Lepage and Gache, 1990; Gache et al., 1992). The ~ 50 kDa hatching enzyme is secreted into the perivitelline space, between the hyaline layer and the fertilization envelope (Lepage and Gache, 1989). Hatching enzyme then proteolytically degrades components of the fertilization envelope, allowing the blastula to swim free (Mozingo et al., 1993). Since HE mRNA accumulates in dissociated blastomere

cultures (with no cell-cell contacts) at the same time and approximately to the same degree as in unperturbed embryos, HE expression is cell-autonomous (Ghiglione et al., 1993.) HE is a zygotic gene that is transcriptionally activated by an animal transcription factor (Lepage et al., 1992; Ghiglione et al., 1993). This maternal factor, SpEts4, is restricted to mesomere descendents (presumptive ectoderm) by invariant early cleavage divisions (Wei et al., 1999).

1.2.4 Primary Mesenchyme Ontogeny

The spherical hatched blastula consists of a simple, ciliated epithelium surrounding a gel-filled space, the blastocoel. The hyaline layer is an apical extracellular matrix (ECM), comprised of twelve proteins arranged in six layers (Hall and Vacquier, 1982; Alliegro et al., 1988; Campbell and Crawford, 1991; Burke et al., 1998). Embryonic sea urchin basal lamina, an internal ECM structure that contacts the basal surfaces of blastomeres, contains many of the same glycoproteins as vertebrate basal lamina (Wessel et al., 1984).

A few hours after hatching, the embryo begins a series of morphological changes. Coincident with the initiation of invagination, PMCs decrease levels of adhesion to echinonectin, hyalin, and to adjacent cells (Fink and McClay, 1985; Burdsal et al., 1991). As PMCs lose affinity for hyaline layer glycoproteins, they undergo epithelial-to-mesenchymal transformation and migrate into the blastocoel through fenestrations in the basal lamina (McClay et al., 1995). Migrating PMCs extend long, slender filopodia, which appear to contact the basal lamina (Katow and Solursh, 1981). PMCs then use the basal lamina as a

substrate for migration (Malinda and Ettensohn, 1994). The sea urchin basal lamina appears to contain ECM components such as heparan sulfate proteoglycan, laminin, and collagen types I and IV (Wessel et al., 1984). PMCs express adhesion molecules such as integrins on the surfaces of their filopodial extensions, allowing these cells to attach to/detach from ECM molecules (Marsden and Burke, 1997, 1998).

Following ectoderm-derived cues, which have yet to be identified (Malinda and Ettensohn, 1994), PMCs migrate along the basal lamina to characteristic locations within the blastocoel (Armstrong and McClay, 1994; Guss and Ettensohn, 1997). The mesenchymal ring consists of 16-32 PMCs encircling the vegetal blastocoel, and a branch of about 18 PMCs extends from each ventrolateral cluster toward the animal pole (Galileo and Morrill, 1985). By mid-gastrulation, the filopodial plasma membranes of adjacent PMCs fuse by an unknown mechanism, forming a syncytium (Okazaki, 1960; Wolpert and Gustafson, 1961; Malinda et al., 1995). The calcareous larval skeleton is deposited in spaces within the PMC syncytium (Ingersoll and Wilt, 1998). Triradiate spicules form at the two ventrolateral PMC clusters in the mesenchymal ring, and each spicule elongates to form the larval skeleton (Malinda et al., 1995).

The ectoderm's involvement in embryonic sea urchin skeletal pattern determination was proposed by Wolpert and Gustafson (1961), based on observations of PMC behaviour. The first experimental evidence suggesting

that the ectoderm plays an important role in spiculogenesis came from Harkey and Whiteley (1980), who found that the spicules formed by isolated PMCs exhibited normal morphology only when these PMCs were allowed to form aggregates with ectodermal cells.

In normal embryos, a thickened area of ectoderm overlies the two ventrolateral PMC clusters (Okasaki, 1960; Galileo and Morrill, 1985). Treatment with $NiCl_2$ results in embryos that have no dorsal-ventral axis, are radially symmetrical, and form multiple enlarged triradiated spicules in a radial pattern around the base of the archenteron (Hardin et al., 1992). Armstrong et al. (1993) found that chimeric sea urchin embryos composed of normal PMCs recombined with $NiCl_2$-treated PMC-less host embryos (supplying the ectoderm) formed abnormal skeletons identical to those of the $NiCl_2$-treated control embryos, whereas chimeras composed of $NiCl_2$-treated PMCs in normal ectoderm produced normal spicules. In $NiCl_2$-treated sea urchin embryos, the thickened ectodermal region is expanded into a band encircling the vegetal plate (Hardin et al., 1992). Since normal embryos with two dorsolateral ectodermal thickenings form two spicular rudiments regardless of how the mesenchyme is treated, and $NiCl_2$-treated embryos with an annular ectodermal thickening form multiple triradiate spicules even with untreated mesenchyme, the ectoderm appears to determine the number of locations within the blastocoel at which spicule nucleation and initial growth can occur (Armstrong et al., 1993).

1.2.5 *Secondary Mesenchyme Ontogeny*

The secondary mesenchyme is distinguished from primary mesenchyme by its later ingression into the blastocoel. Secondary mesenchyme forms pigment cells, blastocoelar cells, and circumesophageal muscles.

A monoclonal antibody (SP1) identifying pigment cell precursors in the vegetal plate just after PMC ingression has revealed that all presumptive pigment cells appear to ingress from the vegetal plate and archenteron tip prior to 1/3 gastrula stage (when the archenteron has reached one-third of the way across the blastocoel; Gibson and Burke, 1985, 1987, 1988). These SP 1-immunoreactive pigment cell precursors then migrate across the blastocoel and penetrate basal lamina, invading the ectoderm (Gibson and Burke, 1985, 1987). SP1-immunoreactive cells in the late gastrula ectoderm develop pigment and continue to migrate, eventually assuming a characteristic distribution in the pluteus (Gibson and Burke, 1988).

Blastocoelar cells are a subset of SMCs that release from the tip of the lengthening archenteron after the initial phase of gastrulation (Tamboline and Burke, 1992). Unlike PMCs, which use basal lamina as a substrate for migration, blastocoelar cells migrate with their cell bodies completely surrounded by blastocoelar matrix (Tamboline and Burke, 1992). During gastrulation, blastocoelar cells are capable of fusing with one another by a molecular pathway believed to be distinct from that involved in the formation of the PMC syncytium (Hodor and Ettensohn, 1998). Although PMCs and blastocoelar cells

come into contact with one another, they are incapable of heterotypic fusion (Hodor and Ettensohn, 1998).

In the late gastrula/early prism stage embryo, the coeloms begin to form from cells at the tip of the invaginating archenteron (Burke and Alvarez, 1988). The cells that form the circumesophageal musculature originate in the coelomic epithelium (Gustafson and Wolpert, 1967). In late gastrula/early prism stage embryos (45-48 h), anti-actin and phalloidin staining is found in the basal regions of coelomic pouch and gut epithelial cells (Burke and Alvarez, 1988). In early plutei (60-72 h), about six cells in each coelomic sac contain abundant actin, and processes from these myoblasts extend around the upper esophagus, appearing to fuse along its midline (Burke and Alvarez, 1988). The circular upper esophageal muscle cells then send longitudinal collateral branches that form a basket-like network around the lower esophagus (Burke, 1981; Burke and Alvarez, 1988).

1.2.6 Larval Nervous System

The feeding echinopluteus larva possesses effectors (circumesophageal muscle fibres and ciliary band cells) and neurons which appear to innervate them (Burke, 1978). Peristaltic contractions of the circumesophageal musculature and coordinated control of ciliary band cells are thought to be governed by the larval nervous system (Strathmann, 1971; Burke, 1978).

The apical plate is a region of ectoderm in the prism stage embryo (50 -

60 h) where serotonergic cells differentiate and form the apical ganglion (Gustafson and Wolpert, 1967; Hörstadius, 1973; Burke, 1983). The week-old larval nervous system consists of the apical ganglion in the pre-oral hood, the oral ganglia in lower lip regions on either side of the mouth, and axon tracts beneath the circumesophageal musculature and ciliary band (Burke, 1978, 1983; Bisgrove and Burke, 1987).

1.3 Objectives

The initial goal of this research project was to determine if sea urchin embryos contain ADAM-like mRNAs and proteins. The temporal and spatial patterns of ADAM expression would then be determined. From this data, hypotheses of embryonic sea urchin ADAM functions would be developed and tested.

CHAPTER 2

MATERIALS AND METHODS

2.1 Embryo Culture

Strongylocentrotus purpuratus were collected locally and kept at 12°C in recirculating sea water. Embryos were cultured at 12-14° C following conventional procedures (Strathmann, 1987).

2.2 Homology RT-PCR

Poly (A+) RNA was prepared from staged embryos using a MicroPoly(A)Pure mRNA Isolation Kit (Ambion). Precipitated RNA from $5x10^4$ embryos was resuspended in nuclease-free H_2O, primed with random hexamers, and reverse transcribed (Marsden and Burke, 1997). First strand cDNA was immediately used as template in PCR amplifications with a semi-nested set of degenerate primers (primers 1, 5, and 4, Alfandari et al., 1997) (Fig. 2). A 1:500 dilution of first-round product was used as template in a second-round of amplification. Cycling parameters were: 39 cycles of (94°C 1 min, 40°C 2 min, 72°C 2 min) followed by a 10 min extension at 72°C. A 425 bp product was band purified using Sephaglas (Pharmacia), TA cloned using the pGEM®-T Vector (Promega), and then sequenced using M13 primers (Amersham) on an ABI 377 automated sequencer. Nucleic acid sequences were analyzed initially using the Blastx algorithm (Altschul et al., 1990) and the non-

Figure 2. Primers used to clone, subclone, and sequence SpADAM.

A domain map of unprocessed SpADAM protein shows the locations of primers. Sequences for the semi-nested degenerate primers (1, 5, and 4), used to amplify the original 425 bp SpADAM fragment, were taken from Alfandari et al. (1997). The remaining primers were designed using Gene Runner™ software. SP, signal peptide; TM, transmembrane domain.

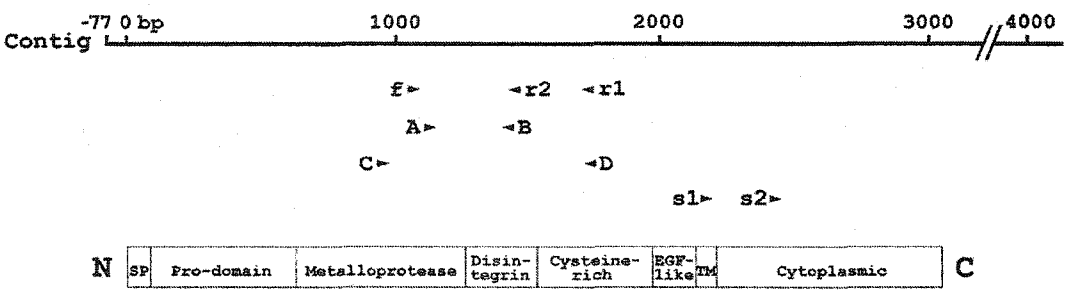

Primer	Sequence (5' to 3')	Location on contig	Product size	Experimental use
f	CA(C/T)GA(A/G)(C/T)TNGGNCA(C/T)AA	1052-1069	695 bp	Template for second round homology RT-PCR
r1	CA(T/A/G)ATNA(G/A)(C/T)TTNCC(G/A)CA	1747-1731		
f	CA(C/T)GA(A/G)(C/T)TNGGNCA(C/T)AA	1052-1069	425 bp	Probes for *in situ* hybridizations
r2	TA(T/C)TCNGGNA(G/A)(G/A)TC(G/A)CA	1477-1461		
A	TGCTCCGTCCAATGTAGGC	1115-1133	335 bp	Developmental RT-PCR
B	AGATCCCGGCAAACCTCAC	1450-1431		Screening Lambda library
C	*Bam HI* CGGGATCCGGGTGTGTCGTTTGATGG	925-942	832 bp	Subcloning into expression vector
D	GGGGTACCTCCTCCAACGCACATCAGC *Kpn I*	1757-1739		
s1	CCTGGCTCTCATTGGAATCC	2177-2196	n/a	Sequencing 57 M5 clone
s2	TCCAGTGCCAAACCTCAG	2688-2705	n/a	Sequencing 57 M5 clone

redundant sequence database available at the National Center for Biotechnology Information (NCBI) website. ADAM sequences were aligned using GENESTREAM alignment tools (IGH Montpellier, France). DNAMAN (Lyon Biosoft v4.03) was used to construct phylogenetic trees using a neighbour joining algorithm (Saitou and Nei, 1987). Hydrophilicity profiles were generated using the Kyte-Doolittle method for calculating amino acid hydropathy indices (Kyte and Doolittle, 1982).

2.3 Screening Lambda and Arrayed cDNA Libraries

A mid-gastrula λ phage cDNA library (Marsden and Burke, 1997) was screened with a 336 bp SpADAM PCR product (1115 - 1450), radiolabeled using Rad Prime DNA Labeling System (GibcoBRL). Hybridization was carried out as previously described (Marsden and Burke, 1997). Following secondary and tertiary screens, the pBluescript plasmid was rescued using the ExAssist helper phage (Stratagene). This yielded a single 1054 bp SpADAM clone, which was used to screen *S. purpuratus* 20-h (mesenchyme blastula) and 40-h (late gastrula) high density, arrayed cDNA libraries (E. Davidson, CalTech).

Arrayed cDNA library membranes (Fig. 3) were wet with sterile deionized H_2O, and incubated 2 h at 65°C in hybridization buffer (5X SSPE, 5X Denhardt's reagent, 0.5% SDS). Radiolabeled, purified, and denatured SpADAM probe was added to the buffer ($1x10^6$ counts per ml), and

Figure 3. Arrayed library membrane and clone identification scheme.

Each high-density filter array consists of a 48X48 square block, which may be subdivided into six 16X24 square blocks. There are (48x48) or 2304 squares per membrane, and 5 or 6 membranes per library. Each 16X24 square block represents the clones in a 384-well plate, and each square is a 4X4 grid of eight clones applied in duplicate. The pair of dots form a unique angle that is used to identify the plate from which the clone was sampled. In the membrane depicted in Fig. 3 (20 h mesenchyme blastula arrayed library, membrane D#4), the angle of the dot pair indicates plate number 29. For each subsequent membrane after the first (A) one in a set, 48 must be added to the plate number. So, for the D filter shown in Fig. 4, 144 must be added to 29 to get the actual decoded plate number (173). The X-Y coordinates of the dot pair can then be used to determine well position within this plate. The dot pair in Fig. 3 lies in the left lower sub-field at position H19. This clone, therefore, is identified as 173 H19, and its position on the SpADAM contiguous cDNA sequence may be seen in Fig. 4.

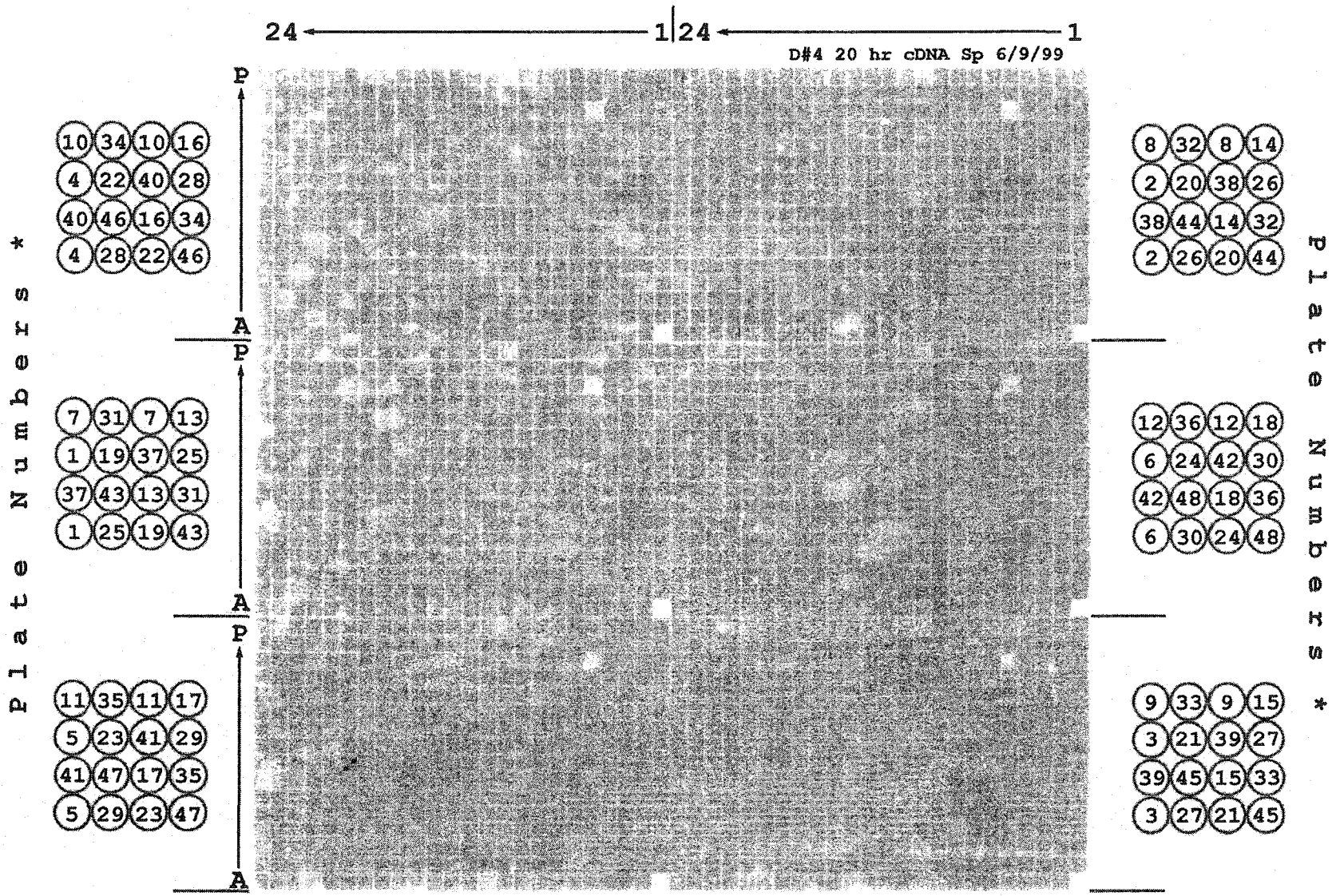
24 ← 1 | 24 ← 1
D#4 20 hr cDNA Sp 6/9/99
P
A
P
A
P
A
Plate Numbers *
10 34 10 16
4 22 40 28
40 46 16 34
4 28 22 46
7 31 7 13
1 19 37 25
37 43 13 31
1 25 19 43
11 35 11 17
5 23 41 29
41 47 17 35
5 29 23 47
8 32 8 14
2 20 38 26
38 44 14 32
2 26 20 44
12 36 12 18
6 24 42 30
42 48 18 36
6 30 24 48
9 33 9 15
3 21 39 27
39 45 15 33
3 27 21 45
Plate Numbers *

hybridization was done at 65°C overnight. Membranes were washed in 2X SSPE, 0.1% SDS two times 10 min at RT; 1X SSPE, 0.1% SDS once 15 min at 65°C; 1X SSPE, 0.1% SDS once 10 min at 65°C. Membranes were exposed to a CRST-VN Imaging Plate (Fuji) for 1 h, and detected using the Storm 860 Phosphoimager (Molecular Dynamics) (Fig. 3).

2.4 *In Situ* RNA Hybridization

A 425 bp SpADAM fragment (1052-1477) was used to transcribe digoxygenin-labeled RNA probes (Ransick et al., 1993). Embryo fixation and RNA hybridization followed Harkey et al. (1992).

2.5 RT-PCR

RT-PCR was performed using the ProSTAR™ First-Strand RT-PCR Kit (Stratagene). SpADAM-specific RT-PCR primers were designed to give a 336 bp product (Fig. 2). First-strand cDNA was synthesized using 300 ng of mRNA (quantified using spectrophotometry) from each stage. 300 ng mRNA (in 0.65 to 0.80 µl dH_2O/0.1 mM EDTA) was brought to 38 µl with DEPC-treated H_2O. 3 µl of 100 ng/µl random primers was added to each sample, and the volumes were mixed gently by pipette. The tubes were incubated at 65°C for 5 min, and then allowed to cool passively at 23°C for 20 min. The first-strand cDNA synthesis reaction consisted of this 41 µl volume plus 5 µl of 10x RT buffer, 40 U of RNase Block Ribonuclease Inhibitor, 4 mM dNTPs, and 50 U of MMLV-RT. These

reactants were mixed gently by pipette, and then incubated at 37°C for 1 h. Reactions were heated at 90°C for 5 min, and placed on ice until thermal cycling reactions were assembled.

PCR amplifications included the following reactants: 40 µl of sterile dH_2O, 5 µl 10x *Taq* DNA polymerase buffer, 2 µl of first-strand cDNA, 0.4 mM of each primer, 0.2 mM dNTPs, and 5 U *Taq* DNA polymerase. After adding polymerase and mixing by pipette, reactions were overlayed with sterile mineral oil. Cycling parameters were 95°C 45 s, 50°C 1 min, 72°C 1 min for 35 cycles, with a 10 min 72°C extension. 5 µl of each PCR product and a 100 bp ladder (Gibco BRL) were then run at 90 constant volts on a 1.5% agarose gel containing ethidium bromide. The gel, transilluminated with UV light, was photographed using the EagleEye (Stratagene) photodocumentation station.

2.6 Northern Blot

Following Sambrook et al. (1989), 1 µg mRNA (quantified using spectrophotometry) from each stage was separated on a formaldehyde agarose gel, and the gel was washed and capillary transferred. A 0.24-9.5 Kb RNA ladder (GibcoBRL) was run alongside embryonic samples, then removed, stained with ethidium bromide, and photographed next to a UV fluorescent ruler. Following transfer, nylon filters were soaked in 2X SSC, 0.1% SDS for 5 min at 23°C, dried flat on 3MM paper for 30 min at 23°C, and UV crosslinked using the 1200 µJoule preset of the UVStratalinker 1800 (Stratagene).

The 1054 bp SpADAM clone from the Lambda library (Fig. 4) was band purified (Sephaglas, Pharmacia), radiolabeled using ^{32}P as previously described, purified using the Wizard PCR kit (Promega), heated to 100°C for 5 min, chilled on ice for 2 min, and used to probe the blots. Membranes were wet in sterile deionized H_2O, and prehybridized for 1-2 h at 65°C in 10 ml/blot ULTRAhyb ultrasensitive hybridization buffer (Ambion). Membranes were hybridized overnight (16-20 h) at 65°C with constant rotation. Following hybridization, membranes were washed twice in (2X SSC, 0.2% SDS, 15 min, 65°C), and twice in (0.2X SSC, 0.2% SDS, 30 min, 65°C). Membranes were wrapped in Saran wrap and exposed to a flashed, standard CRST-VN Imaging Plate (Fuji) for 24 h. Latent images were detected using the Storm 860 Phosphoimager (Molecular Dynamics).

2.7 Antibody Production

A 832 bp SpADAM fragment (925-1757) was subcloned into the expression plasmid pQE31 (Qiagen) (Fig. 2). Expression and purification of the 6xHis-tagged SpADAM fragment followed manufacturer's procedures (Qiagen). Purified SpADAM protein was concentrated (1 mg/ml) and buffer exchanged into sterile PBS. SpADAM protein, injected subcutaneously into a New Zealand White rabbit, served as antigen for the production of a polyclonal antibody. 500 µg of SpADAM protein was mixed with an equal volume (500 µl) of Freund's complete adjuvant, and sonicated 5 s on ice prior to injection. Four

boosts of 500 μg SpADAM in Freund's incomplete adjuvant were given at monthly intervals. Anti-SpADAM serum was collected fourteen days after the final boost. Bacterially expressed SpADAM+His protein was purified using nickel columns, subjected to SDS-PAGE, electrophoretically transferred to nitrocellulose, and probed with anti-His antibodies to ensure the bacterially expressed protein was of the expected size (~30 kDa).

2.8 Immunoblots

For each sample, 3×10^4 embryos were pelleted, resuspended in 300 μl sterile deionized H_2O containing Complete™ protease inhibitor (Boehringer Mannheim), and sonicated 5 s on ice. Samples were centrifuged at 25,000 X G (4°C, 30 min), and supernatants were concentrated to 1/5 volume using Centricon 10 centrifugal filters (Amicon). Samples were dissolved in reducing sample buffer and separated by SDS-PAGE (Laemmli, 1970), and transferred to nitrocellulose (Towbin et al., 1979). Blots were blocked, incubated, washed, and detected as in Marsden and Burke (1997). Antiserum or pre-immune serum was diluted 1:1000, and alkaline phosphatase-conjugated goat anti-rabbit (Sigma) was diluted 1:10,000 in 3% milk/TBST (3% skim milk powder, 0.1% Tween 20 in TBS).

2.9 Immunoprecipitations

Pelleted embryos were resuspended in sterile PBS containing 1 mM AEBSF (pH 8.0) and sonicated 10 s on ice. Lysates were centrifuged (25,000 X G, 4°C, 25 min). EZ Link Sulfo NHS LC Biotin (Pierce) was added to 1 mg/ml. Samples were vortexed and incubated at 4°C for 1 h. Biotinylated embryonic supernatants were washed and concentrated with a Centricon 10 filter (Amicon) and resuspended with PBS containing 1 mM AEBSF. After a second concentration and resuspension, samples were diluted 1:10 with 0°C pH 8.0 PBS containing 1 mM AEBSF. Immunoprecipitation, PAGE, immunoblotting, and chemilluminescent detection followed Murray et al. (2000). Primary antiserum and pre-immune serum were diluted 1:50.

2.10 Whole Mount Immunofluorescence

Embryo fixation followed Nakajima and Burke (1996). Embryos were blocked, incubated with primary antibody, and rinsed following Marsden and Burke (1997). Embryos were then incubated 1 h in 1:400 dilution of AlexaFluor™ 488 goat anti-rabbit IgG (H+L) conjugate (Molecular Probes) in filtered PBS. Embryos were rinsed 3 times in PBS, and mounted 1:1 in SlowFade® Light Antifade in glycerol buffer (Molecular Probes). Specimens were viewed and images acquired with a Zeiss LSM 410 laser confocal microscope. Pre-immune controls were run for all experimental preparations.

Images were adjusted for contrast and brightness and assembled with Adobe Photoshop (V. 4.0).

2.11 Affinity Purification of Anti-SpADAM Antibodies

40 μg of purified, bacterially expressed SpADAM fragment was electrophoretically separated on a preparative 10% polyacrylamide gel and blotted to nitrocellulose. A strip containing the SpADAM polypeptide was removed and blocked overnight in 5% milk/TBST (TBS + 0.1% Tween 20) and incubated with a 1:50 dilution of the anti-SpADAM antiserum. The membrane strip was washed extensively in TBST and TBS, and antibodies bound to the strip were eluted with 3.0 ml 0.2 M glycine pH 2.2 (4°C, 10 min). The pH of the eluted antibodies was immediately adjusted to 7.4 using 2 M Tris HCl (pH 9.0).

2.12 Genomic Southern Blot

DNA was isolated from the sperm of two sea urchins (Sambrook et al., 1989; Blin and Stafford, 1976), digested with *Bam*HI, *Eco*RI, *Hind*III, or *Pst*I, and separated on 0.8% agarose gels. Gels were depurinated, denatured, neutralized, and capillary transferred to Hybond N+ nylon membranes (Peterson et al., 1999). Membranes were soaked in 6X SSPE (23°C, 5 min), air dried, and UV crosslinked. Southern blots were incubated in pre-hybe buffer (5X SSPE, 5X Denhardt's reagent, 0.5% SDS) for 2 h at 65°C. Hybridization was done (60°C, overnight) with radiolabeled SpADAM probe (912-1927). Membrane washes

follow the Northern blot protocol, but at 60°C. Membranes were exposed to a CRST-VN Imaging Plate (Fuji) for 12 h, and detected using a Storm 860 Phosphoimager (Molecular Dynamics).

2.13 Purification of Anti-SpADAM IgG and Isolation of Fab Fragments

IgG fractions were purified from anti-SpADAM serum using a protein A agarose column (Pierce). IgGs were eluted into 0.2 M glycine (pH 2.5), neutralized with 2 M Tris (pH 9.0), and concentrated (to 5 mg/ml) and buffer exchanged into 100 mM sodium acetate (pH 5.5) using a stirred cell with a YM30 ultrafiltration membrane (Amicon). Papain digestion of anti-SpADAM IgG was carried out as described by Harlow and Lane (1988). Fab and Fc fragments were separated using a protein A agarose column (Pierce), and the Fab fragments were concentrated (10 mg/ml) and buffer exchanged several times into sterile PBS. Fab fragments were kept at 4°C and used within one week of isolation.

2.14 Micromere Isolation and Culture

For micromere isolation, eggs were fertilized in ASW containing 1 mM aminotriazole (Showman and Foerder, 1979) and fertilization envelopes removed by pouring eggs through 102 μm Nitex. Embryos were cultured to 16 cell stage and dissociated following McClay (1986). Micromeres were isolated with a 5-25% linear sucrose gradient following Kabakoff and Lennarz (1990). The micromere band was collected, $CaCl_2$ was added to a final concentration of

10 mM, and an equal volume of the micromere suspension was added to each well of a sterile 12-well tissue culture dish (Costar). After cell attachment, the sucrose solution was replaced with ASW (14°C). After 1h incubation, the ASW was replaced with the appropriate experimental or control medium (ASW, 4% horse serum, 100 units/ml penicillin, 100 μg/ml streptomycin). Cells were cultured at 14°C.

2.15 Spicule Measurement

Micromeres were cultured in the presence of anti-SpADAM serum in ASW, heat-inactivated anti-SpADAM serum in ASW, purified anti-SpADAM IgG in ASW, normal rabbit IgG in ASW, anti-SpADAM Fab fragments in ASW, heat-inactivated anti-SpADAM Fab fragments in ASW, or ASW alone. All cultures contained 4% horse serum, 100 units/ml penicillin, and 100 μg/ml streptomycin, and were incubated at 14°C. Spicules were analyzed 46-68 h after micromere isolation. Starting at a position on the edge of each dish, a transect of adjacent fields was photographed. Spicules in adjacent fields were measured either on prints or the computer screen. Results were analyzed using Unpaired t tests when comparing two groups, and ANOVA with Tukey post tests when comparing three groups (GraphPad Instat v3.05).

2.16 Deduced Amino Acid Sequence Comparisons

To determine regional levels of identity and similarity between SpADAM and other ADAMs of known function, SpADAM was individually aligned with each ADAM using GENESTREAM Align tools (Person et al., 1997). Human ADAM 12 domain boundaries of Gilpin et al. (1998) were used. Within a given aligned domain, the number (#) of identical amino acids was divided by (# of SpADAM residues + # of SpADAM gaps in that domain) to give % identity. (# of identical + similar amino acids in domain) ÷ (# of SpADAM residues + SpADAM gaps in domain) yielded % similarity.

CHAPTER 3

RESULTS

3.1 Identification of SpADAM

Homology RT-PCR using mesenchyme blastula mRNA as template and degenerate semi-nested primers (Alfandari et al., 1997) yielded a fragment of the predicted size (425 bp) (Fig. 2). Blast searches indicate this is a fragment of a novel sea urchin ADAM. A PCR amplified internal region of this fragment was used as a probe to screen a mid-gastrula phage library (Fig. 2). This yielded a 1054 bp SpADAM fragment, which was used as probe to screen 20 h (mesenchyme blastula) and 40 h (late gastrula) high density, arrayed cDNA libraries. The four clones identified from these libraries were sequenced several times in both directions. Sequencing primers were designed for internal sequences of clone 57 M5 (Fig. 2) to sequence the 3' end of the open reading frame. The sequences were assembled into a contiguous sequence containing a complete 3072 bp open reading frame encoding a 1023 amino acid protein with a predicted molecular weight of 111.2 kDa. Two clones identified in the 20 h library (35 O14 and 57 M5) contained 69 bp inserts in their EGF-like domains (Fig. 4). Primers designed from the 5' and 3' untranslated sequences, were used to amplify a single band of the predicted size from embryonic cDNA (data not shown).

A hydrophilicity profile of the deduced SpADAM amino acid sequence (Kyte and Doolittle, 1982) reveals a potential signal peptide and transmembrane

domain (Fig. 4). The putative signal peptide is 30 amino acids long and ends with a predicted cleavage site (Nielsen et al., 1997). The predicted protein also contains a pro-domain (31-208), a metalloproteinase domain (209-417), a disintegrin domain (418-511), a cysteine-rich domain (512-653) and an EGF-like domain (654-706). SpADAM contains the conserved HEXGHXXGXXHD zinc-binding catalytic site sequence characteristic of active metalloproteinases (Black and White, 1998; Schlöndorff and Blobel, 2000). The putative transmembrane domain is 28 amino acids in length (707-734) and separates a 676 residue extracellular domain (31-706) from a 289 residue cytoplasmic domain (735-1023) (Figs. 5, 6). The cytoplasmic domain is 22.8% proline and contains sequences such as RPPTPVTRP, which are similar to the SH3 binding consensus, RPLPXXP.

3.2 SpADAM Similarities

With protein-protein Blast searches (Altschul et al., 1997), SpADAM is most similar to mammalian ADAM 12 (meltrin α), ADAM 19 (meltrin β), and ADAM 9 (meltrin γ), and *Xenopus* ADAM 13. When the SpADAM amino acid sequence is aligned and compared with the amino acid sequences of all ADAMs with known functions, SpADAM is most similar to Human ADAM 12 (34.8 % identity/59.5 % similarity) and *Xenopus* ADAM 13 (35.5 % identity/59.0 % similarity) (Table 1). Within the metalloproteinase active site, the SpADAM sequence is 66.7 % identical and 91.7 % similar to human ADAM 12 and

Figure 4. Clone map showing SpADAM domain structure and hydrophilicity profile.

Hydrophilicity profile for SpADAM was generated using the Kyte-Doolittle method for calculating amino acid hydropathy indices (Kyte and Doolittle, 1982). N (amino terminus), SP (signal peptide), EGF (epidermal growth factor), TM (transmembrane), C (carboxyl terminus), aa (amino acid). On the hydrophilicity plot, a single bar marks the hydrophobic signal sequence, and a double bar marks the hydrophobic transmembrane domain.

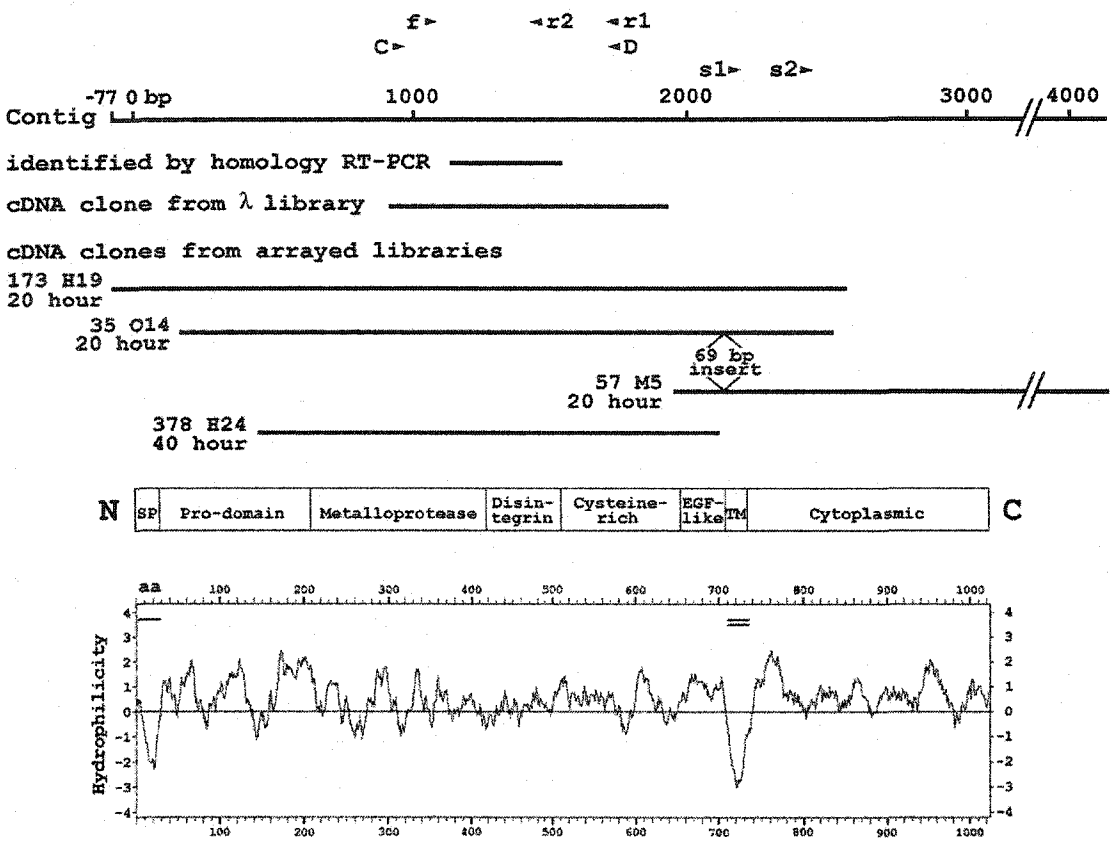
f►
◄r2
◄r1
C►
◄D
s1►
s2►
-77 0 bp
1000
2000
3000
4000
Contig
identified by homology RT-PCR
cDNA clone from λ library
cDNA clones from arrayed libraries
173 H19
20 hour
35 O14
20 hour
69 bp
insert
57 M5
20 hour
378 H24
40 hour
N
SP
Pro-domain
Metalloprotease
Disin-
tegrin
Cysteine-
rich
EGF-
like
TM
Cytoplasmic
C
aa
100
200
300
400
500
600
700
800
900
1000
Hydrophilicity
4
3
2
1
0
-1
-2
-3
-4

Figure 5. Alignment of deduced amino acid sequences of SpADAM and human ADAM 12.

Domain boundaries are from Gilpin et al. (1998). Gaps are indicated by dashes, large black arrows show predicted signal peptide cleavage sites, and asterisks show potential N-linked glycosylation sites. Signal peptide cleavage sites were predicted using the SignalP V1.1 World Wide Web Server. N-linked glycosylation consensus sequences, N{P}[ST]{P} (where N represents asparagine, {P} denotes any amino acid except proline, and [ST] indicates either serine or threonine), were identified using Gene Runner™ software. Amino acid identities are shown in gray. The metalloproteinase active site and disintegrin loop are boxed. The underlined tripeptide aligns with the RGD sequence found in many soluble snake venom metalloproteinase disintegrins (SVMPs). This SVMP tripeptide is presented on the tip of the disintegrin loop, where it functions as an integrin ligand. (SpADAM Accession Number: AY029303)

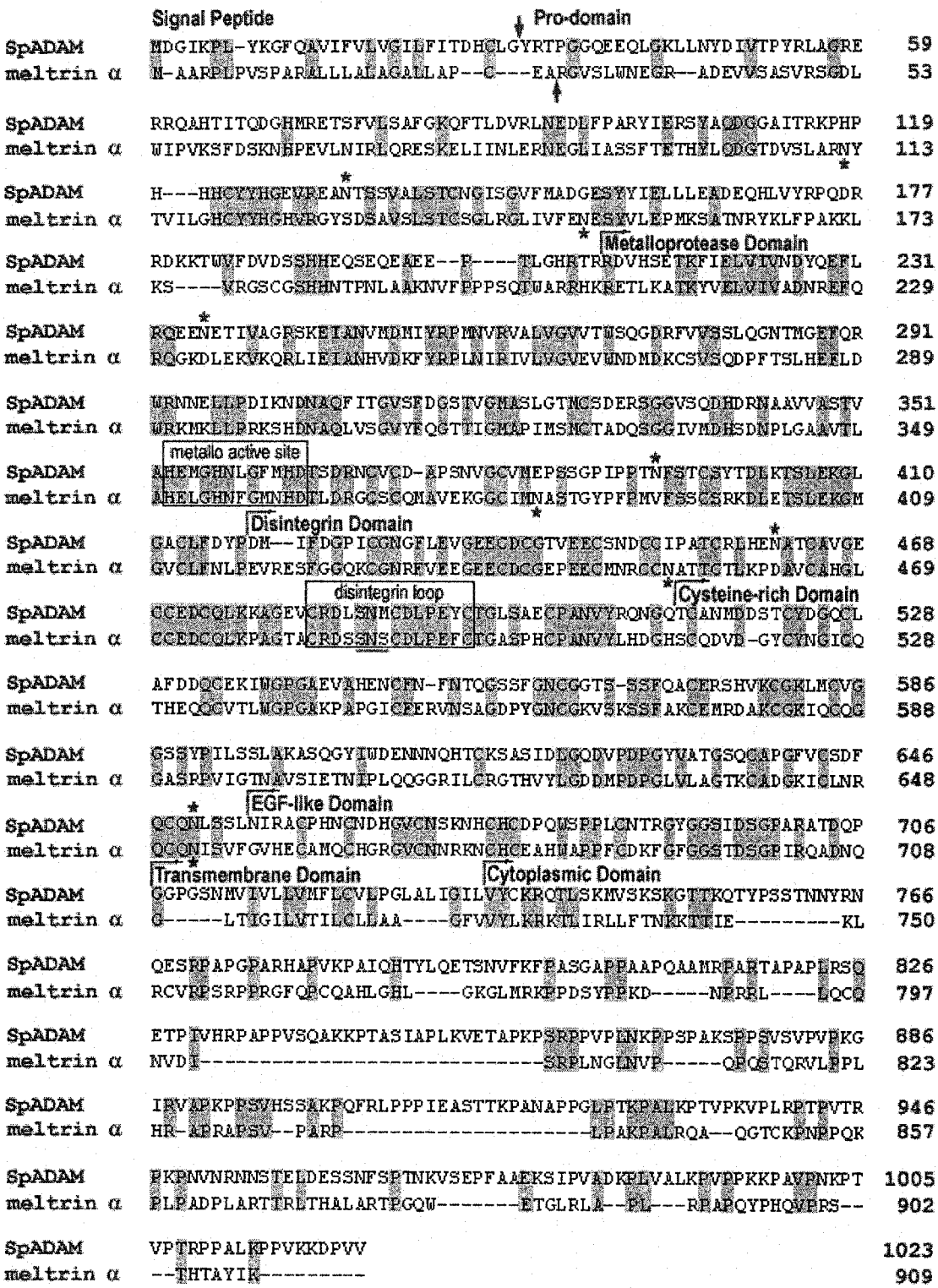
Signal Peptide
Pro-domain
SpADAM
meltrin α
Metalloprotease Domain
metallo active site
Disintegrin Domain
disintegrin loop
Cysteine-rich Domain
EGF-like Domain
Transmembrane Domain
Cytoplasmic Domain

Figure 6. SpADAM cDNA sequence with deduced amino acid translation.

The 3381 bp SpADAM contiguous cDNA sequence is shown, 5′ to 3′, with the encoded amino acid residues. 77 bp of the 5′ untranslated region (UTR) and 231 bp of the 3′ UTR are shown. A black triangle indicates the predicted signal peptide cleavage site, asterisks denote possible N-linked glycosylation sites, and domains are assigned according to Gilpin et al. (1998). The putative zinc-binding metalloproteinase catalytic site is shown in bold italics, the disintegrin loop is boxed, and the tripeptide aligned with the integrin-binding RGD of SVMPs in bold. The putative fusogenic peptide, aligned with a hydrophobic region of mouse ADAM 12 that is similar in amino acid sequence to a Sendai virus fusion peptide (Yagami-Hiromasa et al, 1995; Huovila et al, 1996), is underlined. The stop codon is indicated by "&", and the contiguous sequence does not include a polyadenylation signal.

```
-77   ttcgttacattacatgcgtatcgtattttgctcgagaacggagagacccgcgaccgagta
-17   gtgaaataggagaaagATGGATGGAATTAAACCCCTTTACAAGGGATTCCAAGCTGTG
  1                    M  D  G  I  K  P  L  Y  K  G  F  Q  A  V

 43   ATTTTCGTGCTGGTTGGAATATTATTTATCACAGATCATTGTTTAGGTTACAGAACACCA
 15    I  F  V  L  V  G  I  L  F  I  T  D  H  C  L  G  Y  R  T  P
                                        Signal Peptide ▲ Pro-domain
103   GGAGGACAAGAGGAACAACTAGGGAAATTATTGAACTACGACATCGTCACACCGTATCGT
 35    G  G  Q  E  E  Q  L  G  K  L  L  N  Y  D  I  V  T  P  Y  R

163   TTAGCCGGCAGGGAGCGCAGGCAAGCCCACACAATTACTCAGGATGGTCACATGCGAGAA
 55    L  A  G  R  E  R  R  Q  A  H  T  I  T  Q  D  G  H  M  R  E

223   ACTTCCTTTGTTCTGTCTGCATTTGGAAAACAATTTACATTGGATGTCAGGCTGAATGAA
 75    T  S  F  V  L  S  A  F  G  K  Q  F  T  L  D  V  R  L  N  E

283   GACCTATTTCCTGCAAGATACATTGAGAGGTCTTATGCACAGGATGGCGGAGCTATTACT
 95    D  L  F  P  A  R  Y  I  E  R  S  Y  A  Q  D  G  G  A  I  T

343   AGGAAGCCTCACCCACATCATCATTGTTACTACCACGGAGAAGTAAGAGAAGCTAATACA
115    R  K  P  H  P  H  H  H  C  Y  Y  H  G  E  V  R  E  A  N  T
                                                              *
403   TCATCCGTAGCACTCAGTACTTGCAATGGAATCAGTGGAGTGTTTATGGCAGATGGTGAA
135    S  S  V  A  L  S  T  C  N  G  I  S  G  V  F  M  A  D  G  E

463   AGTTATTATATCGAACTACTGCTTGAGGCGGACGAACAACATCTAGTCTACAGACCGCAG
155    S  Y  Y  I  E  L  L  L  E  A  D  E  Q  H  L  V  Y  R  P  Q

523   GATAGGCGTGACAAGAAGACGTGGGTGTTTGACGTAGATTCATCACATCATGAGCAATCT
175    D  R  R  D  K  K  T  W  V  F  D  V  D  S  S  H  H  E  Q  S

583   GAGCAAGAAGCAGAGGAGCCGACCCTCGGGCACCGAACCCGGAGAGACGTCCATTCCGAA
195    E  Q  E  A  E  E  P  T  L  G  H  R  T  R  R  D  V  H  S  E
                                                 [Metalloprotease domain
643   ACTAAATTTATCGAGCTAGTCATCGTTAACGACTATCAGGAGTTTCTACGCCAAGAGGAG
215    T  K  F  I  E  L  V  I  V  N  D  Y  Q  E  F  L  R  Q  E  E

703   AATGAAACTATCGTTGCAGGAAGAAGTAAAGAAATAGCCAATGTCATGGACATGATCTAC
235    N  E  T  I  V  A  G  R  S  K  E  I  A  N  V  M  D  M  I  Y
       *
763   CGTCCAATGAATGTTCGGGTAGCGCTGGTGGGCGTGGTCACCTGGAGTCAAGGAGACCGT
255    R  P  M  N  V  R  V  A  L  V  G  V  V  T  W  S  Q  G  D  R

823   TTTGTTGTTAGCTCCCTTCAAGGAAACACGATGGGCGAGTTTCAAAGATGGAGAAACAAC
275    F  V  V  S  S  L  Q  G  N  T  M  G  E  F  Q  R  W  R  N  N

883   GAACTACTCCCAGATATCAAGAACGACAATGCACAGTTCATAACGGGTGTGTCGTTTGAT
295    E  L  L  P  D  I  K  N  D  N  A  Q  F  I  T  G  V  S  F  D

943   GGAAGCACGGTAGGGATGGCCTCGCTAGGAACGATGTGCTCTGATGAGAGATCAGGTGGA
315    G  S  T  V  G  M  A  S  L  G  T  M  C  S  D  E  R  S  G  G
```

```
1003  GTCAGCCAGGACCATGATCGCAACGCAGCTGTTGTTGCCAGCACCGTCGCCCATGAGATG
335    V  S  Q  D  H  D  R  N  A  A  V  V  A  S  T  V  A  H  E  M

1063  GGCCATAATCTAGGCTTCATGCACGATACCTCCGATAGAAACTGCGTATGTGATGCTCCG
355    G  H  N  L  G  F  M  H  D  T  S  D  R  N  C  V  C  D  A  P

1123  TCCAATGTAGGCTGTGTGATGGAGCCCTCTAGTGGACCGATCCCTCCTACAAACTTCTCA
375    S  N  V  G  C  V  M  E  P  S  S  G  P  I  P  P  T  N  F  S
                                                          *

1183  ACGTGTTCTTACACGGACTTGAAGACATCTCTTGAGAAGGGTCTAGGAGCGTGTCTCTTT
395    T  C  S  Y  T  D  L  K  T  S  L  E  K  G  L  G  A  C  L  F

1243  GACTATCCTGATATGATCTTTGACGGACCCATCTGCGGCAACGGCTTCTTGGAGGTCGGG
415    D  Y  P  D  M  I  F  D  G  P  I  C  G  N  G  F  L  E  V  G
               Disintegrin domain

1303  GAAGAGTGCGATTGCGGAACAGTAGAGGAATGCTCCAATGACTGCTGTATTCCTGCTACC
435    E  E  C  D  C  G  T  V  E  E  C  S  N  D  C  C  I  P  A  T

1363  TGTCGCCTGCATGAGAATGCAACCTGTGCTGTAGGAGAATGCTGTGAAGATTGCCAGCTG
455    C  R  L  H  E  N  A  T  C  A  V  G  E  C  C  E  D  C  Q  L
                     *

1423  AAGAAAGCCGGTGAGGTTTGCCGGGATCTCAGTAACATGTGCGACCTCCCTGAATACTGC
475    K  K  A  G  E  V  C  R  D  L  S  N  M  C  D  L  P  E  Y  C

1483  ACTGGTCTGTCTGCTGAGTGTCCAGCCAACGTGTACAGGCAGAACGGTCAGACGTGTGCC
495    T  G  L  S  A  E  C  P  A  N  V  Y  R  Q  N  G  Q  T  C  A
                                                    Cys-rich domain

1543  AACATGGACGATTCCACCTGTTATGATGGCCAATGTTTGGCCTTTGATGACCAGTGTGAG
515    N  M  D  D  S  T  C  Y  D  G  Q  C  L  A  F  D  D  Q  C  E

1603  AAGATATGGGGGCCAGGAGCGGAGGTAGCTCATGAAAACTGCTTCAATTTTAACACTCAG
535    K  I  W  G  P  G  A  E  V  A  H  E  N  C  F  N  F  N  T  Q

1663  GGCAGCTCTTTTGGCAACTGTGGAGGGACTAGTTCATCATTCCAAGCATGCGAAAGAAGT
555    G  S  S  F  G  N  C  G  G  T  S  S  S  F  Q  A  C  E  R  S

1723  CATGTGAAGTGTGGTAAGCTGATGTGCGTTGGAGGAAGCTCCTATCCCATCTTGAGTTCC
575    H  V  K  C  G  K  L  M  C  V  G  G  S  S  Y  P  I  L  S  S

1783  CTAGCCAAGGCCAGTCAGGGTTATATCTGGGACGAGAACAACAACCAGCATACCTGCAAG
595    L  A  K  A  S  Q  G  Y  I  W  D  E  N  N  N  Q  H  T  C  K

1843  TCTGCCTCCATTGACCTGGGTCAAGACGTACCAGATCCGGGTTATGTCGCCACAGGATCG
615    S  A  S  I  D  L  G  Q  D  V  P  D  P  G  Y  V  A  T  G  S

1903  CAATGTGCACCGGGATTTGTATGCAGTGACTTCCAATGCCAGAACTTATCATCTCTCAAC
635    Q  C  A  P  G  F  V  C  S  D  F  Q  C  Q  N  L  S  S  L  N
                                              *                EGF-like

1963  ATCAGGGCTTGTCCTCATAACTGCAATGACCATGGGGTGTGCAACAGCAAGAACCACTGC
655    I  R  A  C  P  H  N  C  N  D  H  G  V  C  N  S  K  N  H  C
```

```
2023  CACTGTGACCCTCAGTGGAGCCCTCCTCTGTGTAACACTCGTGGGTATGGAGGTAGCATT
675    H  C  D  P  Q  W  S  P  P  L  C  N  T  R  G  Y  G  G  S  I

2083  GATAGTGGTCCTGCAAGAGCTACAGATCAACCAGGCGGTCCTGGATCCAACATGGTCATT
695    D  S  G  P  A  R  A  T  D  Q  P  G  G  P  G  S  N  M  V  I
                                      Transmembrane domain

2143  GTGCTCCTAGTCATGTTCCTCTGTGTACTCCCAGGCCTGGCTCTCATTGGAATCCTAGTC
715    V  L  L  V  M  F  L  C  V  L  P  G  L  A  L  I  G  I  L  V
                                                                Cyto.

2203  TACTGCAAGAGACAAACTCTTTCTAAGATGGTCTCCAAGTCCAAGGGAACTACAAAGCAA
735    Y  C  K  R  Q  T  L  S  K  M  V  S  K  S  K  G  T  T  K  Q
      Cytoplasmic domain

2263  ACTTATCCCTCAAGCACAAACAACTATCGCAATCAAGAGAGTAGACCTGCGCCCGGGCCT
755    T  Y  P  S  S  T  N  N  Y  R  N  Q  E  S  R  P  A  P  G  P

2323  GCACGCCACGCCCCTGTCAAACCTGCAATACAGCACACCTATCTACAGGAGACATCTAAT
775    A  R  H  A  P  V  K  P  A  I  Q  H  T  Y  L  Q  E  T  S  N

2383  GTCTTTAAATTCCCTGCCTCAGGTGCCCCTCCAGCTGCTCCTCAAGCCGCTATGAGACCT
795    V  F  K  F  P  A  S  G  A  P  P  A  A  P  Q  A  A  M  R  P

2443  GCACGAACAGCACCGGCACCGCTAAGATCCCAGGAGACACCGATAGTTCACCGGCCTGCA
815    A  R  T  A  P  A  P  L  R  S  Q  E  T  P  I  V  H  R  P  A

2503  CCTCCAGTTTCACAAGCTAAGAAACCGACAGCAAGTATAGCACCATTGAAAGTGGAAACA
835    P  P  V  S  Q  A  K  K  P  T  A  S  I  A  P  L  K  V  E  T

2563  GCACCGAAACCATCAAGGCCTCCGGTACCGTTAAACAAACCTCCCAGCCCAGCTAAGAGC
855    A  P  K  P  S  R  P  P  V  P  L  N  K  P  P  S  P  A  K  S

2623  CCTCCCTCGGTGTCGGTACCGGTGCCAAAGGGCATCAGGGTAGCGCCCAAACCCCCCTCT
875    P  P  S  V  S  V  P  V  P  K  G  I  R  V  A  P  K  P  P  S

2683  GTACATTCCAGTGCCAAACCTCAGTTCAGGTTACCACCTCCTATAGAGGCTAGCACCACC
895    V  H  S  S  A  K  P  Q  F  R  L  P  P  P  I  E  A  S  T  T

2743  AAACCTGCAAATGCACCACCAGGACTACCCACGAAACCGGCTCTAAAGCCAACGGTACCC
915    K  P  A  N  A  P  P  G  L  P  T  K  P  A  L  K  P  T  V  P

2803  AAGGTGCCGCTCAGACCAACCCCAGTTACAAGGCCCAAACCGAACGTAAATCGTAACAAC
935    K  V  P  L  R  P  T  P  V  T  R  P  K  P  N  V  N  R  N  N

2863  TCTACAGAACTCGATGAAAGCTCGAACTTTTCACCAACTAATAAAGTCTCAGAACCCTTT
955    S  T  E  L  D  E  S  S  N  F  S  P  T  N  K  V  S  E  P  F

2923  GCTGCAGAGAAGTCGATACCGGTAGCAGATAAACCTCTTGTGGCTCTTAAACCAGTACCG
975    A  A  E  K  S  I  P  V  A  D  K  P  L  V  A  L  K  P  V  P

2983  CCCAAGAAACCAGCGGTACCGAACAAACCGACCGTGCCAACTAGGCCACCTGCTCTTAAA
995    P  K  K  P  A  V  P  N  K  P  T  V  P  T  R  P  P  A  L  K
```

```
3043  CCACCTGTCAAGAAGGACCCTGTTGTATGAcgatagtgtctcaacaatctaggcttttat
1015   P   P   V   K   K   D   P   V   V   &

3103  taatgaactctttatcatcggtactcaactcagtcttttctgtgattccagtttatttaa
3163  gagggatgtgctatggttgtcatgaatgtctacgcataagatgttactgcctttcctgtg
3223  cagatggacaaatccacatcggcagaaatctgcaaataatggttttaaaatgttgttgtg
3283  atctacaagactagtttttctg
```

Table 1. Regional sequence similarities of SpADAM and other ADAMs of known function.

SpADAM deduced amino acid sequence was individually aligned with deduced amino acid sequences of other ADAMs. Levels of identity and similarity in each domain were evaluated using the human ADAM 12 domain boundaries of Gilpin et al. (1998). Although functions are not yet known for the *Xenopus* ADAMs, they are included because of high degrees of sequence similarity with SpADAM. ADAM synonyms and references follow: ADAM 1 = fertilin α, Ph-30α (Blobel et al., 1992); ADAM 2 = fertilin β, PH-30 β (Cho et al., 1998); ADAM 3 = cyritestin, tMDC1 (Yuan et al., 1997; Linder and Heinlein, 1997); ADAM 9 = xMDC 9 (Cai et al., 1998), MDC 9 (Izumi et al., 1998; Howard et al., 1999; Nath et al., 2000); ADAM 10 = *Drosophila* kuzbanian (Sotillos et al., 1997; Pan and Rubin, 1997), *C. elegans* Sup 17 (Wen et al., 1997). ADAM 12 = meltrin α (Loechel et al., 1998; Gilpin et al., 1998; Iba et al., 1999, 2000); ADAM 13 (Alfandari et al., 1997); ADAM 15 = metargidin, MDC 15 (Zhang et al., 1998; Howard et al., 1999; Nath et al., 1999); ADAM 17 = tumour necrosis factor α converting enzyme, TACE (Black et al., 1997). ADAM 19 = meltrin β (Kurisaki et al., 1998). Identity boxes are white if 0-20% (ADAM 17 signal peptide), pale gray if 20.1-30% (ADAM 17 Pro-domain), medium gray if 30.1-40% (ADAM 17 Disintegrin domain), dark gray if 40.1-50% (ADAM 13 Metalloproteinase domain), and black if >50% identity (ADAM 13 Disintegrin domain). Similarity boxes are white if 0-40% (ADAM 17 signal peptide), pale gray if 40.1-50% (ADAM 17 Pro-domain),

medium gray if 50.1-60% (ADAM 17 Disintegrin domain), dark gray if 60.1-70% (ADAM 13 Cysteine-rich domain), and black if >70% similarity (ADAM 13 Disintegrin domain). For functional motifs (metalloproteinase active site and disintegrin loop), percent identity is shown, with percent similarity in parentheses below.

SpADAM aligned with	Protease	Adhesion	Fusion	Signaling	Overall		Signal peptide		Pro-domain		Metallo-protease		Disintegrin domain		Cysteine-rich domain		EGF-like + transmemb.		Cytoplasmic domain		Metallopro. active site	Disintegrin loop
					% Ident.	% Simil.	% Ident.	% Simil.	% Ident.	% Simil.	% Ident.	% Simil.	% Ident.	% Simil.	% Ident.	% Simil.	% Ident.	% Simil.	% Ident.	% Simil.		
Rat ADAM 1			*		23.8	43.4	14.3	35.7	22.7	48.3	29.7	62.7	46.9	65.3	32.7	49.3	35.0	57.5	6.2	12.8	75.0 (91.7)	62.3 (78.6)
Mouse ADAM 2		*			21.6	44.6	20.0	36.7	21.3	56.8	22.8	57.2	40.8	61.2	26.3	55.6	20.3	29.1	12.5	21.5	16.7 (75.0)	50.0 (71.4)
Mouse ADAM 3		*			21.4	45.7	16.7	30.0	25.9	54.6	20.1	55.6	35.3	58.8	27.1	47.2	31.1	60.0	9.3	24.6	41.7 (75.0)	50.0 (85.7)
Mouse ADAM 9	*			*	31.3	56.7	18.8	46.9	28.5	64.5	37.1	68.1	48.5	71.1	35.4	65.3	42.9	65.5	19.0	32.9	75.0 (91.7)	57.1 (78.6)
Xenopus ADAM 9	*			*	32.5	59.9	26.7	50.0	29.1	62.6	36.7	70.5	50.5	75.3	34.7	67.4	40.7	69.1	22.9	40.4	75.0 (91.7)	71.4 (85.7)
Mouse ADAM 10	*				19.6	37.0	20.0	33.3	18.5	47.8	24.4	48.8	38.8	61.2	13.3	21.7	17.7	29.1	12.8	20.4	66.7 (83.3)	42.9 (50.0)
C. elegans ADAM 10	*				21.2	42.7	26.7	50.0	19.8	50.7	21.3	45.6	29.8	54.5	20.7	40.0	19.0	32.9	18.7	32.1	66.7 (83.3)	35.7 (64.3)
Mouse ADAM 12	*	*	*		34.6	57.6	21.9	56.3	24.3	51.9	47.6	73.8	57.3	74.0	38.6	69.0	38.0	72.2	23.1	34.9	66.7 (91.7)	71.4 (78.6)
Human ADAM 12	*	*	*		34.8	59.5	25.8	58.1	23.4	55.9	47.6	74.3	60.4	74.0	40.0	69.7	39.2	72.2	21.5	38.1	66.7 (91.7)	78.6 (85.7)
Xenopus ADAM 13					35.5	59.0	34.4	50.0	31.5	56.0	43.5	70.8	53.6	76.3	35.6	66.4	45.6	67.1	23.5	42.0	66.7 (91.7)	57.1 (92.9)
Mouse ADAM 15		*			28.5	52.1	20.0	36.7	22.6	49.2	42.7	73.0	42.1	71.6	35.2	68.3	27.8	59.5	15.6	23.9	66.7 (91.7)	57.1 (78.6)
Mouse ADAM 17	*				19.7	40.9	20.0	36.7	21.1	47.9	21.1	49.1	30.9	56.7	16.8	32.2	17.7	44.3	15.6	27.3	66.7 (83.3)	26.7 (53.3)
Mouse ADAM 19	*				31.1	57.0	19.4	41.9	28.0	52.8	43.5	70.3	51.1	70.8	31.1	64.2	42.5	68.8	22.9	40.3	66.7 (91.7)	57.1 (78.6)

Xenopus ADAM 13 (Table 1). Within the disintegrin loop, SpADAM is 78.6 % identical and 85.7 % similar to human ADAM 12, and 57.1 % identical and 92.9 % similar to *Xenopus* ADAM 13 (Table 1). Phylogenetic trees constructed from aligned protein sequences consistently group SpADAM with human and mouse ADAM 12, mouse ADAM 19, and *Xenopus* ADAM 13 (Fig. 7). Aligned extracellular domains (excluding signal sequences) gave the most robust bootstrap values (Fig. 7). Phylogenetic trees were generated for all single domain alignments and all possible multiple domain alignments, including entire sequence (data not shown). In these, the SpADAM sequence always clusters with ADAM 12, ADAM 13, and ADAM 19.

3.3 SpADAM is a Single Copy Gene

In Southern blots, there are single bands in *Hind*III and *Pst*I digests of sperm DNA from male 1, as well as in *Bam*HI and *Pst*I digests of sperm DNA from male 2 (Fig. 8). These data indicate that the SpADAM gene is present once per haploid genome.

3.4 RT-PCR

Developmental RT-PCR indicates that SpADAM mRNA is present in all developmental stages from egg to pluteus (Fig. 9). In these reactions, identical quantities of mRNA from each stage (300 ng) were used to generate cDNA, and identical volumes of cDNA from each stage (2 μl) were used to amplify the 335

Figure 7. Phylogenetic analysis of all ADAMs for which complete cDNA sequence is available.

Amino acid sequences without their signal peptides and cytoplasmic domains were aligned and a phylogenetic tree constructed using a neighbour joining algorithm (Saitou and Nei, 1987). Bootstrap values are recorded at each node. Alternative nomenclature and NCBI accession numbers follow: ADAM 1 (fertilin α), U46069, Y08616; ADAM 2 (fertilin β), AF086808, NM_001464, X99794, U38806, U46070; ADAM 3 (cyritestin), NM_009619; ADAM 5, U22059, U22060; ADAM 7, NM_007402; ADAM 8, NM_001109, NM_007403; ADAM 9 (meltrin γ), NM_003816, NM_007404, AF032382; ADAM 10 (kuzbanian, SUP-17), NM_001110, NM_007399, U60591, AF024614; ADAM 11, NM_002390; ADAM 12 (meltrin α), NM_003474, NM_007400; ADAM 13, U66003; ADAM 15 (metargidin), NM_003815, NM_009614, AJ251198; ADAM 17 (tumour necrosis factor α converting enzyme, TACE), NM_003183, NM_009615; ADAM 18 (NM_014237); ADAM 19 (meltrin β), NM_009616; ADAM 20, NM_003814; ADAM 21, AF158644; ADAM 22, AF134708; ADAM 23, NM_003812, NM_011780; ADAM 24 (testase 1), AF167402; ADAM 25, NM_011781; ADAM 26 (testase 3), AF167404; ADAM 27, AF167405; ADAM 28, AF153350, NM_014265; ADAM 29, AF171929; ADAM 30, AF171932; ADAM 31, AF251559; ADM-1, U68185; SpADAM, AY029303.

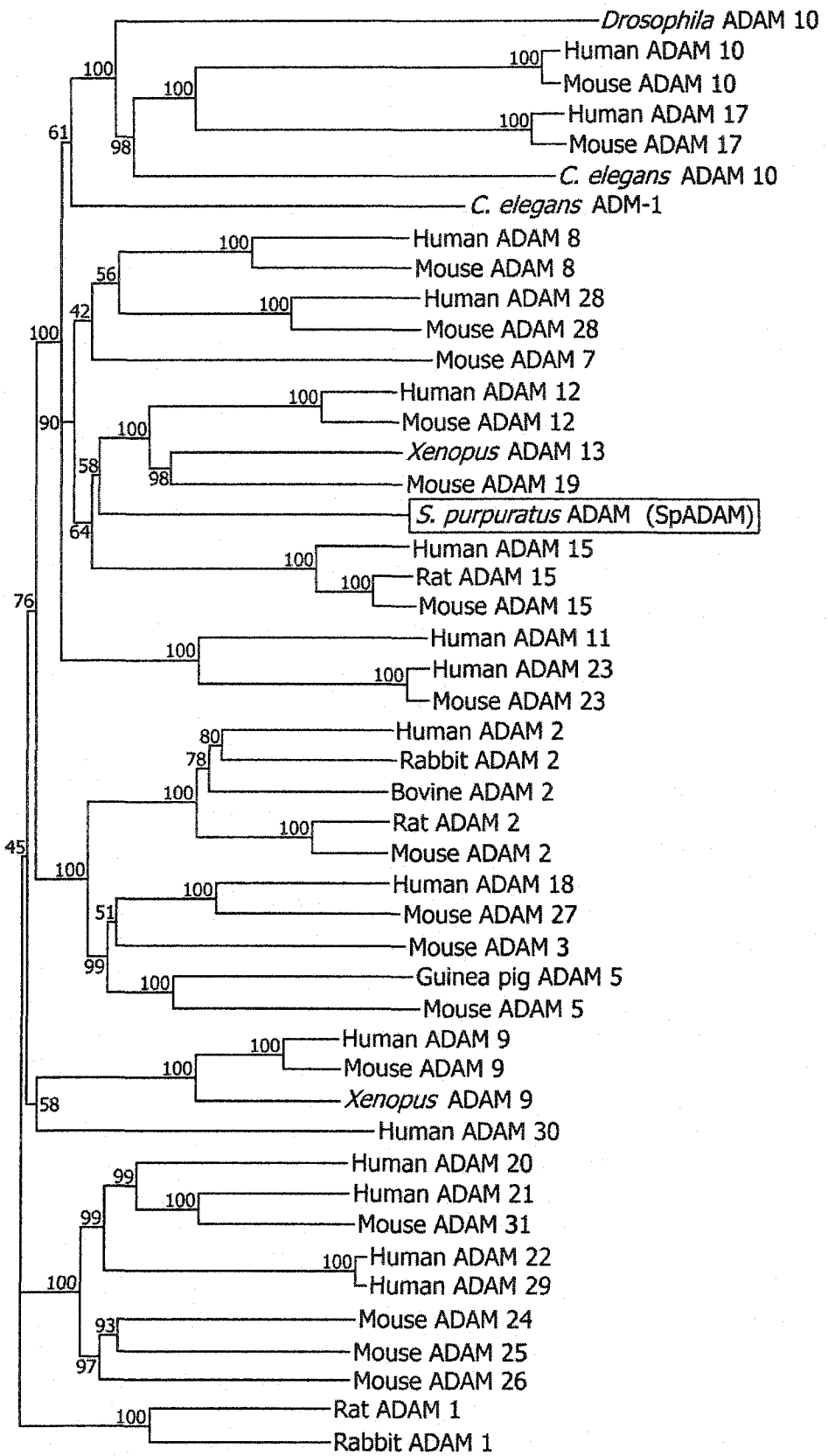
Drosophila ADAM 10
Human ADAM 10
Mouse ADAM 10
Human ADAM 17
Mouse ADAM 17
C. elegans ADAM 10
C. elegans ADM-1
Human ADAM 8
Mouse ADAM 8
Human ADAM 28
Mouse ADAM 28
Mouse ADAM 7
Human ADAM 12
Mouse ADAM 12
Xenopus ADAM 13
Mouse ADAM 19
S. purpuratus ADAM (SpADAM)
Human ADAM 15
Rat ADAM 15
Mouse ADAM 15
Human ADAM 11
Human ADAM 23
Mouse ADAM 23
Human ADAM 2
Rabbit ADAM 2
Bovine ADAM 2
Rat ADAM 2
Mouse ADAM 2
Human ADAM 18
Mouse ADAM 27
Mouse ADAM 3
Guinea pig ADAM 5
Mouse ADAM 5
Human ADAM 9
Mouse ADAM 9
Xenopus ADAM 9
Human ADAM 30
Human ADAM 20
Human ADAM 21
Mouse ADAM 31
Human ADAM 22
Human ADAM 29
Mouse ADAM 24
Mouse ADAM 25
Mouse ADAM 26
Rat ADAM 1
Rabbit ADAM 1

Figure 8. Genomic Southern blot

High molecular weight DNA, isolated from the sperm of two male sea urchins, was independently digested to completion with *Bam*HI (B), *Eco*RI (E), *Hind*III (H), and *Pst*I (P). Digested DNA samples and a λ*Hind*III size marker were separated on agarose gels, blotted to nylon membranes, and probed with a radiolabeled SpADAM fragment. Marker bands are shown in kb. Single bands in *Hind*III and *Pst*I digests of sperm DNA from male 1, and in *Bam*HI and *Pst*I digests of sperm DNA from male 2, were confirmed by running a duplicate Southern on the same samples (data not shown). Single bands indicate the SpADAM gene is present once per haploid genome. Multiple bands are seen in select digests because the probe spans more than one exon.

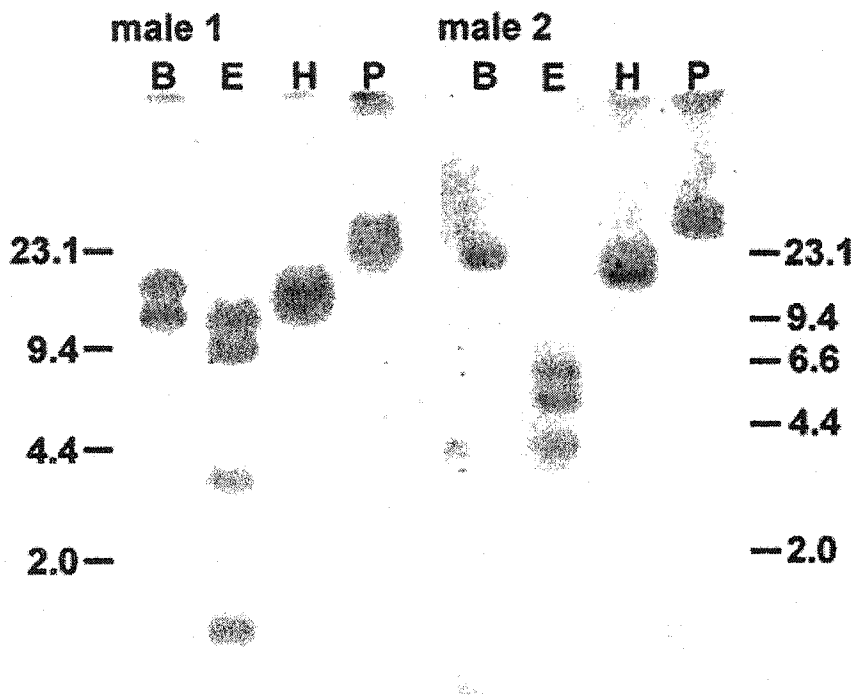
male 1
male 2
B E H P
B E H P
23.1—
9.4—
4.4—
2.0—
—23.1
—9.4
—6.6
—4.4
—2.0

Figure 9. RT-PCR

An equal quantity (300 ng) of poly (A+) RNA from each stage was reverse transcribed to cDNA, and an equal volume (2 μl) of cDNA from each stage used as template in polymerase chain reaction (PCR) with SpADAM specific primers designed to amplify a 335 bp fragment (Fig. 2). SpADAM is present as template in all stages tested.

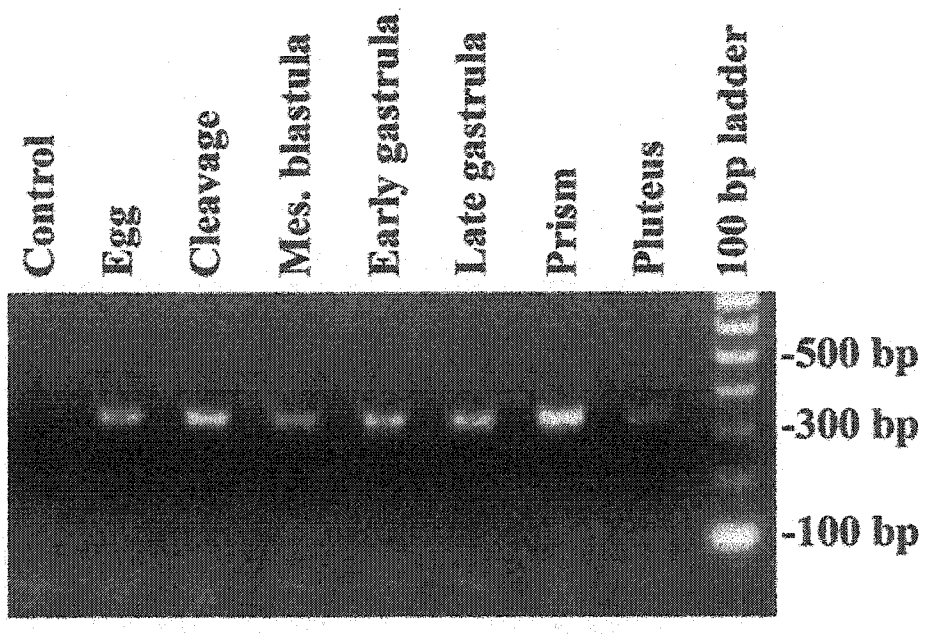
Control
Egg
Cleavage
Mes. blastula
Early gastrula
Late gastrula
Prism
Pluteus
100 bp ladder
-500 bp
-300 bp
-100 bp

bp SpADAM band. The highest RT-PCR product band intensity is seen in the prism (50 h) sample, while the lowest band intensity is in the early pluteus (72 h) sample.

3.5 Northern Blot

Northern blots reveal the presence of two SpADAM transcripts (Fig. 10). In cleavage, mesenchyme blastula, early gastrula, and prism stages, 4.4 and 2.3 kb SpADAM bands are present. Mid-gastrula, late gastrula, and pluteus samples contain only the smaller transcript. To control for loading, an equal quantity of mRNA from each stage was used. Band intensity, therefore, reflects the prevalence of SpADAM transcript in the sample. The highest levels of the 4.4 kb SpADAM transcript are seen in cleavage, mesenchyme blastula, and early gastrula stage embryos. The 4.4 kb SpADAM mRNA drops to undetectable in mid and late gastrulae, rises to a moderate level in prism stage embryos, and then drops back to undetectable in plutei (Fig. 10). The 2.3 kb SpADAM transcript level is steadily high from cleavage through early gastrula stages, decreases during gastrulation to its lowest level in late gastrulae, rises to its highest level in prism stage embryos, and then drops to moderate levels in plutei (Fig. 10).

3.6 *In Situ* RNA Hybridization

In mesenchyme blastulae and early gastrulae, vegetal plates and PMCs

Figure 10. Northern blot

Locations of RNA size marker bands are shown. SpADAM probe recognizes a 2.2 kb band in all stages, with the highest level of this sized transcript present in prism stage embryos. SpADAM probe also recognizes a less intense 4.4 kb band in early stages. The 4.4 kb SpADAM transcript is undetectable in mid and late gastrulae, present at low levels in prisms, and undetectable in plutei.

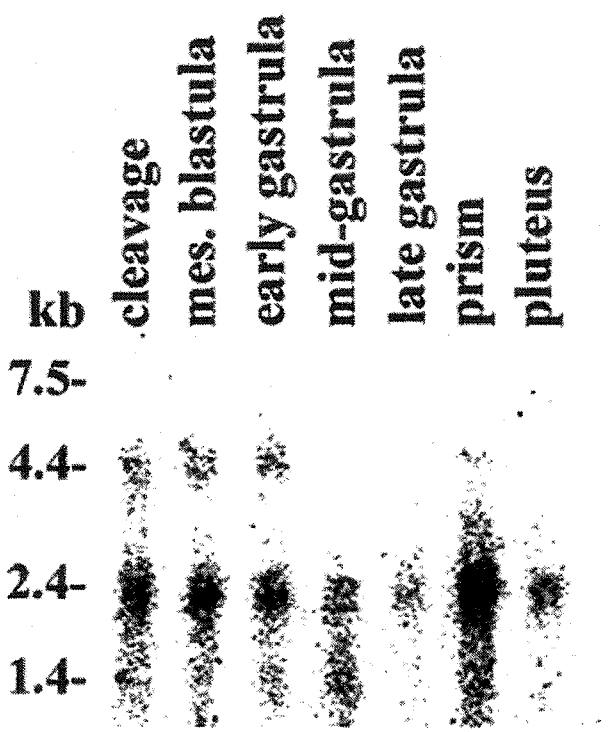
kb
7.5-
4.4-
2.4-
1.4-
cleavage
mes. blastula
early gastrula
mid-gastrula
late gastrula
prism
pluteus

hybridize probe (Fig. 11A). In late gastrulae, SpADAM expression is high in SMCs as they release from the archenteron tip, as well as in the thickened apical plate and blastopore rim (Fig. 11B). In prisms (50 h), the highest level of hybridization of SpADAM probe is in the apical plate, coelomic pouches, intestine, pigment cells, blastocoelar cells, and some PMCs (Fig. 11C,E, F). Typically, there is one PMC in each ventrolateral cluster that stains more intensely than all the others. The remaining tissues have pale blue staining (Fig. 11A,B,C,E,F). In 5-week larvae, the highest levels of SpADAM probe binding were in ciliary band, epaulettes, vestibule, somatocoels, and the five primary podia of the adult rudiment (Fig. 12B,C,D). Again, there appeared to be a low level of SpADAM expression in remaining tissues. There was an absence of staining in all tissues of all embryos and larvae hybridized with the sense riboprobe (Figs. 11D, 12A).

3.7 Immunoblots and Immunoprecipitations

A polyclonal antiserum (CR 15) was raised against a His-tagged bacterially expressed 277 amino acid SpADAM fragment containing all of the disintegrin domain and parts of the metalloproteinase and cysteine-rich domains (Fig. 2). On Western blots of purified bacterially expressed SpADAM+His, anti-His antibodies recognized a major band of approximately the expected size (30 kDa). In cleavage stage pellet (crude membrane) fractions,

Figure 11. Whole mount *in situ* hybridizations of early embryos using 425 bp sense (D) and antisense (A-C, E, F) digoxygenin-labeled SpADAM riboprobes.

(A) Late mesenchyme blastula/early gastrula stage embryo (28 h), showing intense staining in the vegetal plate, moderate staining in the presumptive apical plate and fully ingressed PMCs, and low levels of SpADAM expression in presumptive ectoderm.

(B) Late gastrula stage embryo (36 h), showing moderate staining of SMCs, blastopore rim, and apical plate, and low levels of staining in remaining tissues.

(C, E, F) Prism stage embryos (50 h), showing high levels of SpADAM transcript in apical plate, coelomic pouches (cp), intestine (i), pigment and blastocoelar cells, and some PMCs. Faint staining is seen in remaining tissues such as esophagus (e), stomach (s), ectoderm, and some PMCs. (F) Same embryo as (E) in a surface focal plane showing staining of cells which, due to their appearance and location, are believed to be pigment cells.

(D) Control prism stage embryo, hybridized with digoxygenin-labeled sense SpADAM riboprobe. Bars = 25 μm. Bar is C applies to C-F.

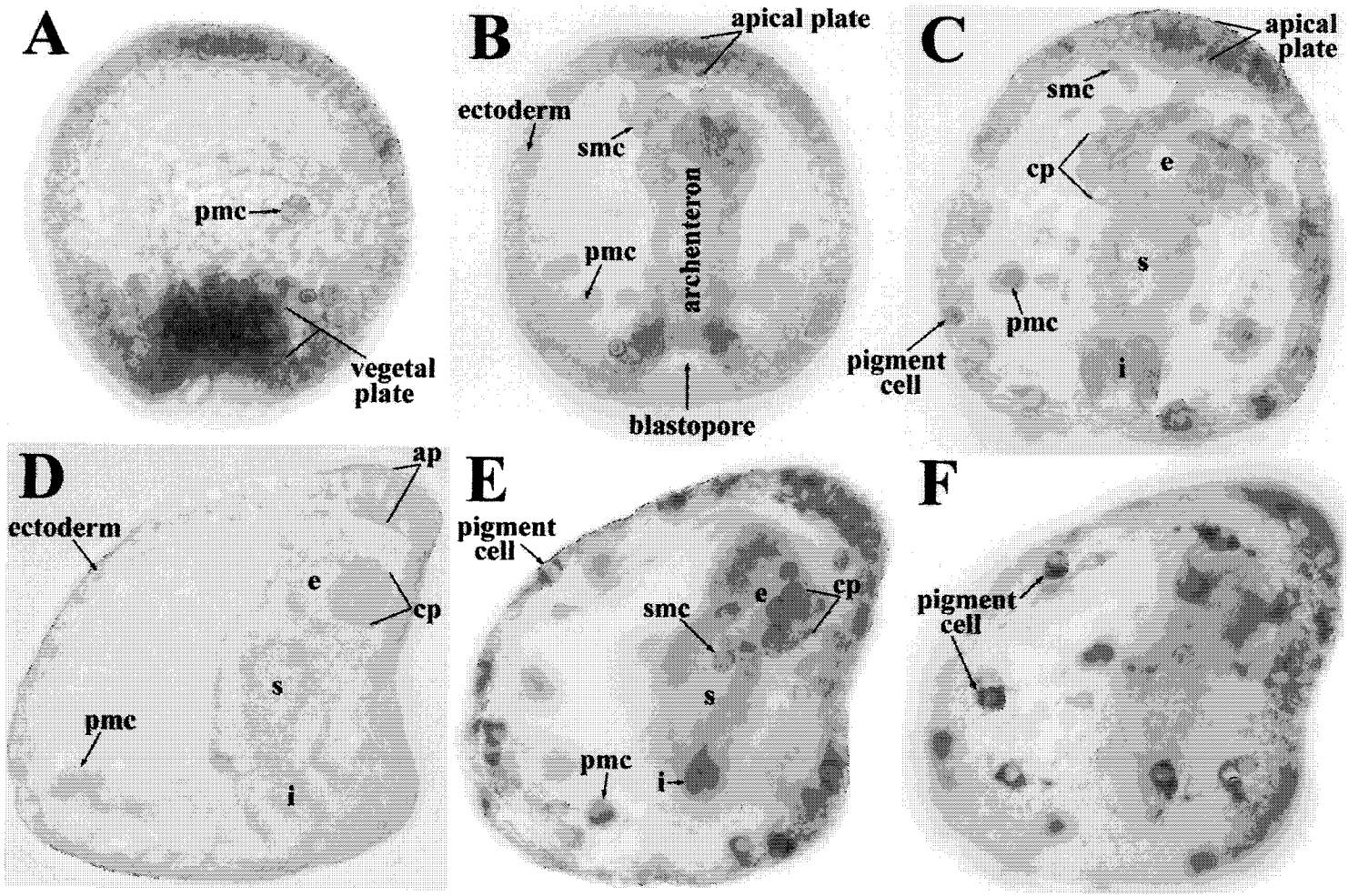
A
pmc
vegetal plate
B
apical plate
ectoderm
smc
archenteron
pmc
blastopore
C
apical plate
smc
cp
e
s
pmc
pigment cell
i
D
ap
ectoderm
e
cp
s
pmc
i
E
pigment cell
smc
e
cp
s
pmc
i
F
pigment cell

Figure 12. Whole mount *in situ* hybridizations of late larvae with sense (A) and antisense (B-D) digoxygenin-labeled SpADAM riboprobes.

(A) Larvae labeled with sense SpADAM riboprobe have no staining in all tissues.

(B) Staining is more intense in the left somatocoel (s) and invaginating vestibule (v), but not in the left hydrocoel (h).

(C) A more advanced stage than (B), in which the vestibule, somatocoels, and ciliated band (cb) display high levels of SpADAM transcript.

(D) More advanced than (C), this larva has formed an adult rudiment. SpADAM is expressed at high levels in the five primary podia (pp), the ciliated band, and the epaulettes (e). Remaining tissues are faintly stained.

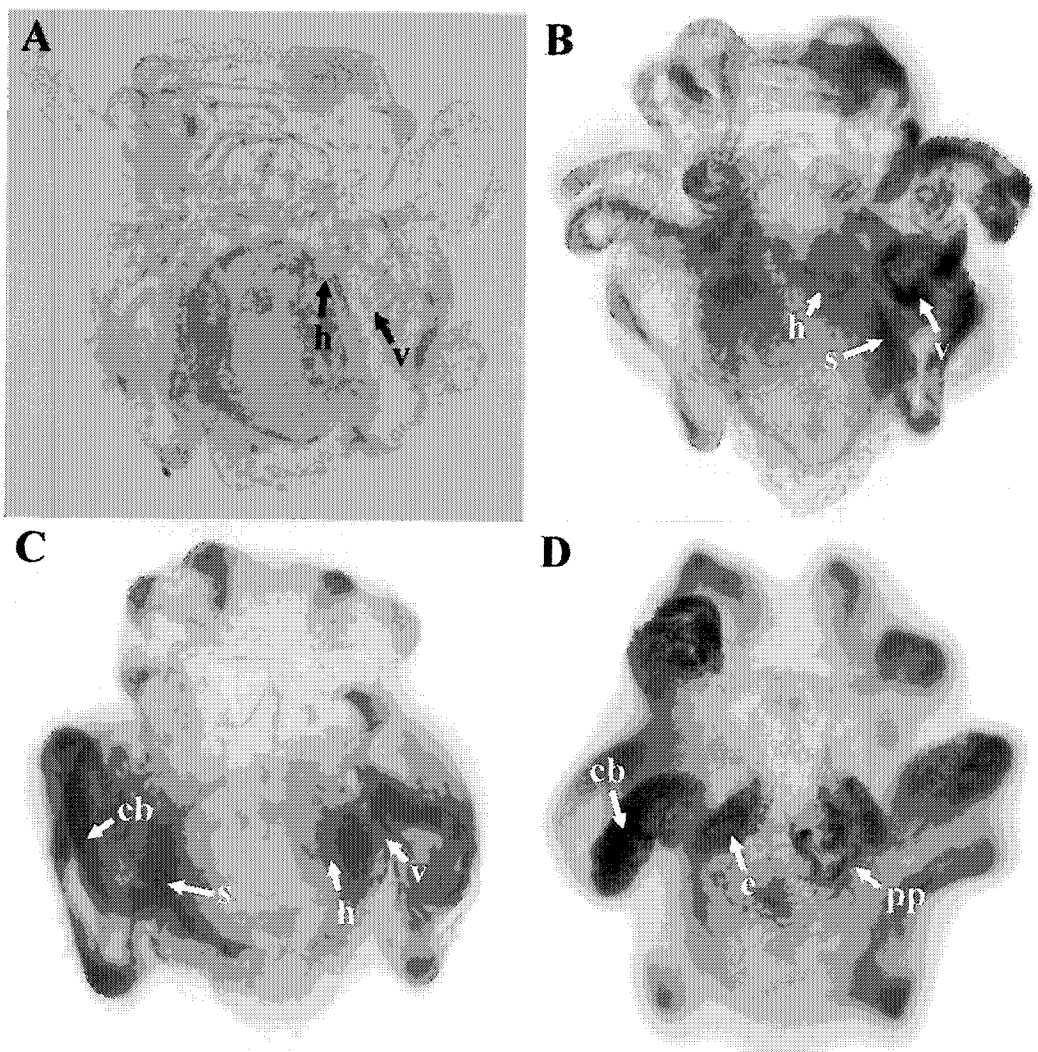
A
h
v
B
h
s
v
C
cb
s
h
v
D
cb
c
pp

the dominant protein recognized by anti-SpADAM serum is of apparent molecular weight (MW) 131 kDa (Fig. 13A, lane 1). The 131 kDa band is not present in cleavage stage supernatant fractions (data not shown). In mesenchyme blastula (28 h) crude membrane fractions, the dominant band is 95 kDa (Fig. 13A, lane 3). Anti-SpADAM antibodies also recognize a 131 kDa protein in this fraction, but not in mesenchyme blastula supernatant (Fig. 13A, lane 2). Weaker bands of 51 and 44 kDa are seen in all cleavage and mesenchyme blastula fractions (Fig. 13A, lanes 1, 2, and 3). No bands are recognized, in any fractions of any stage, by pre-immune serum (Fig. 13A, lane 4). Immunoprecipitates of prism (52 h) lysates with anti-SpADAM antibodies have specific bands at 95 and 72 kDa (Fig. 13B, lane 1).

3.8 SpADAM Immunolocalization

Anti-SpADAM immunoreactivity is first detected at the intercellular interface of the 2-cell cleavage embryo (Fig. 14A). In 4-cell and 8-cell embryos, immunoreactivity is seen on all blastomere surfaces, although more intensely where blastomeres contact (Fig. 14C). At the 16-cell stage, all mesomere and macromere surfaces are immunoreactive (Fig. 14D). Staining in micromeres appears more diffuse and less clearly associated with cell surfaces (Fig. 14D). In 60-cell embryos, all surfaces of macromere daughters are immunoreactive (Fig. 14G). The apical and lateral surfaces of an_1 (mesomere daughter) blastomeres

Figure 13. SpADAM protein expression assessed by immunoblot and immunoprecipitation.

A. Immunoblot of samples from cleavage stage (32-cell) and mesenchyme blastula (28 h) crude membrane pellets (lanes 1 and 3) and mesenchyme blastula aqueous supernatant (lane 2). Equal loadings of protein were separated by SDS-PAGE, electroblotted, and incubated with anti-SpADAM antiserum (lanes 1-3) or pre-immune serum (lane 4). A 131 kDa band is indicated with a black arrowhead, and a 95 kDa band with a hollow arrowhead. B. Biotinylated prism (52 h) lysates were immunoprecipitated with anti-SpADAM (lane 1) or pre-immune serum (lane 2). The specific bands recognized by anti-SpADAM antibodies are at 72 kDa (gray arrowhead) and 95 kDa.

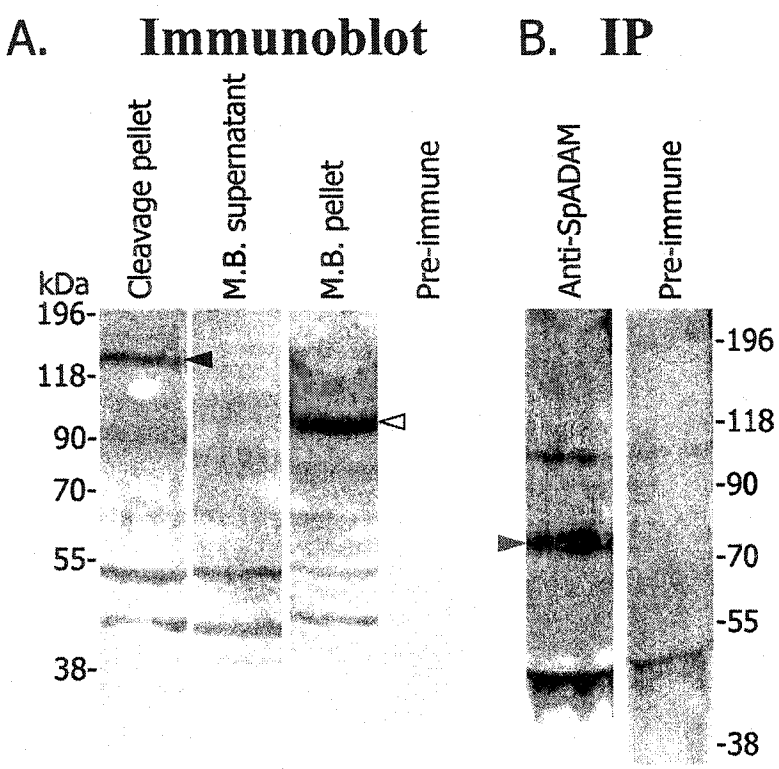
A.
Immunoblot
B.
IP
Cleavage pellet
M.B. supernatant
M.B. pellet
Pre-immune
Anti-SpADAM
Pre-immune
kDa
196-
118-
90-
70-
55-
38-
-196
-118
-90
-70
-55
-38

Figure 14. Confocal laser scanning images of cleavage stage embryos, prepared for immunofluorescence with anti-SpADAM (A,C,D,F,G) or pre-immune serum (B,E).

All images are 1 μm optical sections except A and B, which are projections of 8-1 μm sections. (A) 2-cell embryo shows anti-SpADAM immunoreactivity at cell-cell interface. (B) Pre-immune control of 2-cell embryo shows no staining. (C) 8-cell embryo shows immunoreactivity on all blastomere surfaces. (D) 16-cell embryo shows immunoreactivity on all mesomere and macromere surfaces, with more diffuse fluorescence of micromeres (m). (E) Pre-immune control of 16-cell embryo. (F) Optical section through animal tier of blastomeres of 32-cell embryo showing anti-SpADAM immunoreactivity on apical and lateral surfaces. (G) Vegetal view of 60-cell embryo showing anti-SpADAM immunoreactivity on all surfaces of veg_1 and veg_2 blastomeres. Micromeres are not immunoreactive, and lack the diffuse internal staining seen in 16-cell micromeres. Bar = 25 μm, and applies to A-G.

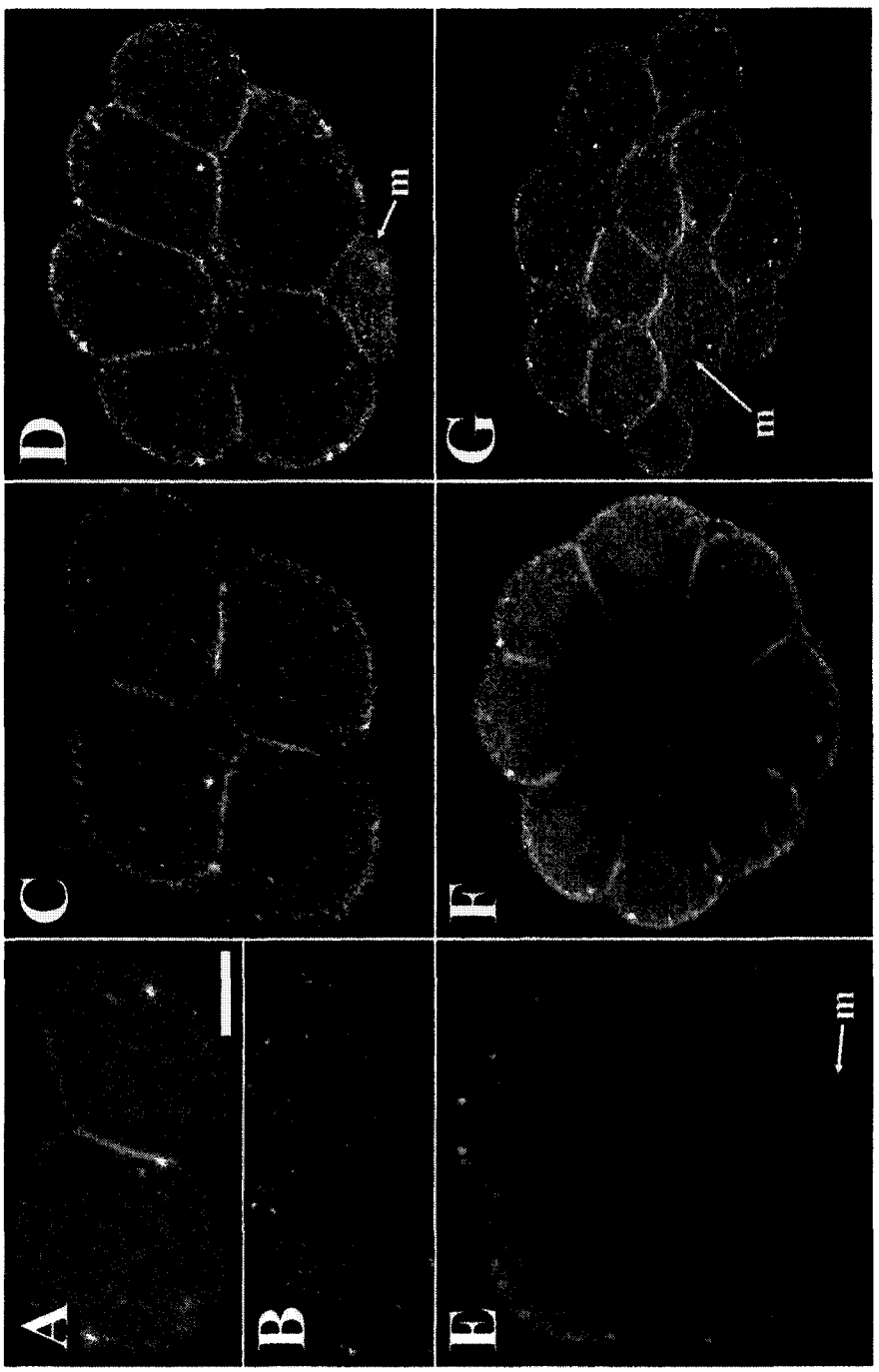
A
B
C
D
E
F
G
m
m
m

are immunoreactive, whereas their basal surfaces are not (Fig. 14F). Although the 60-cell macromere-micromere interface is highly immunoreactive, there is no immunoreactivity between micromeres (Fig. 14G). Additionally, the diffuse immunoreactivity seen in 16-cell micromeres is no longer present in the 60-cell micromeres (Fig. 14G).

At the mesenchyme blastula stage, the apical surfaces of vegetal plate cells are immunoreactive (Fig. 15A). The apical surfaces of cells in the apical plate are weakly immunoreactive (data not shown). As PMCs are released into the blastocoel, some have small foci of anti-SpADAM immunoreactivity (Fig. 15A). Throughout gastrulation, SMCs released from the tip of the archenteron are immunoreactive (Fig. 15B,C). In early gastrulae (Fig. 15B), PMCs are weakly immunofluorescent. The level of immunoreactivity in PMCs rises throughout gastrulation (Fig. 15C). In late gastrula/early prism stage embryos, surfaces of PMC ventrolateral clusters with spicule rudiments and elongating spicules are strongly immunoreactive (Fig. 15D,F). The skeletogenic cells remain immunoreactive throughout larval life (Figs. 16C, 17E). In late gastrulae, the cells of the coelomic pouches and pigment cells dispersed within the ectoderm are immunoreactive (Fig. 15D, E).

In early plutei, skeletogenic mesenchyme associated with the larval skeleton is immunoreactive (Fig 16A-F). The sheath of cytoplasm surrounding the spicules, and the cells associated, are fluorescent. Although the spicule sheath is almost uniformly immunofluorescent, there are regions of brighter

Figure 15. Confocal laser scanning images of mesenchyme blastula to late gastrula stage embryos prepared for immunofluorescence with anti-SpADAM (A-F) or pre-immune (D inset) serum.

All images are 1 μm optical sections. (A) Mesenchyme blastula (28 h); (B) Mid-gastrula (33 h); (C) Late gastrula (38 h); (D) Late gastrula/early prism stage embryo (45 h). (D inset) Pre-immune 45 h control embryo showing no immunoreactivity. (E) Detail of (D), showing apical immunoreactivity on cells of coelomic pouch and esophagus. Mesenchyme cells and their filopodial extensions are also immunoreactive. (F) Detail of (D), showing intense fluorescence of PMCs and spicule sheath in ventrolateral cluster. Ectoderm staining is not above background levels. PMC, primary mesenchyme cell; SMC, secondary mesenchyme cell; a, archenteron; sp, spicule sheath; cp, coelomic pouch; eso, esophagus; ect, ectoderm. Bar = 25 μm in A-D, bar = 10 μm in E and F.

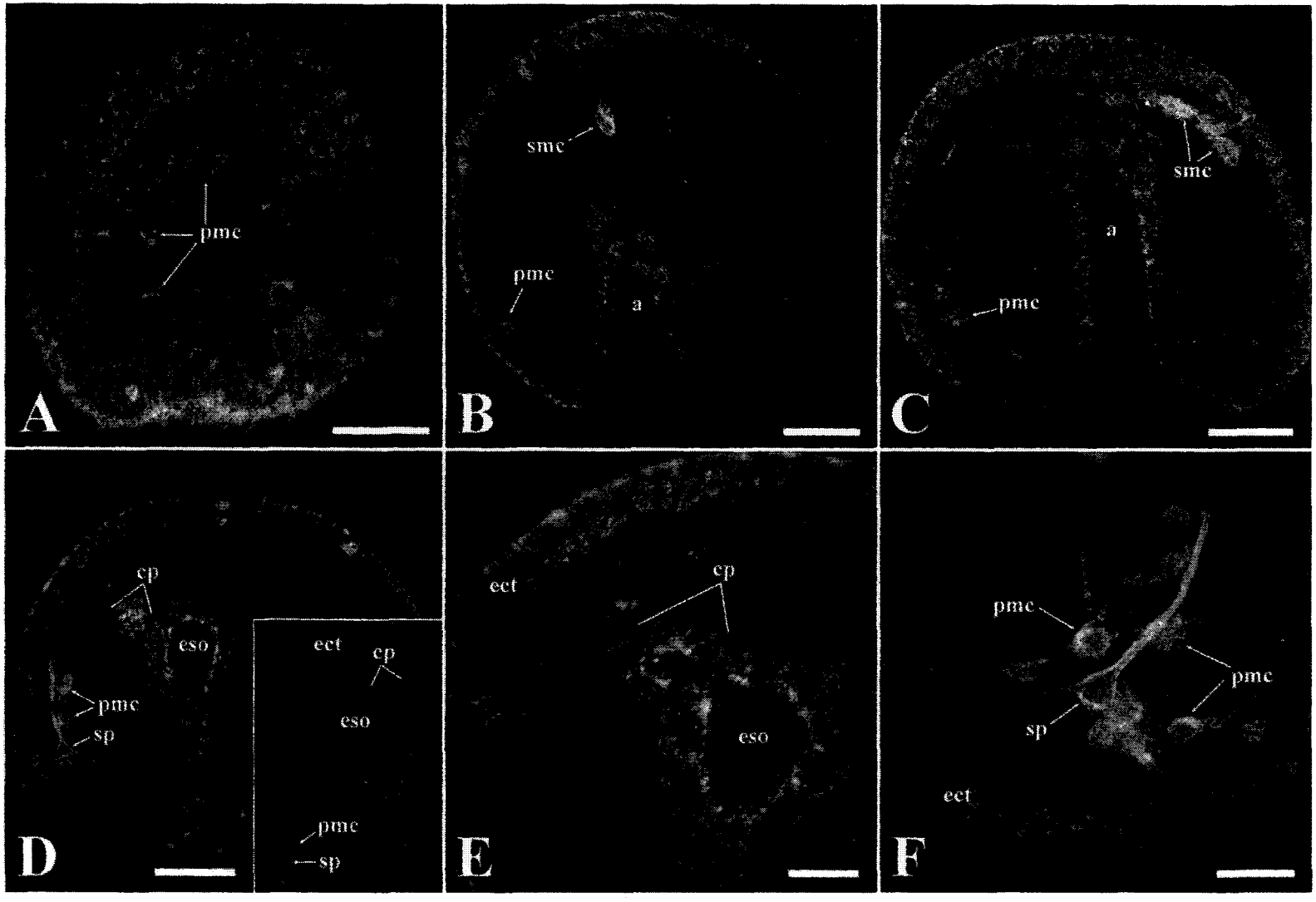
A
pmc
B
smc
pmc
a
C
smc
a
pmc
D
cp
eso
pmc
sp
ect
cp
eso
pmc
sp
E
ect
cp
eso
F
pmc
pmc
sp
ect

Figure 16. Confocal laser scanning images of 4-arm plutei (72 h) prepared for immunofluorescence with affinity-purified anti-SpADAM antibodies (A), anti-SpADAM serum (B-H), or pre-immune serum (E inset).

(A) 1 μm optical section showing immunoreactivity only in mesenchyme. PMC, primary mesenchyme cell; sp, spicule sheath; b, blastocoelar cell; i, intestine; ect, ectoderm. (B) Maximum projection reconstruction of 6-0.6 μm sections, showing patches of bright anti-SpADAM immunoreactivity in regions of ectoderm overlying spicule tips. (C) 1 μm section. Immunoreactivity is associated with coelomic pouch (cp), and filopodial extensions (f) of PMC at tip of body rod. mo, mouth; eso, esophagus; sto, stomach. (D) Projection of 6-1 μm sections. Muscle cells (mu) surrounding the esophagus bind anti-SpADAM antibodies. (E) Projection of 7-1 μm sections. (E inset) Projection of 10-1 μm sections. (F) 1 μm section. (G) Projection of 7-1 μm sections of cross section of pluteus esophageal region. There is a single immunoreactive cell in each coelomic pouch (on either side of the esophagus). (H) Projection of 8-1 μm sections of longitudinal section of pluteus in esophageal region. Circumesophageal muscle fibres, as well as the apical surfaces (ap) of cells lining the stomach, are recognized by anti-SpADAM antibodies. bl, basal lamina. Bar = 25 μm in A,B,G,H; bar = 50 μm in C-F.

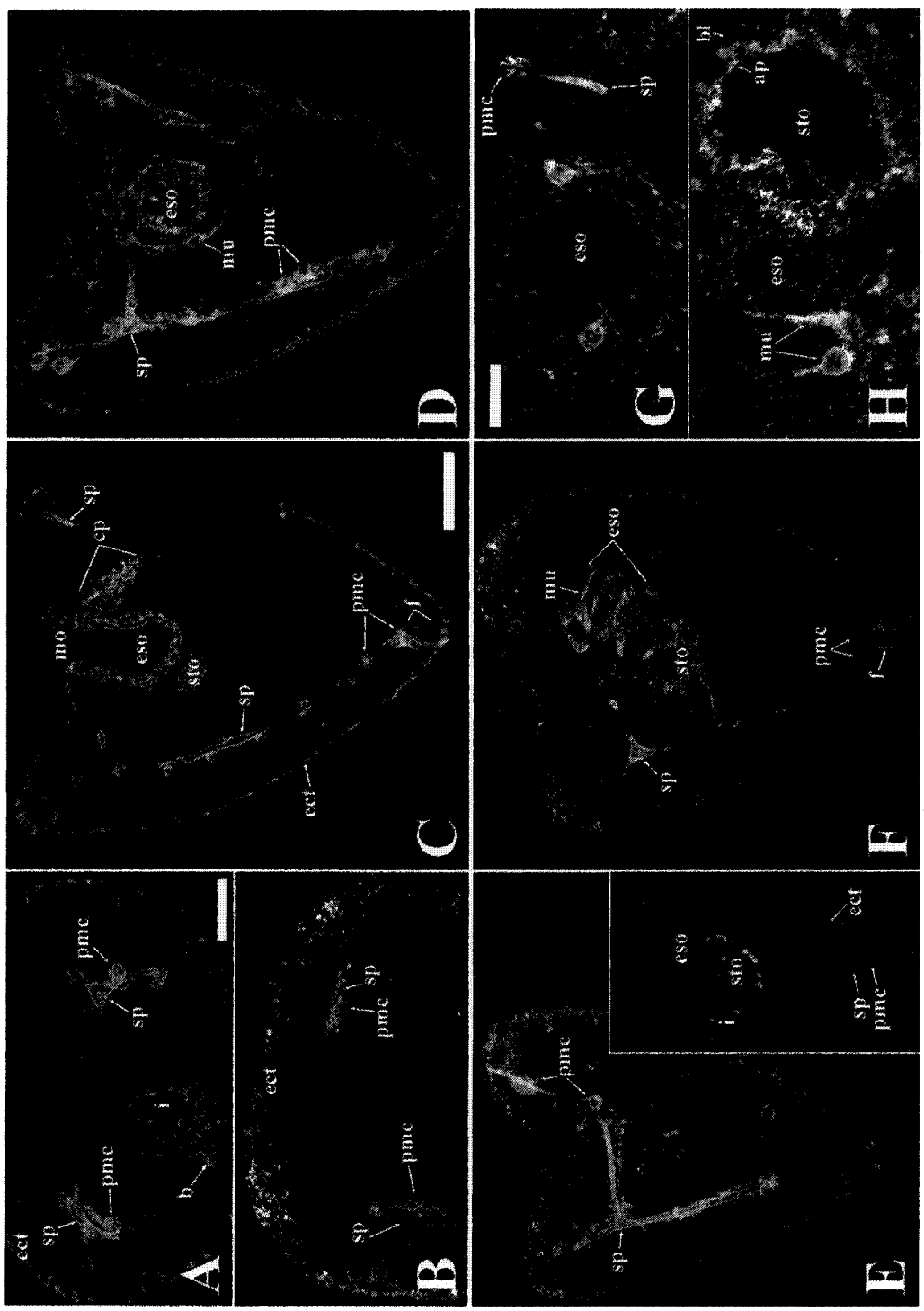
A
B
C
D
E
F
G
H
ect
sp
pmc
b
i
ect
sp
pmc
pmc
sp
mo
cp
sp
eso
sto
sp
ect
pmc
f
sp
pmc
mu
eso
sto
sp
pmc
eso
i
sto
sp
pmc
ect
pmc
f
sp
pmc
eso
sp
mu
eso
sto
bl
mu
eso
ap
sto

fluorescence at the tips of the spicules and interspersed along the length of the skeletal rods (Fig. 16C-E). Blastocoelar cells are diffusely immunoreactive (Fig. 16A). In early plutei, a single cell in each coelomic pouch, and the circumesophageal muscle fibers express SpADAM (Fig. 16F-H). Unfertilized eggs were not immunoreactive (data not shown). All early control embryos (to 100 h) treated with pre-immune serum showed no immunofluorescence above background (Fig. 14B,E; Fig. 15D inset; Fig. 16E inset).

In 7-day plutei, the highest levels of anti-SpADAM immunoreactivity are in the skeletogenic mesenchyme, esophageal muscles, and cells of the preoral ectoderm surrounding the apical ganglion (Fig. 17). Preoral ectoderm fluorescence is initially in a small number of cells, but in later plutei, the thickened ectoderm between the preoral arms is brightly fluorescent (Fig. 17A-C). In 7-day larvae, anti-serotonin antibodies recognize a group of neurons in the apical ganglion (Fig. 17D left inset). Other potentially neural tissues expressing SpADAM include adoral ciliated band, ciliated band, and oral ganglia (Fig. 17D,E). The circumesophageal musculature is also strongly immunoreactive in plutei, most prominently in the longitudinal muscles forming a basket around the lower esophagus (Fig. 17F).

Figure 17. Confocal laser scanning images of 7 day larvae prepared for immunofluorescence with anti-SpADAM (A-F), pre-immune serum (D right inset and F inset), or anti-serotonin (D left inset).

All images are 1 μm optical sections except (D, left inset), which is a projection of 5-1 μm sections. (A) Prism stage embryo showing SpADAM expression in a few cells of the apical plate (ap), PMCs, SMCs, and spicule (sp) sheaths. eso, esophagus; sto, stomach; i, intestine; ect, ectoderm. Images B-F are of 7 day fasted larvae. (B) Immunofluorescence is in the thickened region of ectoderm containing the apical ganglion (ag), epithelium surrounding the mouth (mo), spicule sheaths, and blastocoelar fibres. poa, postoral arm. (C) Detail of (B). (D) Immunoreactivity in the region of the apical ganglion, oral ectoderm, PMCs, and adoral ciliated band (ad). Oral ganglia (og) are more strongly stained than background (D and F, insets). ala, anterolateral arm; ue, upper esophagus; le, lower esophagus. (D left inset) Oral field and apical ganglion prepared with anti-serotonin, showing cell bodies and processes of neurons. (D right inset) Same region as (D left inset), but stained with pre-immune serum. (E) Detail of oral field and upper digestive tract. ul, upper lip; cb, ciliated band; ll, lower lip. (F) Detail of upper digestive tract, showing immunoreactive longitudinal fibres on the surface of the lower esophagus. (F inset) Upper digestive tract of larva stained with pre-immune serum. Stomach endoderm, oral ganglia, and the circular muscle fibres surrounding the upper esophagus stain weakly in pre-immune controls. Bars in A, C, E, and F = 50 μm. Bars in B and D = 100 μm.

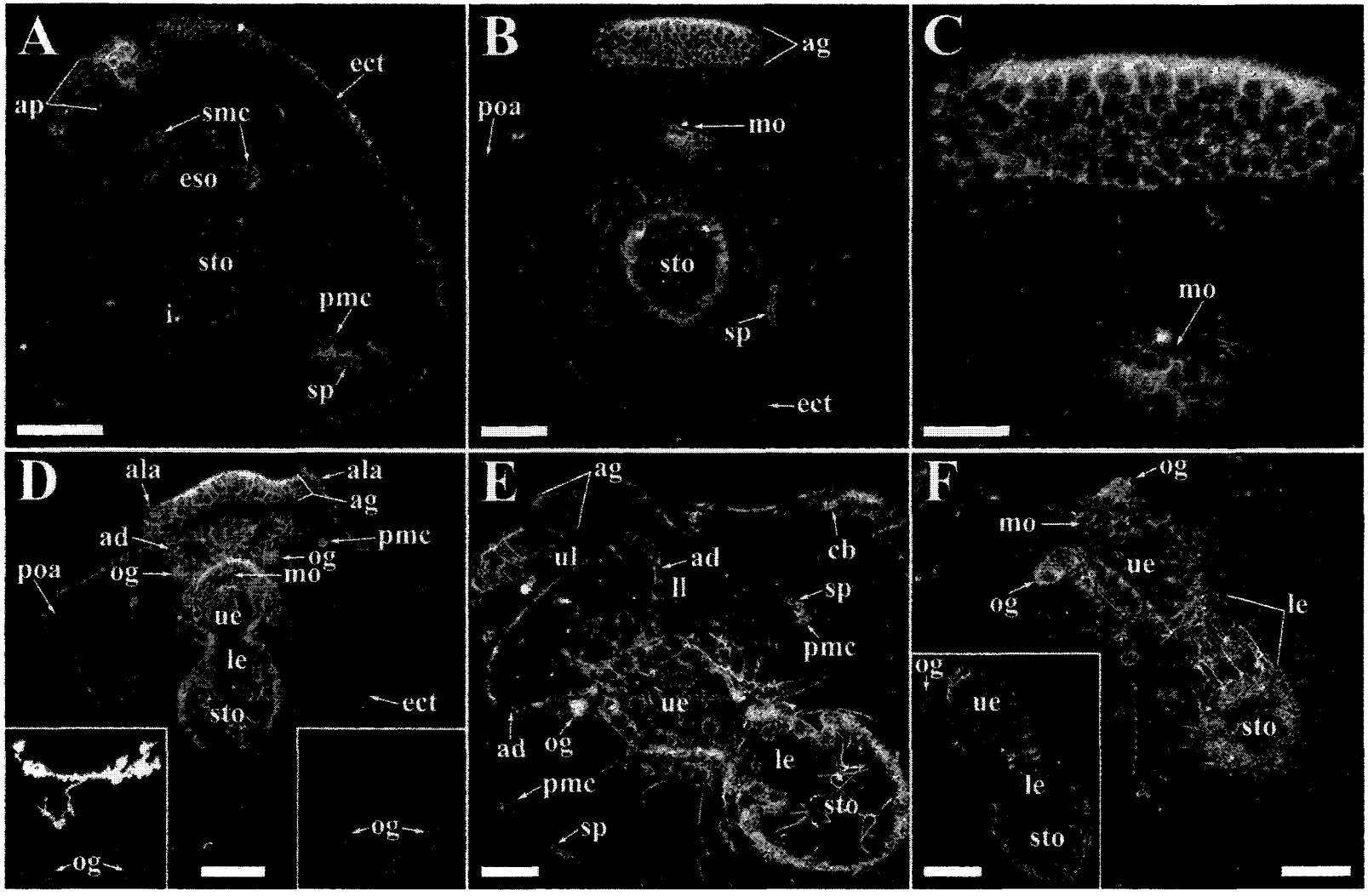
A
ect
ap
smc
eso
sto
pmc
sp
B
ag
poa
mo
sto
sp
ect
C
mo
D
ala
ala
ag
ad
pmc
poa
og
mo
ue
le
sto
ect
og
og
E
ag
ul
ad
cb
ll
sp
pmc
ue
ad
og
le
pmc
sto
sp
F
og
mo
ue
og
le
og
ue
le
sto
sto

3.9 SpADAM and Skeletogenesis

To identify potential functions for SpADAM, PMCs were cultured with anti-SpADAM antibodies throughout the development of spicules. 46 h PMC cultures with 1 μl anti-SpADAM serum/ml artificial seawater (ASW) had spicules (mean=43.63 μm, n=43) significantly longer ($p< 0.001$) than those without anti-SpADAM (mean=27.5 μm, n=43) (Figs. 18, 19). 68 h PMC cultures with 1 μl anti-SpADAM serum/ml ASW had spicules (mean=103.4 μm, n=109) significantly longer ($p< 0.0001$) than those without anti-SpADAM (mean=72.1 μm, n=112) or in 1 μl heat-inactivated anti-SpADAM serum/ml ASW (mean=75.2 μm, n=104) (Figs. 20, 21). Micromeres cultured in the presence of purified anti-SpADAM IgG (7 μg/ml) grew significantly longer spicules than micromeres cultured with an identical concentration of normal rabbit IgG ($p< 0.0001$) (Fig. 22). At 60 h post-isolation, mean spicule length of micromeres cultured with anti-SpADAM IgG was 75.4 ± 6.0 μm (SEM), compared with 40.2 ± 3.9 μm for micromeres cultured with normal rabbit IgG ($P<0.0001$) (Fig. 22). Similarly, micromeres cultured in the presence of 1.7 μg/ml anti-SpADAM Fab fragments grew significantly longer spicules (mean=73.3 ± 5.6 μm) than micromeres cultured with an identical concentration of heat-inactivated anti-SpADAM Fab fragments (51.4 ± 3.0 μm) ($P=0.001$) (Fig. 22). PMC morphology, the number of PMCs per spicule, spicule thickness, and degree of branching were not different in any of the treatments (data not shown).

Figure 18. Results of experiment in which micromeres were cultured in the presence of anti-SpADAM serum in ASW(1a-1c), or ASW alone (2a-2c). ASW, Artificial Sea Water. Spicules were analyzed 46 h after micromere isolation. Three representative adjacent fields are shown for each condition. The 6 anti-SpADAM frames contained 43 spicules ranging in length from 10.05-103.85 μm, and the 6 ASW frames contained 48 spicules ranging in length from 6.7-70.35 μm. Spicule lengths less than 10 μm were removed as these were considered spicule "nuclei", and this adjustment resulted in 43 spicules from each condition. Bar = 50 μm, and applies to all frames.

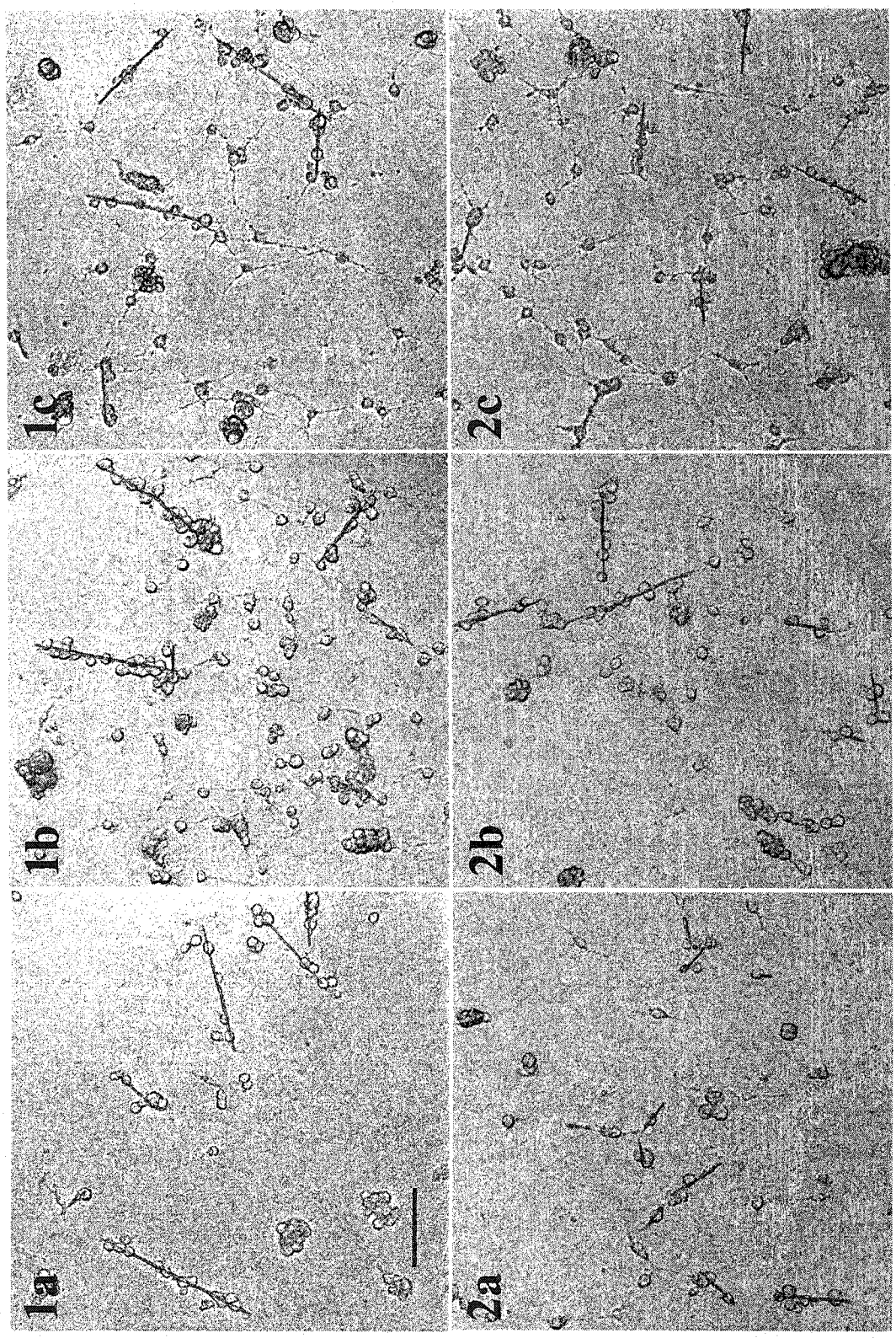
1c
2c
1b
2b
1a
2a

Figure 19. Frequency histograms of spicule length from micromeres cultured in the presence of anti-SpADAM serum in ASW, or ASW alone. ASW, Artificial Sea Water; SEM, standard error of the mean in μm. Spicules were analyzed 46 h after micromere isolation.

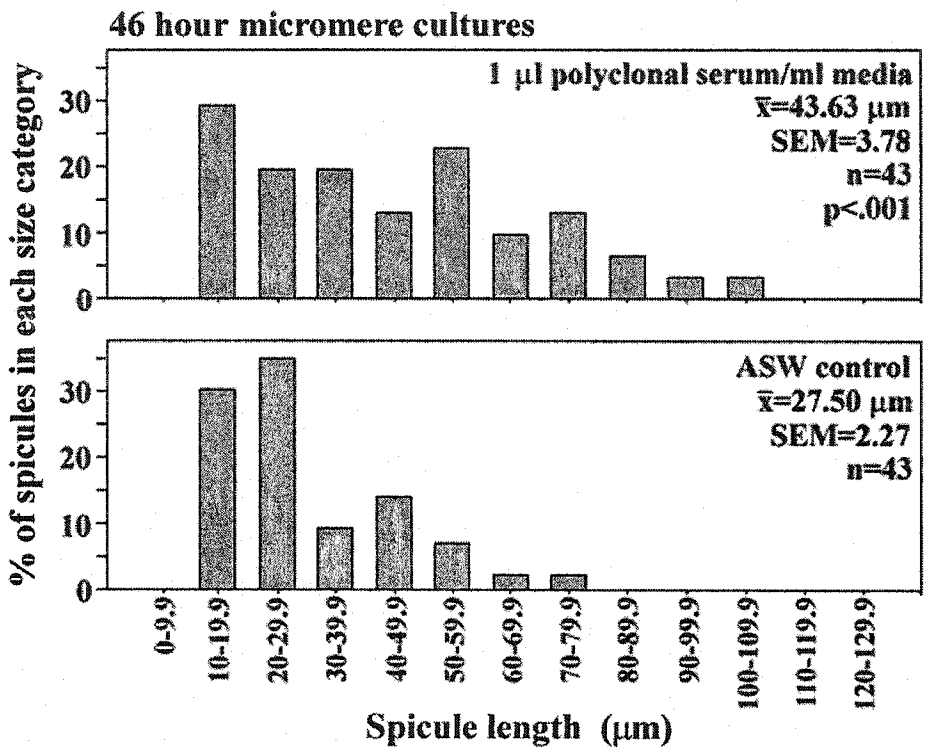
46 hour micromere cultures
1 µl polyclonal serum/ml media
x̄=43.63 µm
SEM=3.78
n=43
p<.001
ASW control
x̄=27.50 µm
SEM=2.27
n=43
% of spicules in each size category
0
10
20
30
0-9.9
10-19.9
20-29.9
30-39.9
40-49.9
50-59.9
60-69.9
70-79.9
80-89.9
90-99.9
100-109.9
110-119.9
120-129.9
Spicule length (µm)

Figure 20. Results of experiment in which micromeres were cultured in the presence of anti-SpADAM serum in ASW (1a-1c), heat-inactivated anti-SpADAM serum in ASW (2a-2c), or ASW alone (3a-3c). ASW, Artificial Sea Water. Spicules were analyzed 68 h after micromere isolation. 12 anti-SpADAM frames contained 109 spicules ranging in length from 16.8-227.8 μm. 7 heat-inactivated anti-SpADAM frames contained 104 spicules ranging in length from 13.4-160.8 μm. 13 ASW frames contained 112 spicules ranging in length from 10.1-187.6 μm. Bar = 25 μm, and applies to all frames.

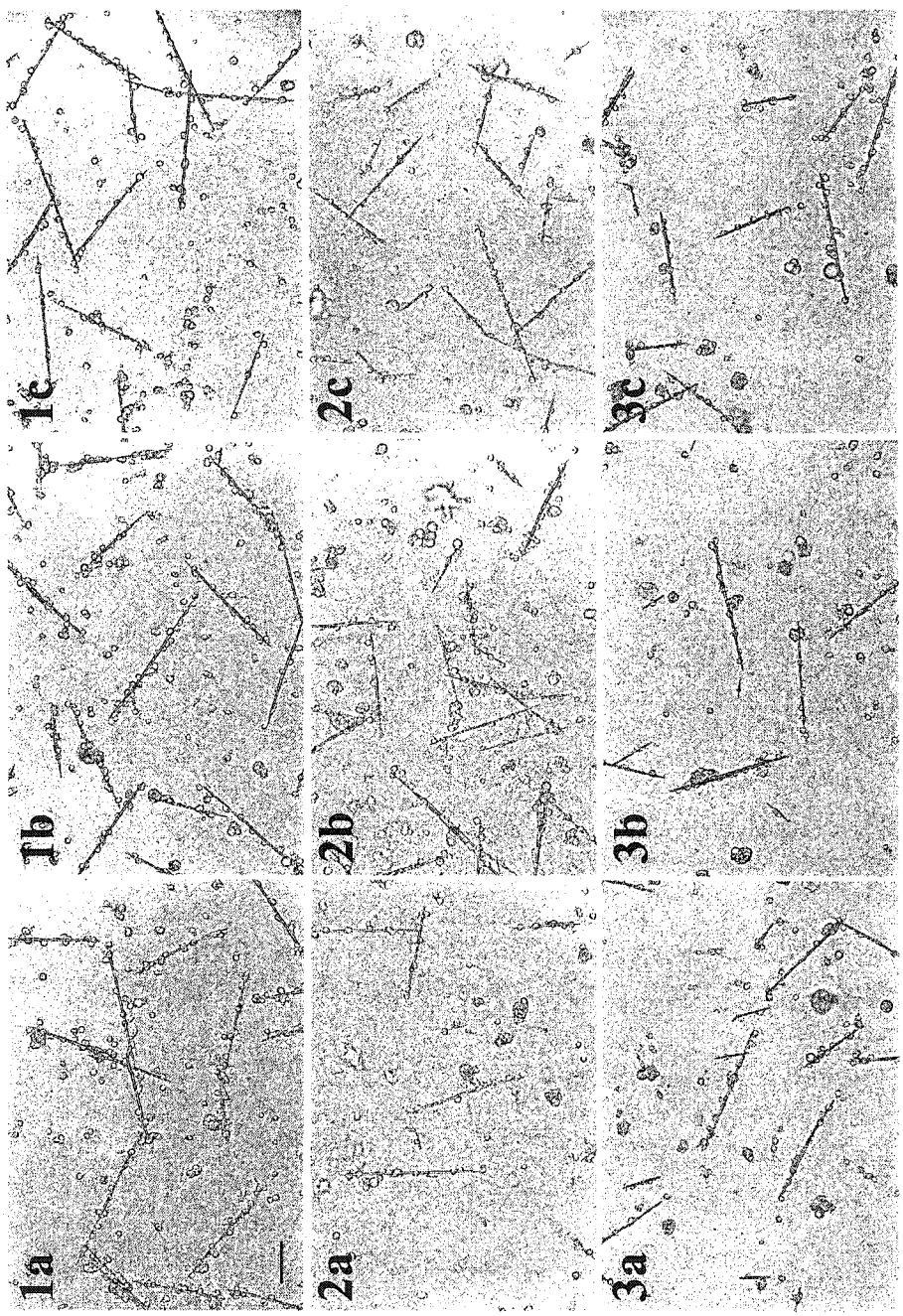
1c
2c
3c
1b
2b
3b
1a
2a
3a

Figure 21. Frequency histograms of spicule lengths from micromeres cultured in the presence of anti-SpADAM serum in ASW, heat-inactivated anti-SpADAM serum in ASW, or ASW alone. Spicules were analyzed 68 h after micromere isolation. ASW, Artificial Sea Water; SEM, standard error of the mean in μm.

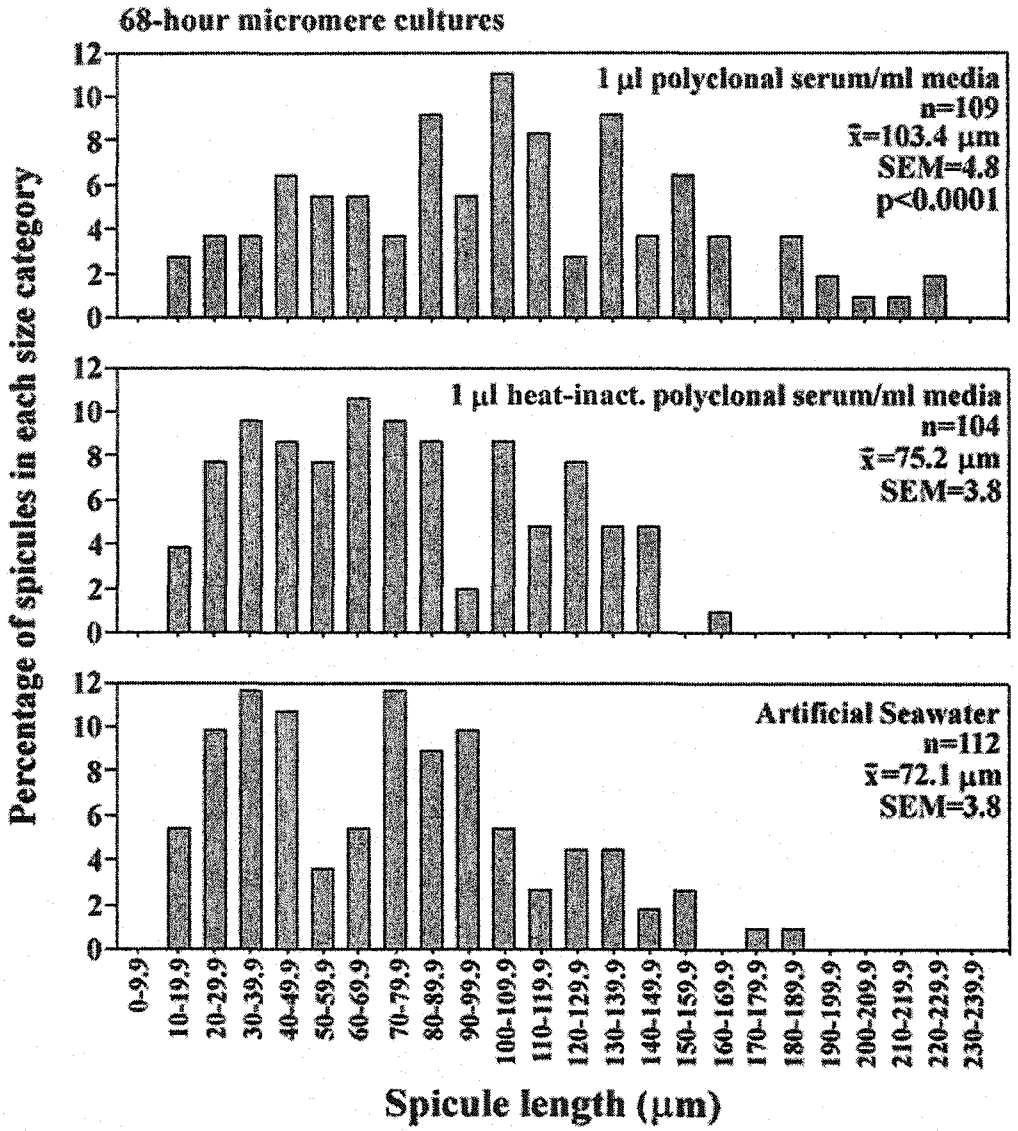
68-hour micromere cultures
1 µl polyclonal serum/ml media
n=109
x̄=103.4 µm
SEM=4.8
p<0.0001
1 µl heat-inact. polyclonal serum/ml media
n=104
x̄=75.2 µm
SEM=3.8
Artificial Seawater
n=112
x̄=72.1 µm
SEM=3.8
Percentage of spicules in each size category
0
2
4
6
8
10
12
0-9.9
10-19.9
20-29.9
30-39.9
40-49.9
50-59.9
60-69.9
70-79.9
80-89.9
90-99.9
100-109.9
110-119.9
120-129.9
130-139.9
140-149.9
150-159.9
160-169.9
170-179.9
180-189.9
190-199.9
200-209.9
210-219.9
220-229.9
230-239.9
Spicule length (µm)

Figure 22. Results of experiment in which micromeres were cultured in the presence of purified anti-SpADAM IgG in ASW, normal rabbit IgG in ASW, anti-SpADAM Fab fragments in ASW, or heat-inactivated anti-SpADAM Fab fragments in ASW. Spicules were analyzed 60 h after micromere isolation. One representative field is shown for each condition. Bar graphs show the length/frequency distribution of spicules within each culture.

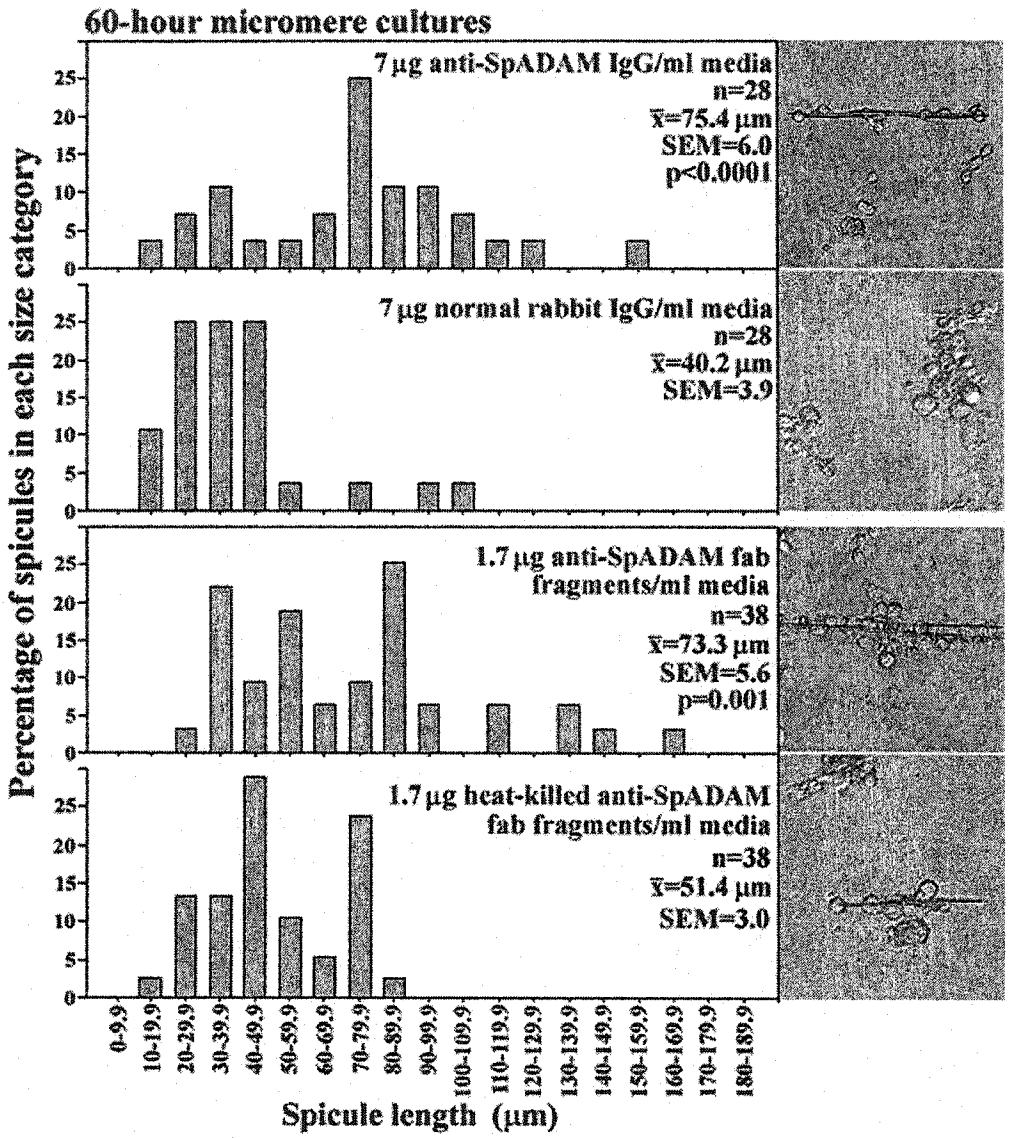
60-hour micromere cultures
7 µg anti-SpADAM IgG/ml media
n=28
x̄=75.4 µm
SEM=6.0
p<0.0001
7 µg normal rabbit IgG/ml media
n=28
x̄=40.2 µm
SEM=3.9
1.7 µg anti-SpADAM fab fragments/ml media
n=38
x̄=73.3 µm
SEM=5.6
p=0.001
1.7 µg heat-killed anti-SpADAM fab fragments/ml media
n=38
x̄=51.4 µm
SEM=3.0
Percentage of spicules in each size category
0
5
10
15
20
25
0-9.9
10-19.9
20-29.9
30-39.9
40-49.9
50-59.9
60-69.9
70-79.9
80-89.9
90-99.9
100-109.9
110-119.9
120-129.9
130-139.9
140-149.9
150-159.9
160-169.9
170-179.9
180-189.9
Spicule length (µm)

To confirm the antibodies were bound to cell surface SpADAM, cells cultured in anti-SpADAM were fixed and probed with an Alexa 488 conjugated Goat anti-rabbit antibody. PMC surfaces were immunoreactive throughout the cellular sheath surrounding spicules and there were large immunoreactive granules within the cells. In cultures not incubated with anti-SpADAM, there was no immunoreactivity (data not shown).

CHAPTER 4

DISCUSSION

4.1 SpADAM is Most Closely Related to ADAMs 12, 13, and 19.

The deduced primary structure of the SpADAM protein indicates it is an authentic member of the family of ADAM proteins. In addition to having the requisite domain organization, phylogenetic analyses suggest SpADAM is most closely related to ADAM 12 (meltrin α), ADAM 13, and ADAM 19 (meltrin β). Although the overall similarity of ADAM 12 with SpADAM is about 59%, notably greater similarity occurs in some domains. The similarities within the metalloproteinase and the disintegrin domains exceed 70%, suggesting these regions of the proteins are strongly conserved. Potential SpADAM activities may be hypothesized given the functions of closely related ADAMs. For example, ADAM 12 and ADAM 19 are active metalloproteinases (Loechel et al., 1998; Wei et al., 2001). ADAM 19 proteolytically processes membrane-bound Neuregulin-1, a member of the epidermal growth factor family that plays important roles in the development of neural crest and glial cells (Garratt et al., 2000; Shirakabe et al., 2001). SpADAM, like ADAMs 12, 13, and 19, contains the zinc binding consensus sequence HEXXH characteristic of a subset of ADAMs with metalloproteinase activity.

In addition to having similar primary structures, SpADAM and vertebrate ADAMs 12, 13, and 19 are also expressed in similar tissues during embryogenesis. Mouse ADAMs 12 and 19 are highly expressed in neonatal

muscle, where they play roles in myogenesis (Yagami-Hiromasa et al., 1995; Inoue et al., 1998). *Xenopus* ADAM 13 is expressed in somitic mesoderm and cranial neural crest cells, where it is thought to function in myoblast differentiation and neural crest cell adhesion and migration (Alfandari et al., 1997). SpADAM is strongly expressed in cells of the larval muscular and nervous systems, supporting the hypothesis that this ADAM plays conserved roles in potentially homologous processes used by deuterostomes to form these cell types. Several events in sea urchin embryogenesis could involve the proteolytic, adhesive, and putative fusogenic, activities of this group of ADAMs. These events include mesenchyme ingression, PMC syncytia formation, spiculogenesis, SMC-SMC adhesion and fusion, and neurogenesis.

4.2 SpADAM Protein Occurs in Various Forms.

Data from RT-PCR, immunoblots, and immunoprecipitations indicate that SpADAM protein is expressed and, like other ADAMs, the protein occurs in various forms and is developmentally regulated. Two SpADAM clones with 69 bp inserts in their EGF-like domains were isolated. However, as SpADAM appears to be a single copy gene, these are most likely alternative splice variants. SpADAM is a modular protein that potentially can be cleaved proteolytically to expose different functional domains. Immunoblots and immunoprecipitates identified major bands at 131, 95, and 72 kDa. The 131 kDa band presumably represents the SpADAM precursor. The deduced full-length

(pre-processed) SpADAM protein is 1023 amino acids in length, with a predicted molecular weight of approximately 111 kDa. This polypeptide contains five potential N-linked glycosylation sites, which likely explain the discrepancy between predicted and apparent molecular weights. The deduced amino acid sequence of the *C. elegans* ADAM MIG-17, with nine potential N-linked glycosylation sites, has a predicted MW of 58 kDa and an apparent MW of 105 kDa (Nishiwaki et al., 2000). The 95 kDa form probably represents the mature SpADAM protein lacking the pro-domain. The 72 kDa SpADAM protein, which was the predominant band in prisms, may be a form that has been further processed proteolytically. Cleavage of SpADAM on the carboxyl end of its metalloproteinase domain, exposing the potentially adhesive disintegrin domain, would yield a 606 amino acid polypeptide with two predicted N-linked glycosylation sites and a predicted MW of 64 kDa. In *Xenopus*, there have been three forms of ADAM 13 protein identified on immunoblots: a fully glycosylated form at 120 kDa, a form thought to lack the pro-domain at 97 kDa, and a 50 kDa form (Alfandari et al. 1997). In mammals, three forms of ADAM 12 protein have been identified with immunoblots. There is a 115 kDa form, a form lacking the pro-domain (86 kDa), and a form lacking the metalloproteinase domain (67 kDa) (Yagami-Hiromasa et al., 1995). Having multiple forms of the SpADAM protein is consistent with the proteolytic processing found in other ADAMs.

4.3 SpADAM Functions in Skeleton Formation.

PMCs express SpADAM after ingression, but both *in situ* RNA hybridization and immunolocalization suggest it is at low levels. Peak levels of immunoreactivity in PMCs are not reached until late in gastrulation after PMC syncytium formation, and expression persists throughout larval development. This suggests that SpADAM may function in the formation of spicules, rather than during PMC migration and fusion. This hypothesis was tested by culturing micromeres in anti-SpADAM antibodies and Fab fragments throughout their differentiation into skeletogenic syncytia. As SpADAM is predicted to be a cell surface molecule, antibody interference is a reasonable approach to assessing function. Controls indicated that anti-SpADAM in the culture medium bound to PMCs, confirming SpADAM is a membrane protein. The number of nuclei per syncytium and number of syncytia formed were not different in treated and control preparations. Thus, the antibody did not appear to have an effect on the early phases of skeletogenesis. However, there was a marked difference in the length of spicules in cultures treated with anti-SpADAM. Treatment with anti-SpADAM serum, purified anti-SpADAM IgG, or anti-SpADAM Fab fragments all resulted in significantly longer spicules than control treatments. There were no differences in the number of branch points or overall form of the spicules between treated and control cultures. These experiments suggest that SpADAM functions in skeletal morphogenesis, specifically in regulation of the growth of the spicule.

Control experiments, in which PMCs cultured with anti-SpADAM antibodies contained immunoreactive granules, suggest antibodies are capped and removed from the cell surface. Thus, it appears most likely that the antibodies are blocking function by causing removal of SpADAM from the surface of the PMCs. As longer spicules result from blocking, it seems possible that SpADAM functions in degradation of spicules. Growth of spicules into 3-dimensionally complex structures must involve regulation of the rate and location of matrix deposition and removal. As spicules form only simple or branched rods in culture, it is thought that regulation of skeletogenic mesenchyme *in vivo* is responsible for this aspect of skeleton morphogenesis (Harkey and Whiteley, 1980; Ettensohn et al., 1997). There are several lines of evidence that indicate the ectoderm provides positional information and the context for the proper development of the 3-dimensional form of the skeleton (Armstrong et al., 1993; Armstrong and McClay, 1994). Guss and Ettensohn (1997) have shown that the rates of skeletal rod growth are not uniform *in vivo*. They also present a model in which ectoderm regulates the expression of skeleton specific genes to enhance regional growth. Although they have emphasized growth resulting from matrix deposition, the model can accommodate regulated matrix removal equally well. Localization indicates that skeletogenic cells do not express SpADAM uniformly, which suggests cells may be responding to localized cues. Thus, SpADAM appears to have some properties of the types of molecules that Guss and Ettensohn (1997) speculate

may mediate skeletal morphogenesis. As antibody treatments indicate that SpADAM may mediate matrix removal, localized activation may function in slowing growth. SpADAM appears to be a good candidate for a molecule that is part of the process by which ectoderm regulates spicule growth.

Metalloproteinases have been identified in sea urchin embryos and inhibitors of matrix metalloproteinases (MMP) have been shown to block spicule elongation (Roe et al. 1989; Quigley et al., 1993; Mayne and Robinson, 1996; Ingersoll and Wilt, 1998). Ingersoll and Wilt (1998) identified a 51 kDa protease that they believed to be the target of metalloproteinase inhibitors. Although they were unable to identify the precise role of metalloproteinases, they have proposed that inhibitors interfere with the delivery of calcium carbonate and matrix to the spicule. Treatment of skeletogenic mesenchyme with anti-SpADAM antibodies appears to have the opposite effect on spicule growth, suggesting that the MMP inhibitors used by Ingersoll and Wilt (1998) are not acting on SpADAM. Clearly, metalloproteinases appear to be important components in the process of biomineralization in sea urchins.

4.4 Hypothetial Role for SpADAM in SMC Ingression and Migration

During gastrulation, SMCs such as presumptive pigment cells and blastocoelar cells undergo epithelial-mesenchymal transformations, and migrate through fenestrations in the basal lamina into the blastocoel (Gibson and Burke, 1987; Tamboline and Burke, 1992). Embryonic sea urchin pigment cells

apparently migrate using ECM substrates distinct from those used by migratory PMCs (Gibson and Burke, 1987). SMCs extend long, slender filopodia as they migrate (Tamboline and Burke, 1992). The mechanisms by which SMCs breach basal lamina and migrate through blastocoelar ECM are not known. Whole mount *in situ* hybridizations and immunolocalizations show high levels of SpADAM expression in blastocoelar cells and pigment cells when they are invasive. Hypothetically, SpADAM could be involved in the proteolytic ECM remodeling that allows SMCs to penetrate basal lamina. The metalloproteinase activity of MIG-17, an ADAM involved in *C. elegans* gonad formation, is thought to be involved in ECM remodeling, allowing distal tip cells to adhere to basement membrane and respond appropriately to directional cues such as UNC-6 (Nishiwaki et al., 2000).

SMCs express the βC integrin subunit while ingressing and migrating (Marsden and Burke, 1997). Integrins are transmembrane heterodimeric proteins that serve as the primary links between ECM components (i.e. laminin, fibronectin) and the actin cytoskeletons of migrating embryonic cells (Alberts et al., 1994; Holly et al., 2000). For a cell to detach from neighbouring cells and migrate individually through the embryo, dynamic cell-ECM interactions involving regulated integrin adhesion must occur (Alberts et al., 1994; Holly et al., 2000). It is speculated that the disintegrin domains of some ADAMs may mediate cellular interactions with ECM components and/or other cells (Black and White, 1998; Primakoff and Myles, 2000). Hypothetically, the regulated

expression of adhesion molecules (i.e. βC integrin), and their antagonists (i.e. SpADAM with exposed disintegrin domain), on SMC surfaces might allow these cells to attach to and detach from ECM molecules during their migratory phases.

Function-blocking experiments could be used to test the hypothesis that SpADAM metalloproteinase activity is involved in SMC ingression. All presumptive pigment cells migrate into the blastocoel during early gastrulation, after the vegetal plate has buckled and before the archenteron has reached one-third of the way across the blastocoel (Gibson and Burke, 1985). Hatched blastulae (26 h) could be microinjected with mouse monoclonal antibodies (mAbs) raised against bacterially expressed SpADAM metalloproteinase domain, or control mAbs directed to irrelevant antigens. 8 h after injection, when uninjected and control injected siblings are late gastrulae with fully ingressed SMCs, control and experimental embryos would be fixed, and SMC numbers and locations determined using the pigment cell specific SP1/20.3.1 antibody (Gibson and Burke, 1985). If SpADAM is involved in SMC ingression, the anti-SpADAM mAb might be expected to block ingression in a dose-dependent fashion. Identification of SP1-positive cells in vegetal ectoderm, and absence of SP1-positive cells in the blastocoel, would indicate SMC ingression had been blocked.

To test the hypothesis that the SpADAM disintegrin domain might be involved in SMC migration, blastocoelic injections of mouse mAb directed to

bacterially expressed SpADAM disintegrin domain, or control mAb, could be performed after SMC ingression had begun (34 h). Similarly, a synthetic peptide corresponding to the integrin recognition sequence (SNM) of SpADAM's disintegrin loop, and a control nonspecific peptide, would be microinjected into the blastocoels of 34 h embryos. Embryos would be fixed 12 h after injection, when the pigment cells of control embryos are dispersed in the ectoderm, and SP1 antibody would be used to identify SMCs. The ratios of SP1-positive cells in the ectoderm to SP1-positive cells adhering to archenteron tips would be compared between control and experimental preparations. If SpADAM is involved in SMC migration, then anti-SpADAM mAb or experimental peptide might prevent SMCs from moving away from the archenteron tip after ingression.

4.5 Hypothetical Role for SpADAM in SMC-SMC Adhesion and/or Fusion

Following ingression and migration, blastocoelar cells fuse with one another by a molecular pathway believed to be distinct from that used by PMCs (Hodor and Ettensohn, 1998). Heterotypic (PMC-SMC) fusion does not occur even though these cell types are occasionally in direct contact with one another (Hodor and Ettensohn, 1998). As well, PMC fusion occurs only at the tips of filopodial extensions, whereas SMC fusion sometimes occurs between adjacent cell bodies (Hodor and Ettensohn, 1998). Hodor and Ettensohn (1998) predict that a fusion protein mediating SMC-SMC fusion should be present on the

entire cell surface during gastrulation. Because SpADAM is highly expressed on SMC bodies and filopodia during their fusogenic period, SpADAM is a candidate for mediating SMC-SMC adhesion and/or fusion.

Fertilization, myotube formation, and the pathogenesis of enveloped viruses, also involve the adhesion and fusion of adjacent phospholipid bilayers. Intercellular fusion is a poorly understood phenomenon. Viral fusion, especially that of influenza virus and human immunodeficiency virus, is better understood. Viral adhesion and fusion are usually mediated by the same protein, and viral fusion proteins share characteristics with adhesive and potentially fusogenic molecules on the surfaces of animal cells that fuse (White, 1992). Therefore, viral fusion is used to model intercellular fusion. Both of these types of fusion events begin with the contact of membrane outer leaflets (White, 1992). Virus and host cell membranes adhere via ligand-receptor binding, resulting in protein conformational changes that bring adjacent outer leaflets in close proximity (White, 1992; Vignery, 2000). Entry of enveloped viruses into host cells involves integral membrane proteins often synthesized as precursors that must be proteolytically cleaved to have optimal fusogenic activity. Viral fusion proteins are capable of conferring fusogenicity when expressed in tissue culture cells, and contain short (16 to 24 residue) relatively hydrophobic fusion peptides that are conserved within, but not between, virus families (White, 1992). Some viral fusion peptides contain central prolines that may cause the amphipathic alpha helical peptide to kink (Terwilliger and Eisenberg, 1982;

White, 1992). The viral fusogenic peptide is thought to be buried until a conformational change in the fusion protein exposes it, allowing the hydrophobic peptide to interact with the target phospholipid bilayer (White, 1992; Alberts et al., 1994). The hydrophobic viral fusion peptide overcomes energetic barriers to membrane fusion by dehydrating the space between outer leaflets and destabilizing the host cell bilayer (Vignery, 2000).

SpADAM, ADAM 1, and ADAM 12 contain both adhesive and putative fusogenic motifs, making them candidates for participation in intercellular fusion processes. SpADAM is the first identified sea urchin protein with potential fusogenic activity. Like viral fusion proteins, SpADAM, ADAM 1, and ADAM 12, are all integral membrane proteins synthesized as precursors that could be cleaved to expose N-terminal putative fusogenic peptides (Huovila et al., 1996). The cysteine-rich domains of all three ADAMs have putative fusogenic motifs that, like viral fusion peptides, are hydrophobic and contain central prolines (Blobel et al., 1992; Yagami-Hiromasa et al., 1995) (Fig. 23). ADAM 1 may play a role in sperm-egg plasma membrane fusion (White, 1992; Huovila et al., 1996), while ADAM 12 is involved in the fusion of myoblasts into multinucleate myotubes during the normal development of mammalian skeletal muscle (Yagami-Hiromasa et al., 1995; Gilpin et al., 1998).

Figure 23. Aligned Kyte-Doolittle hydrophilicity profiles of 3 ADAMs with potential fusion peptides.

Hydrophilicity profiles are aligned at their amino (N) terminals with a schematic showing ADAM domain organization. SP: signal peptide, EGF: epidermal growth factor, TM: transmembrane, C: carboxyl terminus, aa: amino acid. On the hydrophilicity plots, putative fusogenic peptide sequences and locations are shown. Within putative fusion peptide sequences, bold residues are hydrophobic (≥ -0.4 on Kyte-Doolittle hydropathy scale; Kyte and Doolittle, 1982).

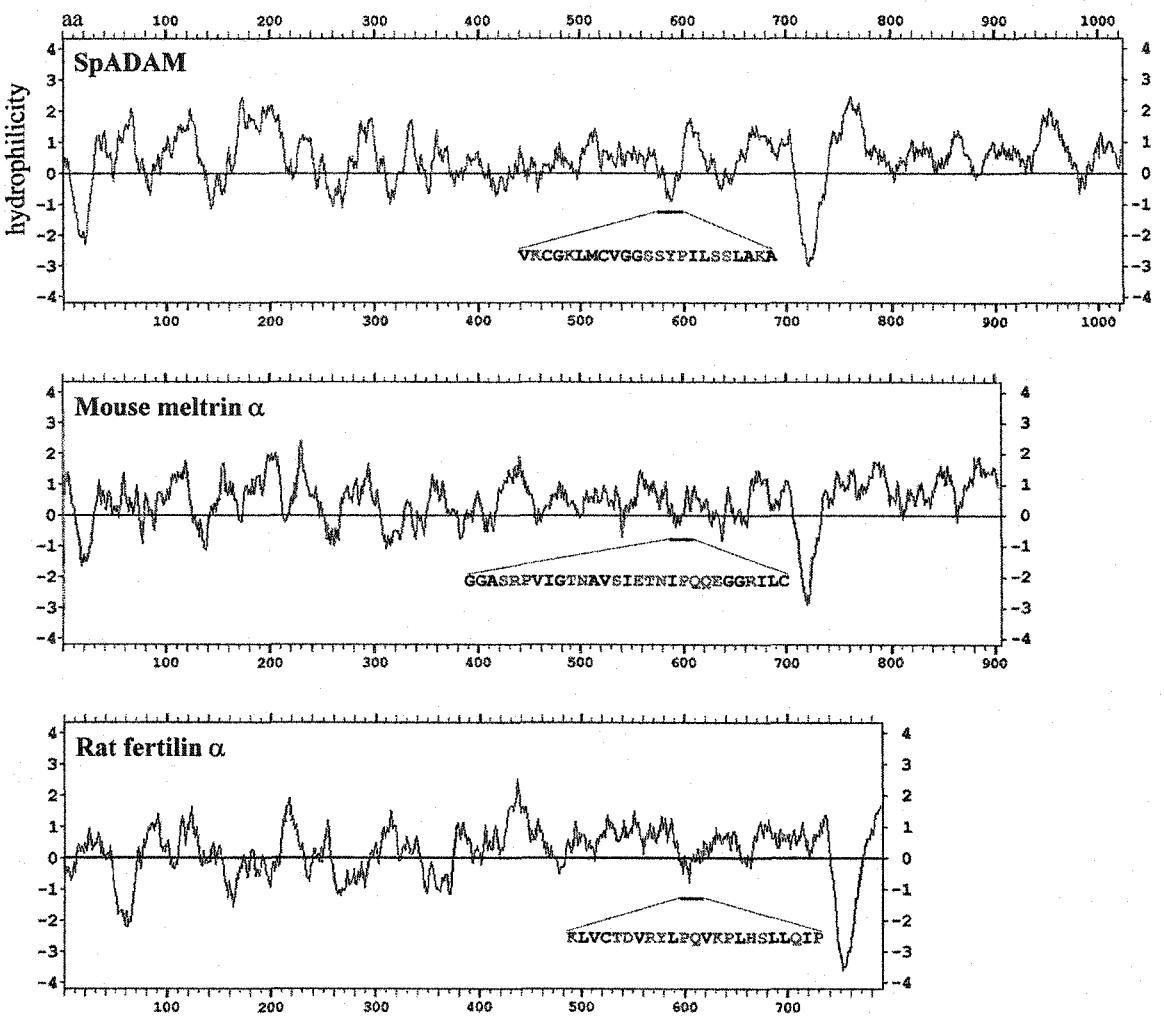
aa
hydrophilicity
SpADAM
VRCGKLMCVGGSSYPILSSLAKA
Mouse meltrin α
GGASRPVIGTNAVSIETNIPQQEGGRILC
Rat fertilin α
RLVCTDVRYLPQVKPLHSLLQIP

Muga et al. (1994) found that a synthetic peptide mimicking the potentially fusogenic region of ADAM 1 bound phospholipid bilayers and induced them to fuse, supporting the notion that this ADAM plays a role in fertilization. Recent evidence, however, indicates that murine sperm-egg fusion is not dependent upon ADAM 1. The mature sperm of ADAM 2 knockout mice also lack ADAM 1 (Cho et al., 2000). While the adhesion of fertilin-minus ($\beta^{-/-}$) sperm to eggs is dramatically reduced (to ~10% wild type levels), the fusion of $\beta^{-/-}$ sperm to eggs is only moderately reduced (to ~50% wild type rate) (Cho et al., 1998, 2000). These findings support the hypothesis that ADAM 2 is required for sperm-egg adhesion, but indicate that ADAM 1 is not essential for sperm-egg fusion. Furthermore, human ADAM 1 is a single-copy expressed, but nonfunctional, pseudogene (Jury et al., 1997). Recent evidence indicates Cd9, a tetraspanin expressed on mouse egg plasma membranes and known to interact with integrins, is required for sperm-egg fusion (Kaji et al, 2000; Miller et al., 2000; Le Naour et al., 2000; Miyado et al, 2000). The mechanism by which Cd9 acts in mammalian gamete fusion is not yet known.

The following is a hypothetical model of SMC-SMC adhesion and fusion that is consistent with expression data (Fig. 24). SpADAM and the βG integrin subunit (Marsden and Burke, 1997) are strongly expressed on all surfaces of all SMCs during their fusogenic period. This may be the ligand-receptor pair mediating SMC-SMC adhesion. Binding of the integrin with its recognition sequence in SpADAM's disintegrin loop could induce clustering of these

Figure 24. Model of hypothetical SpADAM-integrin involvement in SMC-SMC adhesion and fusion.

Both SpADAM (S) and its integrin receptor (i) are expressed on the surfaces of all SMCs. A. Prior to disintegrin-integrin interaction, SpADAM's hydrophobic fusion peptide (black) is buried. The disintegrin loop of SpADAM binds to its integrin receptor, inducing conformational changes in both proteins.

B. Conformational changes in interacting proteins draw adjacent plasma membranes closer together, and expose SpADAM's fusogenic peptide. In this orientation, the hydrophobic peptide makes contact with and destabilizes the target bilayer, and dehydrates the space between membrane outer leaflets.

C. Outer leaflets (ol) fuse first. D. Subsequently, inner leaflets (il) fuse.

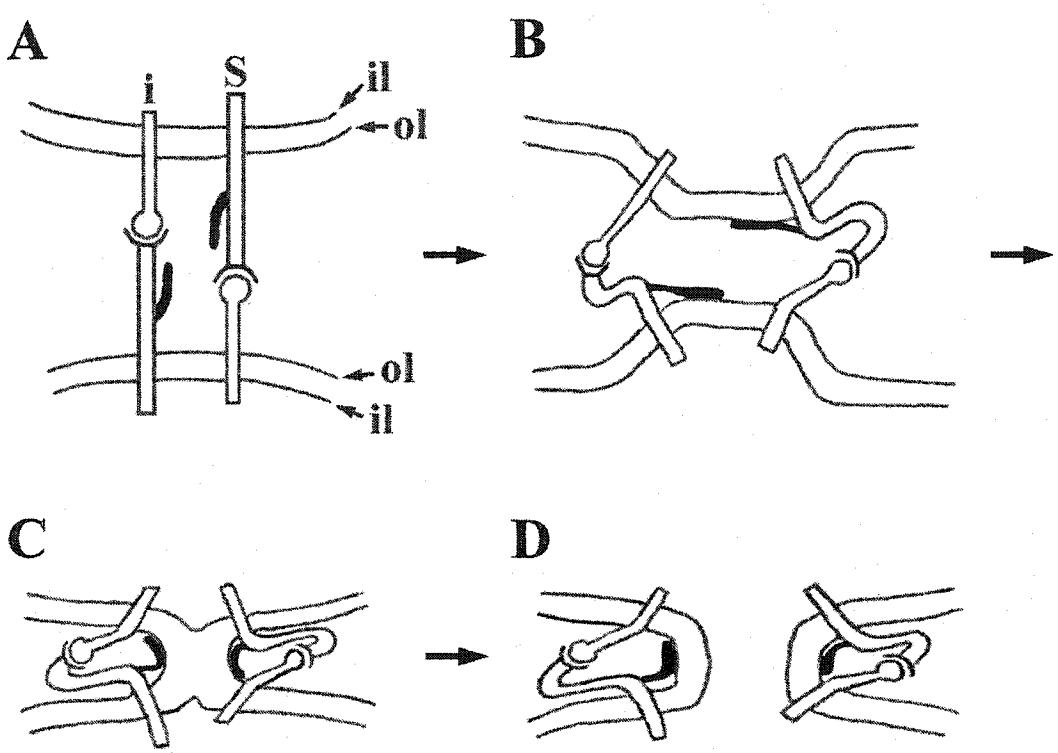
A
i
S
il
ol
ol
il
B
C
D

adhesion molecules to the site of contact and conformational changes in the interacting proteins. These conformational changes might draw the adjacent plasma membranes closer together and expose the hydrophobic fusogenic peptides of clustered SpADAM molecules. In their new orientations, fusion peptides could penetrate the apposed bilayers and dehydrate the space between them, facilitating fusion.

To test this hypothesis, a synthetic peptide corresponding to SpADAM's disintegrin loop sequence and containing the integrin recognition sequence (SNM) would be analyzed for its ability to block SMC-SMC adhesion and/or fusion relative to controls (nonspecific tripeptide). Cultures of fluorescently-labeled SMCs could be prepared by injecting eggs with a fluorescent-labeled dextran, fertilizing them, and culturing in the presence of lithium chloride to generate exogastrulae (Hardin, 1988). Labeled exogastrulae (36 h) would be transferred to calcium-free seawater, agitated to release SMCs from archenteron tips, and passed through 20 μm Nitex to remove embryos. Unlabeled SMCs would be prepared in a similar fashion. After adding $CaCl_2$ to a final concentration of 10 mM, equal numbers of labeled and unlabeled SMCs would be placed in tissue culture dishes with various concentrations of experimental or control peptide. SMC-SMC adhesion would be assessed by determining the ratios of lone cells to attached cells. Fusion would be assessed by acquiring bright field and fluorescence stereo images of cultured cells after various incubation times, and determining the percentage of labeled cells. If SpADAM

mediates SMC-SMC adhesion, or both adhesion and fusion, then the experimental peptide would be expected to block SMC fusion in a dose-dependent manner.

4.6 SpADAM Localization in Cleavage Stage Embryos

The fourth cleavage mesomeres and macromeres appear to express SpADAM uniformly on all surfaces. However, anti-SpADAM immunoreactivity in micromeres is diffuse and less clearly surface-associated. By the 60-cell stage, SpADAM protein has disappeared from micromere surfaces. This progression of surface staining, from diffuse to absent on cells of a specific territory, is intriguing, and warrants further investigation. The movement of Notch receptor from cell surfaces into intracellular vesicles is thought to be involved in activation or inactivation of the Notch signaling pathway (Klueg et al., 1998; Sherwood and McClay, 1997, 1999). The cytoplasmic domain of SpADAM contains proline-rich sequences similar to those found in the cytoplasmic domains of proteins involved in eukaryotic signal transduction (Kay et al., 2000). Since signaling events are critical in cell fate specification, it is possible that SpADAM could play a role in the specification of micromeres to skeletogenic fate, or the specification of remaining blastomeres to non-skeletogenic fate.

4.7 SpADAM and Muscle Cells

In early (50-72 h) larvae, SpADAM expression is seen almost exclusively in mesenchyme derivatives. The larval mesodermal tissues include PMCs, SMCs, and the coeloms. The prevalence of SpADAM mRNA and protein in various types of differentiated mesenchyme cells suggests histospecific roles for SpADAM.

Anti-SpADAM antibodies identify a single cell in each coelomic pouch, as well as the circumesophageal muscle fibres of 72 h larvae, and the basket-like longitudinal lower esophageal musculature of 7 day larvae. Although anti-actin antibodies reveal about 12 muscle cells in the early pluteus (60 h) coelomic sacs (Burke and Alvarez, 1988), anti-SpADAM antibodies recognize only 2. Also, SpADAM is expressed by the circular upper esophageal muscle cells of early (72 h) plutei, whereas in 7 day larvae, SpADAM expression is predominantly in the longitudinal lower esophageal musculature. Therefore, SpADAM protein appears to be present in only a subset of muscle cells at a given time.

Scanning electron micrographs of the surface of the larval esophagus reveal that the processes of muscle cells attach to one another, and appear to fuse at points of contact (Burke and Alvarez, 1988). The disintegrin and cysteine-rich domains of mammalian ADAM 12 mediate cell-cell adhesion (Yagami-Hiromasa et al., 1995; Iba et al., 2000). The disintegrin domains of SpADAM and human ADAM 12 are 60.4% identical/74.0% similar, and the disintegrin loops of these polypeptides are 78.6% identical/85.7% similar. The

cysteine-rich domains of these proteins are 40.0% identical/69.7% similar. High degrees of conservation in these domains likely reflect their functional importance, and suggest that SpADAM may also function as a cell adhesion molecule. Since SpADAM and ADAM 12 both contain hydrophobic, putative fusogenic peptides in their cysteine-rich domains (Fig. 23), and ADAM 12 has been shown to be involved in myoblast fusion (Yagami-Hiromasa et al., 1995; Gilpin et al., 1998), SpADAM is a candidate member of the sea urchin myoblast fusion machinery.

4.8 SpADAM and the Larval Nervous System

Anti-serotonin antibodies recognize from 1 to 4 cells in the apical plates of prism stage (50-60 h) sea urchin embryos (Bisgrove and Burke, 1986, 1987). SpADAM is expressed by select cells in prism apical plates. In 7 day larvae, the apical ganglion of serotonergic neurons is arranged within a thickened pad of ectoderm. At this stage, SpADAM is expressed by most cells in this region having epithelial morphology. The deduced amino acid sequence of SpADAM is strikingly similar to that of ADAM 19. The metalloproteinase domains of SpADAM and mouse ADAM 19 are 43.5% identical/70.3% similar, and their metalloproteinase active sites are 66.7% identical/91.7% similar (Table 1). Both ADAMs have the conserved HEXXH motif characteristic of active metalloproteinases. ADAM 19 proteolytically processes Neuregulin (Shirakabe et al., 2001), a member of the epidermal growth factor family involved in the

differentiation of neural crest-derived neurons and glial cells (Meyer, 1995; Meyer et al., 1997; Cameron et al., 2001; Meintanis et al., 2001). Hypothetically, SpADAM's metalloproteinase domain could process a growth factor involved in the differentiation of neurons or glial cells in the region of the apical ganglion.

CONCLUSIONS

ADAMs are a family of multidomain cell surface proteins thought to have several important functions in early development. Events in sea urchin embryogenesis that could potentially involve the proteolytic, adhesive, or fusogenic activities of ADAMs include primary mesenchyme cell (PMC) ingression, migration, and syncytia formation, spiculogenesis, and secondary mesenchyme cell (SMC) fusion. SpADAM, a sea urchin ADAM, is expressed during embryonic and larval development. Phylogenetic analyses using aligned deduced amino acid sequences reveal that SpADAM is most similar to mammalian ADAM 12 (meltrin α) and ADAM 19 (meltrin β), and *Xenopus* ADAM 13. SpADAM shares many features with these vertebrate ADAMs. For example, all four members of this group of ADAMs are expressed in multiple forms, possibly indicating multiple activities and functions. All of these ADAMs are expressed early in development, initially by mesenchyme. SpADAM, ADAM 12, and ADAM 13 are all expressed in myogenic mesenchyme, and ADAM 12 is involved in the fusion of myoblasts during the development of skeletal muscle (Yagami-Hiromasa et al., 1995; Gilpin et al., 1998; Alfandari et al., 1997). Mouse ADAM 12 and ADAM 19 function in the formation of bone (Harris et al., 1997; Inoue et al., 1998; Abe et al., 1999), and SpADAM likewise is expressed by skeletogenic cells. ADAM 13 is not expressed solely in mesoderm, but also in the neural plate and cranial neural crest cells (Alfandari et al., 1997). In addition to its expression in bone, mouse

ADAM 19 is also expressed in neural crest-derived ganglia and ventral horns of the spinal cord during neurogenesis (Inoue et al., 1998; Kurisaki et al., 1998). The expression of SpADAM in the preoral ectoderm associated with the sea urchin larval apical ganglion may correspond to the expression of ADAM 13 and ADAM 19 in vertebrate neural plate derived tissues.

Analysis of the primary structure of SpADAM indicates it is closely related to vertebrate ADAMs 12, 13, and 19. Expression patterns of SpADAM and these vertebrate ADAMs are also very similar. It appears that not only has molecular structure been preserved, but remarkably, expression in certain types of cells is also shared. It appears possible that within the deuterostomes, structure and function of this group of ADAMs have been strongly conserved.

REFERENCES

Abe, E., Mocharla, H., Yamate, T., Taguchi, Y., and Manolagas, S.C. (1999). Meltrin-alpha, a fusion protein involved in multinucleated giant cell and osteoclast formation. *Calcified Tissue International* 64(6), 508-515.

Alfandari, D., Wolfsberg, T.G., White, J.M., and DeSimone, D.W. (1997). ADAM 13: a novel ADAM expressed in somitic mesoderm and neural crest cells during *Xenopus laevis* development. *Developmental Biology* 182, 314-330.

Alliegro, M.C., Ettensohn, C.A., Burdsal, C.A., Erickson, H.P., and McClay, D.R. (1988). Echinonectin: a new embryonic substrate adhesion protein. *The Journal of Cell Biology* 107, 2319-2327.

Altschul, S.F., Gish, W., Miller, W., Myers, E.W., and Lipman, D.J. (1990). Basic local alignment search tool. *Journal of Molecular Biology* 215: 403-410.

Angerer, L.M. and Angerer, R.C. (2000). Animal-vegetal axis patterning mechanisms in the early sea urchin embryo. *Developmental Biology* 218, 1-12.

Armstrong, N., Hardin, J., and McClay, D.R. (1993). Cell-cell interactions regulate skeleton formation in the sea urchin embryo. *Development* 119, 833-840.

Armstrong, N. and McClay, D.R. (1994). Skeletal pattern is specified autonomously by the primary mesenchyme cells in sea urchin embryos. *Developmental Biology* 162, 329-338.

Artavanis-Tsakonas, S., Matsuno, K., and Fortini, M.E. (1995). Notch signaling. *Science* 268, 225-232.

Artavanis-Tsakonas, S., Rand, M.D., and Lake, R.J. (1999). Notch signaling: cell fate control and signal integration in development. *Science* 284, 770-776.

Benson, S., Jones, E.M.E, Crise-Benson, N., and Wilt, F. (1983). Morphology of the organic matrix of the spicule of sea urchin larvae. *Experimental Cell Research* 148: 249-253.

Bisgrove, B.W. and Burke, R.D. (1986). Development of serotonergic neurons in embryos of the sea urchin *Strongylocentrotus purpuratus*. *Development Growth and Differentiation* 28(6), 569-574.

Bisgrove, B.W. and Burke, R.D. (1987). Development of the nervous system of the pluteus larva of *Strongylocentrotus droebachiensis*. *Cell and Tissue Research* 248, 335-343.

Black, R.A., Rauch, C.T., Kozlosky, C.J., Peschon, J.J., Slack, J.L., Wolfson, M.F., Castner, B.J., Stocking, K.L., Reddy, P., Srinivasan, S., Nelson, N., Boiani, N., Schooley, K.A., Gerhart, M., Davis, R., Fitzner, J.N., Johnson, R.S., Paxton, R.J., March, C.J., and Cerretti, D.P. (1997). A metalloproteinase disintegrin that releases tumour-necrosis factor-alpha from cells. *Nature* 385, 729-733.

Black, R.A. and White, J.M. (1998). ADAMs: focus on the protease domain. *Current Opinion in Cell Biology* 10, 654-659.

Blelloch, R. and Kimble, J. (1999). Control of organ shape by a secreted metalloprotease in the nematode *Caenorhabditis elegans*. *Nature* 399, 586-590.

Blin, N. and Stafford, D.W. (1976). A general method for isolation of high molecular weight DNA from eukaryotes. *Nucleic Acids Research* 3: 2303.

Blobel, C.P., Wolfsberg, T.G., Turck, C.W., Myles, D.G., Primakoff, P., and White, J.M. (1992). A potential fusion peptide and an integrin ligand domain in a protein active in sperm-egg fusion. *Nature* 356, 248-252.

Boveri, T. (1901). Die Polarität von Ovozyte, Ei und Larve des *Strongylocentrotus lividus*. *Zool. Jahrb. Abt. Anat. Ontog. Tiere* 14, 630-653.

Burdsal, C.A., Alliegro, M.C., and McClay, D.R. (1991). Tissue-specific, temporal changes in cell adhesion to echinonectin in the sea urchin embryo. *Developmental Biology* 144, 327-334.

Burke, R.D. (1978). The structure of the nervous system of the pluteus larva of *Strongylocentrotus purpuratus*. *Cell and Tissue Research* 191, 233-247.

Burke, R.D. (1981). Structure of the digestive tract of the pluteus larva of *Dendraster excentricus* (Echinodermata: Echinoidea). *Zoomorphology* 98, 209-225.

Burke, R.D. (1983). Development of the larval nervous system of the sand dollar, *Dendraster excentricus*. *Cell and Tissue Research* 229, 145-154.

Burke, R.D. and Gibson, A.W. (1986). Cytological techniques for the study of larval echinoids, with notes on methods for inducing metamorphosis. *Methods in Cell Biology* 27, 295-308.

Burke, R.D. and Alvarez, C.M. (1988). Development of the esophageal muscles in embryos of the sea urchin *Strongylocentrotus purpuratus*. *Cell and Tissue Research* 252, 411-417.

Burke, R.D., Lail, M., and Nakajima, Y. (1998). The apical lamina and its role in cell adhesion in sea urchin embryos. *Cell Adhesion and Communication* 5, 97-108.

Cai, H., Krätzschmar, J., Alfandari, D., Hunnicutt, G., and Blobel, C.P. (1998). Neural crest-specific and general expression of distinct metalloprotease-disintegrins in early *Xenopus laevis* development. *Developmental Biology* 204, 508-524.

Cameron, J.S., Dryer, L., and Dryer, S.E. (2001). beta-Neuregulin-1 is required for the in vivo development of functional Ca2+-activated K+ channels in parasympathetic neurons. *Proceedings of the National Academy of Sciences U.S.A.* 98, 2832-2836.

Cameron, R.A., Hough-Evans, B.R., Britten, R.J., and Davidson, E.H. (1987). Lineage and fate of each blastomere of the eight-cell sea urchin embryo. *Genes and Development* 1, 75-84.

Cameron, R.A., Fraser, S.E., Britten, R.J., and Davidson, E.H. (1991). Macromere cell fates during sea urchin development. *Development* 113, 1085-1091.

Campbell, S.S. and Crawford, B.J. (1991). Ultrastructural study of the hyaline layer of the starfish embryo, Pisaster ochraceus. *Anatomical Record* 231, 125-135.

Carson, D.D., Farach, M.C., Earles, D.S., Decker, G.L., and Lennarz, W.J. (1985). A monoclonal antibody inhibits calcium accumulation and skeleton formation in cultured embryonic cells of the sea urchin. *Cell* 41, 639-648.

Chan, S.S., Zheng, H., Su, M.W., Wilk, R., Killeen, M.T., Hedgecock, E.M., and Culotti, J.G. (1996). UNC-40, a C. elegans homolog of DCC (Deleted in Colorectal Cancer), is required in motile cells responding to UNC-6 netrin cues. *Cell* 87(2), 187-195.

Cho, C., O'Dell Bunch, D., Faure, J., Goulding, E.H., Eddy, E.M., Primakoff, P., and Myles, D.G. (1998). Fertilization defects in sperm from mice lacking fertilin β. *Science* 281, 1857-1859.

Cho, C., Ge, H., Branciforte, D., Primakoff, P., and Myles, D.G. (2000). Analysis of mouse fertilin in wild-type and fertilin beta (-/-) sperm: evidence for C-terminal modification, alpha/beta dimerization, and lack of essential role of fertilin alpha in sperm-egg fusion. *Developmental Biology* 222, 289-295.

Coulson, B.S., Londrigan, S.L., and Lee, D.J. (1997). Rotavirus contains integrin ligand sequences and a disintegrin-like domain that are implicated in virus entry into cells. *Proceedings of the National Academy of Sciences U.S.A.* 94, 5389-5394.

Czihak, G. (1971). Echinoids. *In*: Experimental embryology of marine and fresh-water invertebrates (G. Reverberi, ed). North-Holland Publ. Co., Amsterdam.

Davidson, E.H. (1989). Lineage-specific gene expression and the regulative capacities of the sea urchin embryo: a proposed mechanism. *Development* 105, 421-445.

Davidson, E.H. (1990). How embryos work: a comparative view of diverse modes of cell fate specification. *Development* 108, 365-389.

Davidson, E. (1991). Spatial mechanisms of gene regulation in metazoan embryos. *Development* 113, 1-26.

Davidson, E.H., Cameron, R.A., and Ransick, A. (1998). Specification of cell fate in the sea urchin embryo: summary and some proposed mechanisms. *Development* 125, 3269-3290.

Driesch, H. (1892). The potency of the first two cleavage cells in echinoderm development. Experimental production of partial and double formations. *In* Foundations of Experimental Embryology (B.H. Willier and J.M. Oppenheimer, eds). Hafner, New York.

Emlet, R.B. (1995). Larval spicules, cilia, and symmetry as remnants of indirect development in the direct developing sea urchin *Heliocidaris erythrogramma*. *Developmental Biology* 167(2), 405-415.

Ettensohn, C.A. and McClay, D.R. (1988). Cell lineage conversion in the sea urchin embryo. *Developmental Biology* 125, 396-409.

Ettensohn, C.A. (1990). The regulation of primary mesenchyme cell patterning. *Developmental Biology* 140, 261-271.

Ettensohn, C.A. (1992). Cell interactions and mesodermal cell fates in the sea urchin embryo. *Development* Suppl., 43-51.

Ettensohn, C.A., Guss, K.A., Hodor, P.G., and Malinda, K.M. (1997). The morphogenesis of the skeletal system of the sea urchin embryo. *In*: Reproductive biology of invertebrates (Volume editor: J.R. Collier; Series editors: K.G. Adiyodi and R.G. Adiyodi). Oxford & IBH Publishing Co. Pvt. Ltd. New Delhi.

Evans, J.P., Schultz, R.M., and Kopf, G.S. (1995). Mouse sperm-egg plasma membrane interactions: analysis of roles of egg integrins and the mouse homologue of PH-30 (fertilin) β. *Journal of Cell Science* 108, 3267-3278.

Evans, J.P., Kopt, G.S., and Schultz, R.M. (1997). Characterization of the binding of recombinant mouse sperm fertilin beta subunit to mouse eggs: evidence for adhesive activity via an egg beta-one integrin-mediated interaction. *Developmental Biology* 187, 79-93.

Fink, R.D. and McClay, D.R. (1985). Three cell recognition changes accompany the ingression of sea urchin primary mesenchyme cells. *Developmental Biology* 107(1), 66-74.

Foerder, C.A. and Shapiro, B.M. (1977). Release of ovoperoxidase from sea urchin eggs hardens the fertilization membrane with tyrosine crosslinks. *Proceedings of the National Academy of Sciences, USA* 74(10), 4214-4218.

Gache, C., Lepage, T., and Ghiglione, C. (1992). Expression pattern of two early genes in the sea urchin embryo. *In*: Echinoderm Research 1991 (L. Scalera-Liaci and C. Canicattì, eds). A.A. Balkema, Rotterdam.

Galileo, D.S. and Morrill, J.B. (1985). Patterns of cells and extracellular material of (Echinodermata: Echinoidea) embryo, from hatched blastula to late gastrula. *Journal of Morphology* 185, 387-402.

Garratt, A.N., Britsch, S., and Birchmeier, C. (2000). Neuregulin, a factor with many functions in the life of a schwann cell. *Bioessays* 22, 987-996.

Ghiglione, C., Lhomond, G., Lepage, T., and Gache, C. (1993). Cell-autonomous expression and position-dependent repression by Li^+ of two zygotic genes during sea urchin early development. *The EMBO Journal* 12(1), 87-96.

Gibson, A.W., and Burke, R.D. (1985). The origin of pigment cells in embryos of the sea urchin *Strongylocentrotus purpuratus*. *Developmental Biology* 107, 414-419.

Gibson, A.W. and Burke, R.D. (1987). Migratory and invasive behavior of pigment cells in normal and animalized sea urchin embryos. *Experimental Cell Research* 173, 546-557.

Gibson, A.W. and Burke, R.D. (1988). Localization and characterization of an integral membrane protein antigen expressed by pigment cells in embryos of the sea urchin *Strongylocentrotus purpuratus*. *Development Growth and Differentiation* 30(3), 283-292.

Gilbert, S.F. (1997). Developmental Biology, 5th Edition. Sinauer Associates, Inc. Publishers, Sunderland, Massachusettes.

Gilpin, B.J., Loechel, F., Mattei, M., Engvall, E., Albrechtsen, R., and Wewer, U.M. (1998). A novel, secreted form of human ADAM 12 (Meltrin alpha) provokes myogenesis *in vivo*. *The Journal of Biological Chemistry* 273(1), 157-166.

Greenwald, I. (1998). LIN-12/Notch signaling: lessons from worms and flies. *Genes and Development* 12, 1751-1762.

Guss, K.A. and Ettensohn, C.A. (1997). Skeletal morphogenesis in the sea urchin embryo: regulation of primary mesenchyme gene expression and skeletal rod growth by ectoderm-derived cues. *Development* 124, 1899-1908.

Gustafson, T., and Wolpert, L. (1961). Studies on the cellular basis of morphogenesis in the sea urchin embryo: Directed movements of primary mesenchyme cells in normal and vegetalized larvae. *Experimental Cell Research* 24, 64-79.

Gustafson, T. and Wolpert, L. (1967). Cellular movement and contact in sea urchin morphogenesis. *Biological Reviews* 42, 442-498.

Hall, H.G. and Vacquier, V.D. (1982). The apical lamina of the sea urchin embryo: major glycoproteins associated with the hyaline layer. *Developmental Biology* 89, 168-178.

Hardin, J., Coffman, J.A., Black. S.D., and McClay, D.R. (1992). Commitment along the dorsoventral axis of the sea urchin embyro is altered in response to $NiCl_2$. *Development* 116, 671-685.

Harkey, M.A. and Whiteley, A.M. (1980). Isolation, culture and differentiation of echinoid primary mesenchyme cells. *Wilhelm Roux Archives of Developmental Biology* 189, 111-122.

Harkey, M.A., Whiteley, H.R., and Whiteley, A.H. (1992). Differential expression of the msp130 gene among skeletal lineage cells in the sea urchin embryo: a three dimensional in situ hybridization analysis. *Mechanisms of Development* 37, 173-184.

Harlow, E. and Lane, D. (1988). Antibodies: a laboratory manual. Cold Spring Harbor Laboratories.

Harris, H.A., Murrills, R.J., and Komm, B.S. (1997). Expression of meltrin-alpha mRNA is not restricted to fusagenic cells. *Journal of Cellular Biochemistry* 67(1), 136-142.

Henry, J.J., Amemiya, S., Wray, G.A., and Raff, R.A. (1989). Early inductive interactions are involved in restricting cell fates of mesomeres in sea urchin embryo. *Developmental Biology* 136, 140-153.

Hodor, P.G. and Ettensohn, C.A. (1998). The dynamics and regulation of mesenchymal cell fusion in the sea urchin embryo. *Developmental Biology* 199, 111-124.

Hörstadius, S. (1928). Über die Determination des Keimes bei Echinodermen. *Acta Zoologica* 9, 1-191.

Hörstadius, S. (1935). Über die Determination im Verlaufe der Eiachse bei Seeigeln. *Pubblicazioni Della Stazione Zoologica di Napoli* 14, 251-479.

Hörstadius, S. (1939). The mechanics of sea urchin development studied by operative methods. *Biological Reviews* 14, 132-179.

Hörstadius, S. (1973). Experimental Embryology of Echinoderms. Oxford Press, London.

Hörstadius, S. and Wolsky, A. (1936). Studien Über die Determination der Bilateralsymmetrie des jungen Seeigelkeimes. *Wilhelm Roux' Archiv fur Entwicklungsmechanik dur Organismen* 135, 69-113.

Howard, L., Nelson, K.K., Maciewicz, R.A., and Blobel, C.P. (1999). Interaction of the metalloprotease disintegrins MDC9 and MDC15 with two SH3 domain-containing proteins, endophilin I and SH3PX1. *The Journal of Biological Chemistry* 274(44), 31693-31699.

Huovila, A.J., Almeida, E.A.C., and White, J.M. (1996). ADAMs and cell fusion. *Current Opinion in Cell Biology* 8, 692-699.

Iba, K., Albrechtsen, R., Gilpin, B.J., Loechel, F., and Wewer, U.M. (1999). Cysteine-rich domain of human ADAM 12 (meltrin α) supports tumor cell adhesion. *American Journal of Pathology* 154(5), 1489-1501.

Iba, K., Albrechtsen, R., Gilpin, B., Fröhlich, C., Loechel, F., Zolkiewska, A., Ishiguro, K., Kojima, T., Liu, W., Langford, J.K., Sanderson, R.D., Brakebusch, C., Fässler, R., and Wewer, U.M. (2000). The cysteine-rich domain of human ADAM 12 supports cell adhesion through syndecans and triggers signaling events that lead to β1 integrin-dependent cell spreading. *The Journal of Cell Biology* 149(5), 1143-1155.

Ingersoll, E.P. and Wilt, F.H. (1998). Matrix metalloproteinase inhibitors disrupt spicule formation by primary mesenchyme cells in the sea urchin embryo. *Developmental Biology* 196, 95-106.

Inoue, D., Reid, M., Lum, L., Krätzschmar, J., Weskamp, G., Myung, Y.M., Baron, R., and Blobel, C.P. (1998). Cloning and initial characterization of mouse meltrin β and analysis of the expression of four metalloprotease-disintegrins in bone cells. *The Journal of Biological Chemistry* 273(7), 4180-4187.

Izumi, Y., Hirata, M., Hasuwa, H., Iwamoto, R., Umata, T., Miyado, K., Tamai, Y., Kurisaki, T., Sehara-Fujisawa, A., Ohno, S., and Mekada, E. (1998). A metalloprotease-disintegrin, MDC9/meltrin-γ/ADAM9 and PKCδ are involved in TPA-induced ectodomain shedding of membrane-anchored heparin-binding EGF-like growth factor. *The EMBO Journal* 17(24), 7260-7272.

Jury, J.A., Frayne, J., and Hall, L. (1997). The human fertilin alpha gene is non-functional: implications for its proposed role in fertilization. *Biochemistry Journal* 321(Pt 3), 577-581.

Kabakoff, B. and Lennarz, W.J. (1990). Inhibition of glycoprotein processing blocks assembly of spicules during development of the sea urchin embryo. *Journal of Cell Biology* 111(2), 391-400.

Kaji, K., Oda, S., Shikano, T., Ohnuki, T., Uematsu, Y., Sakagami, J., Tada, N., Miyazaki, S., and Kudo, A. (2000). The gamete fusion process is defective in eggs of Cd9-deficient mice. *Nature Genetics* 24, 279-282.

Katow, H. and Solursh, M. (1981). Ultrastructural and time-lapse studies of primary mesenchyme cell behavior in normal and sulfate-deprived sea urchin embryos. *Experimental Cell Research* 136: 233-245.

Kay, E.S. and Shapiro, B.M. (1987). Ovoperoxidase assembly in the sea urchin fertilization envelope and dityrosine crosslinking. *Developmental Biology* 121, 325-334.

Kenny, A.P., Kozlowski, D., Oleksyn, D.W., Angerer, L.M., and Angerer, R.C. (1999). SpSoxB1, a maternally encoded transcription factor asymmetrically distributed among early sea urchin blastomeres. *Development* 126(23), 5473-5483.

Klueg, K.M., Parody, T.R., and Muskavitch, M.A.T. (1998). Complex proteolytic processing acts on Delta, a transmembrane ligand for Notch during *Drosophila* development. *Molecular Biology of the Cell* 9, 1709-1723.

Knoll, A.H. and Carroll, S.B. (1999). Early animal evolution: emerging views from comparative biology and geology. *Science* 284, 2129-2137.

Kunisch, M., Haenlin, M., and Campos-Ortega, J.A. (1994). Lateral inhibition mediated by the Drosophila neurogenic gene Delta is enhanced by proneural proteins. *Proceedings of the National Academy of Sciences U.S.A.* 91, 10139-10143.

Kurisaki, T., Masuda, A., Osumi, N., Nabeshima, Y., and Fujisawa-Sehara, A. (1998). Spatially- and temporally-restricted expression of meltrin alpha (ADAM12) and beta (ADAM19) in mouse embryo. *Mechanisms of Development* 73, 211-215.

Kyte, J. and Doolittle, R.F. (1982). A simple method for displaying the hydropathic character of a protein. *Journal of Molecular Biology* 157, 105-132.

Laemmli, U.K. (1970). Cleavage of structural proteins during the assembly of the head of bacteriophage T4. *Nature*, 227, 680-685.

Le Naour, F., Rubinstein, E., Jasmin, C., Prenant, M., and Boucheix, C. (2000). Severely reduced female fertility in CD9-deficient mice. *Science* 287, 319-321.

Lepage, T. and Gache, C. (1989). Purification and characterization of the sea urchin embryo hatching enzyme. *The Journal of Biological Chemistry* 264(9), 4787-4793.

Lepage, T. and Gache, C. (1990). Early expression of a collagenase-like hatching enzyme gene in the sea urchin embryo. *The EMBO Journal* 9(9), 3003-3012.

Lepage, T., Sardet, C., and Gache, C. (1992). Spatial expression of the hatching enzyme gene in the sea urchin embryo. *Developmental Biology* 150, 23-32.

Leung-Hagesteijn, C., Spence, A.M., Stern. B.D., Zhou, Y., Su, M.W., Hedgecock, E.M., and Culotti, J.G. (1992). UNC-5, a transmembrane protein with immunoglobulin and thrombospondin type 1 domains, guides cell and pioneer axon migrations in C. elegans. *Cell* 71(2), 289-299.

Liu, C.Z., and Huang, T.F. (1997). Crovidisin, a collagen-binding protein isolated from snake venom of Crotalus viridis, prevents platelet-collagen interaction. *Archives of Biochemistry and Biophysics* 337, 291-299.

Loechel, F., Gilpin, B.J., Engvall, E., Albrechtsen, R., and Wewer, U.M. (1998). Human ADAM 12 (Meltrin α) is an active metalloprotease. *The Journal of Biological Chemistry* 273, 16993-16997.

Logan, C.Y. and McClay, D.R. (1998). The lineages that give rise to the endoderm and the mesoderm in the sea urchin embryo. *In*: Cell Fate and Lineage Determination (S.A. Moody, ed.). Academic Press, San Diego.

Logan, C.Y., Miller, J.R., Ferkowicz, M.J., and McClay, D.R. (1999). Nuclear beta-catenin is required to specify vegetal cell fates in the sea urchin embryo. *Development* 126, 345-357.

Logeat, F., Bessia, C., Brou, C., LeBail, O., Jarriault, S., Seidah, N.G., and Israel, A. (1998). The Notch1 receptor is cleaved constitutively by a furin-like convertase. *Proceedings of the National Academy of Sciences U.S.A.* 95(14), 8108-8112.

Malinda, K.M. and Ettensohn, C.A. (1994). Primary mesenchyme cell migration in the sea urchin embryo: distribution of directional cues. *Developmental Biology* 164, 562-578.

Malinda, K.M., Fisher, G.W., and Ettensohn, C.A. (1995). Four-dimensional microscopic analysis of the filopodial behavior of primary mesenchyme cells during gastrulation in the sea urchin embryo. *Developmental Biology* 172, 552-566.

Marsden, M. (1995). Cloning and characterization of β integrin subunits in sea urchin embryos. Ph.D. Thesis, University of Victoria.

Marsden, M., and Burke, R.D. (1997). Cloning and characterization of novel beta integrin subunits from a sea urchin. *Developmental Biology* 181, 234-245.

Marsden, M., and Burke, R.D. (1998). The betaL integrin subunit is necessary for gastrulation in sea urchin embryos. *Developmental Biology* 203, 134-148.

Maruyama, Y.K., Nakaseko, Y, and Yagi, S. (1985). Localization of the cytoplasmic determinants responsible for primary mesenchyme formation and gastrulation in the unfertilized eggs of the sea urchin Hemicentrotus pulcherrimus. *Journal of Experimental Zoology* 236, 155-163.

Mayne, J. and Robinson, J.J. (1996). Purification and metal ion requirements of a candidate matrix metalloproteinase: a 41 kDa gelatinase activity in the sea urchin embryo. *Biochemistry and Cell Biology* 74(2), 211-218.

McClay, D.R. (1986). Embryo dissociation, cell isolation, and cell reassociation. *In*: Methods in Cell Biology, Vol. 27. Academic Press.

McClay, D.R., Miller, J.R., Logan, C.Y., Hertzler, P.L., Bachman, E.S., Matese, J.C., Sherwood, D.R., and Armstrong, N.A. (1995). Cell adhesion and cell signaling at gastrulation in the sea urchin. *Theriogenology* 44, 1145-1165.

Meintanis, S., Thomaidou, D., Jessen, K.R., Mirsky, R., and Matsas, R. (2001). The neuron-glia signal beta-neuregulin promotes Schwann cell motility via the MAPK pathway. *Glia* 34, 39-51.

Mendoza, L.M., Nishioka, D., and Vacquier, V.D. (1993). A GPI-anchored sea urchin sperm membrane protein containing EGF domains is related to human uromodulin. *Journal of Cell Biology* 121(6), 1291-1297.

Meyer, D. and Birchmeier, C. (1995). Multiple essential functions of neuregulin in development. *Nature* 378, 386-390.

Meyer, D., Yamaai, T., Garratt, A., Riethmacher-Sonnenberg, E., Kane, D., Theill, L.E., and Birchmeier, C. (1997). Isoform-specific expression and function of neuregulin. *Development* 124, 3575-3586.

Miller, B.J., Georges-Labouesse, E., Primakoff, P., and Myles, D.G. (2000). Normal fertilization occurs with eggs lacking the integrin alpha6beta1 and is CD9-dependent. *Journal of Cell Biology* 149, 1289-1296.

Miller. J.B. (1995). Making one cell from two. *Nature* 377, 575-576.

Miyado, K., Yamada, G., Yamada, S., Hasuwa, H., Nakamura, Y., Ryu, F., Suzuki, K., Kosai, K., Inoue, K., Ogura, A., Okabe, M., and Mekada, E. (2000). Requirement of CD9 on the egg plasma membrane for fertilization. *Science* 287, 321-324.

Mozingo, N.M., Hollar, L.R., and Chandler, D.E. (1993). Degradation of an extracellular matrix: sea urchin hatching enzyme removes cortical granule-derived proteins from the fertilization envelope. *Journal of Cell Science* 104, 929-938.

Murray, G., Reed, C., Marsden, M., Rise, M., Wang, D., and Burke, R.D. (2000). The alphaBbetaC integrin is expressed on the surface of the sea urchin egg and removed at fertilization. *Developmental Biology* 227, 633-647.

Myles, D.G., Kimmel, L.H., Blobel, C.P., White, J.M., and Primakoff, P. (1994). Identification of a binding site in the disintegrin domain of fertilin required for sperm-egg fusion. *Proceedings of the National Academy of Sciences U.S.A.* 91, 4195-4198.

Nagase, H. (1998). Cell surface activation of progelatinase A (proMMP-2) and cell migration. *Cell Research* 8(3), 179-186.

Nakajima, Y., and Burke, R.D. (1996). The initial phase of gastrulation in sea urchins is accompanied by the formation of bottle cells. *Developmental Biology* 179, 436-446.

Nasir, A., Reynolds, S.D., Angerer, L.M., and Angerer, R.C. (1995). VEB4: Early zygotic mRNA expressed asymmetrically along the animal-vegetal axis of the sea urchin embryo. *Development Growth and Differentiation* 37, 57-68.

Nielsen, H., Engelbrecht, J., Brunak, S., and von Heijne, G. (1997). Identification of prokaryotic and eukaryotic signal peptides and prediction of their cleavage sites. *Protein Engineering* 10, 1-6.

Nishiwaki, K., Hisamoto, N., and Matsumoto, K. (2000). A metalloprotease disintegrin that controls cell migration in *Caenorhabditis elegans*. *Science* 288, 2205-2208.

Nomura, K., and Suzuki, N. (1995). Sea urchin ovoperoxidase: solubilization and isolation from the fertilization envelope, some structural and functional properties, and degradation by hatching enzyme. *Archives of Biochemistry and Biophysics* 319, 525-534.

Okazaki, K. (1960). Skeleton formation of the sea urchin larvae. II. Organic matrix of the spicule. *Embryologia* 5, 283-320.

Okazaki, K. (1975). Spicule formation by isolated micromeres of the sea urchin embryo. *American Zoologist* 15, 567.

Pan, D. and Rubin, G.M. (1997). Kuzbanian controls proteolytic processing of Notch and mediates lateral inhibition during Drosophila and vertebrate neurogenesis. *Cell* 90, 271-280.

Person, W.R., Wood, T., Zhang, Z., and Miller, W. (1997). Comparison of DNA sequences with protein sequences. *Genomics* 46, 24-36.

Peschon, J.J., Slack, J.L., Reddy, P., Stocking, K.L., Sunnarborg, S.W., Lee, D.C., Russell, W.E., Castner, B.J., Johnson, R.S., Fitzner, J.N., Boyce, R.W., Nelson, N., Kozlosky, C.J., Wolfson, M.F., Rauch, C.T., Ceretti, D.P., Paxton, R.J., March, C.J., and Black, R.A. (1998). An essential role for ectodomain shedding in mammalian development. *Science* 282, 1281-1284.

Peterson, K.J., Harada, Y., Cameron, R.A., and Davidson, E.H. (1999). Expression pattern of Brachyury and Not in the sea urchin: comparative implications for the origins of mesoderm in the basal deuterostomes. *Developmental Biology* 207, 419-431.

Peterson, K.J., Cameron, R.A., and Davidson, E.H. (2000). Bilaterian origins: significance of new experimental observations. *Developmental Biology* 219, 1-17.

Podbilewicz, B. (1996). ADM-1, a protein with metalloprotease- and disintegrin-like domains, is expressed in syncytial organs, sperm, and sheath cells of sensory organs in Caenorhabditis elegans. *Molecular Biology of the Cell* 7, 1877-1893.

Primakoff, P., Hyatt, H., and Tredick-Kline, J. (1987). Identification and purification of a sperm surface protein with a potential role in sperm-egg membrane fusion. *Journal of Cell Biology* 104, 141-149.

Primakoff, P. and Myles, D.G. (2000). The ADAM gene family: surface proteins with adhesion and protease activity. *Trends in Genetics* 16(2), 83-87.

Qi, H., Rand, M.D., Wu, X., Sestan, N., Wang, W., Rakic, P., Xu, T., and Artavanis-Tsakonas, S. (1999). Processing of the Notch Ligand Delta by the Metalloprotease Kuzbanian. *Science* 283, 91-94.

Quigley, J.P., Braithwaite, R.S., and Armstrong, P.B. (1993). Matrix metalloproteases of the developing sea urchin embryo. *Differentiation* 54, 19-23.

Raff, R.A. (1987). Constraint, flexibility, and phylogenetic history in the evolution of direct development in sea urchins. *Developmental Biology* 119, 6-19.

Ransick, A. and Davidson, E.H. (1993). A complete second gut induced by transplanted micromeres in the sea urchin embryo. *Science* 259, 1134-1138.

Ransick, A., Ernst, S., Britten, R.J., and Davidson, E.H. (1993). Whole mount in situ hybridization shows Endo 16 to be a marker for the vegetal plate territory in sea urchin embyros. *Mechanisms of Development* 42, 117-124.

Ransick, A. and Davidson, E.H. (1995). Micromeres are required for normal vegetal plate specification in sea urchin embryos. *Development* 121, 3215-3222.

Reynolds, S.D., Angerer, L.M., Palis, J., Nasir, A., and Angerer, R.C. (1992). Early mRNAs, spatially restricted along the animal-vegetal axis of sea urchin embryos, include one encoding a protein related to tolloid and BMP-1. *Development* 114, 769-786.

Roe, J.L., Park, H.R., Strittmatter, W.J., and Lennarz, W.J. (1989). Inhibitors of metalloendoproteases block spiculogenesis in sea urchin primary mesenchyme cells. *Experimental Cell Research* 181, 542-550.

Rooke, J., Pan, D., Xu, T., and Rubin, G.M. (1996). KUZ, a conserved metalloprotease-disintegrin protein with two roles in *Drosophila* neurogenesis. *Science* 273, 1227-1231.

Saitou, N. and Nei, M. (1987). The neighbor-joining method: a new method for reconstructing phylogenetic trees. *Molecular Biology and Evolution* 4, 406-425.

Sambrook, J., Fritsch, E.F., and Maniatis, T. (1989). Molecular Cloning: a laboratory manual, 2nd edition. Cold Spring Harbor Laboratory Press, Cold Spring Harbor.

Schlöndorff, J. and Blobel, C.P. (1999). Metalloprotease-disintegrins: modular proteins capable of promoting cell-cell interactions and triggering signals by protein-ectodomain shedding. *Journal of Cell Science* 112, 3603-3617.

Schroeder, T.E. (1980). Expressions of the prefertilization polar axis in sea urchin eggs. *Developmental Biology* 79, 428-443.

Sherwood, D.R. and McClay, D.R. (1997). Identification and localization of a sea urchin Notch homologue: insights into vegetal plate regionalization and Notch receptor regulation. *Development* 124, 3363-3374.

Sherwood, D.R. and McClay, D.R. (1999). LvNotch signaling mediates secondary mesenchyme specification in the sea urchin embryo. *Development* 126, 1703-1713.

Shirakabe, K., Wakatsuki, S., Kurisaki, T., and Fujisawa-Sehara, A. (2001). Roles of meltrin beta/ADAM19 in the processing of neuregulin. *Journal of Biological Chemistry* 276, 9352-9358.

Showman, R.M. and Foerder, C.A. (1979). Removal of the fertilization membrane of sea urchin embryos employing aminotriazole. *Experimental Cell Research* 120: 253-255.

Slack, J.M.W. (1991). From egg to embryo: regional specification in early development. Cambridge University Press, New York.

Sotillos, S., Roch, F., and Campuzano, S. (1997). The metalloprotease-disintegrin Kuzbanian participates in *Notch* activation during growth and patterning of *Drosophila* imaginal discs. *Development* 124, 4769-4779.

Southern, E.M. (1975). Detection of specific sequences among DNA fragments separated by gel electrophoresis. *Journal of Molecular Biology* 98: 503.

Strathmann, R.R. (1971). The behavior of planktotrophic echinoderm larvae: mechanisms, regulation, and rates of suspension feeding. *Journal of Experimental Marine Biology and Ecology* 6, 109-160.

Strathmann, M.F. (1987). Reproduction and development of marine invertebrates of the Northern Pacific Coast. University of Washington Press, Seattle.

Tamboline, C.R. and Burke, R.D. (1992). Secondary mesenchyme of the sea urchin embryo: ontogeny of blastocoelar cells. *The Journal of Experimental Zoology* 262, 51-60.

Terwilliger, T.C. and Eisenberg, D. (1982). The structure of melittin. II. Interpretation of the structure. *The Journal of Biological Chemistry* 257(11), 6016-6022.

Towbin, H., Staehelin, T., and Gordon, J. (1979). Electrophoretic transfer of proteins from polyacrylamide gels to nitrocellulose sheets: Procedure and some applications. *Proceedings of the National Academy of Sciences U.S.A.* 76(9), 4350-4354.

Vignery, A. (2000). Osteoclasts and giant cells: macrophage-macrophage fusion mechanism. *International Journal of Experimental Pathology* 81, 291-304.

Wei, Z., Angerer, L.M., and Angerer, R.C. (1999). Spatially regulated SpEts4 transcription factor activity along the sea urchin embryo animal-vegetal axis. *Development* 126, 1729-1737.

Wen, C., Metzstein, M.M., and Greenwald, I. (1997). SUP-17, a Caenorhabditis elegans ADAM protein related to Drosophila KUZBANIAN, and its role in LIN-12/NOTCH signaling. *Development* 124(23), 4759-4767.

Weskamp, G., Krätzschmar, J., Reid, M.S., and Blobel, C.P. (1996). MDC9, a widely expressed cellular disintegrin containing cytoplasmic SH3 ligand domains. *The Journal of Cell Biology* 132(4), 717-726.

Wessel. G.M., Marchase, R.B., and McClay, D.R. (1984). Ontogeny of the basal lamina in the sea urchin embryo. *Developmental Biology* 103(1), 235-245.

Wessel, G.M. and Berg, L. (1995). A spatially restricted molecule of the extracellular matrix is contributed both maternally and zygotically in the sea urchin embryo. *Development, Growth and Differentiation* 37, 517-527.

White, J.M. (1992). Membrane fusion. *Science* 258, 917-924.

Wikramanayake, A.H., Brandhorst, B.P., and Klein, W.H. (1995). Autonomous and non-autonomous differentiation of ectoderm in different sea urchin species. *Development* 121, 1497-1505.

Wikramanayake, A.H., Huang, L., and Klein, W.H. (1998). Beta-catenin is essential for patterning the maternally specified animal-vegetal axis in the sea urchin embryo. *Proceedings of the National Academy of Sciences U.S.A.* 95, 9343-9348.

Wolfsberg, T.G., Straight, P.D., Gerena, R.L., Huovila, A.J., Primakoff, P., Myles, D.G., and White, J.M. (1995). ADAM, a widely distributed and developmentally regulated gene family encoding membrane proteins with A Disintegrin And Metalloprotease domain. *Developmental Biology* 169, 378-383.

Wolfsberg, T.G. and White, J.M. (1996). ADAMs in fertilization and development. *Developmental Biology* 180, 389-401.

Wolpert, L., and Gustafson, T. (1961). Studies on the cellular basis of morphogenesis of the sea urchin embryo. *Experimental Cell Research* 25: 311-325.

Wray, G.A., Levinton, J.S., and Shapiro, L.H. (1996). Molecular evidence for deep Precambrian divergences among metazoan phyla. *Science* 274, 568-573.

Yagami-Hiromasa, T., Sato, T., Kurisaki, T., Kamijo, K., Nabeshima, Y., and Fujisawa-Sehara, A. (1995). A metalloprotease-disintegrin participating in myoblast fusion. *Nature* 377, 652-656.

Yuan, R., Primakoff, P., and Myles, D.G. (1997). A role for the disintegrin domain of cyritestin, a sperm surface protein belonging to the ADAM family, in mouse sperm-egg plasma membrane adhesion and fusion. *The Journal of Cell Biology* 137, 105-112.

Zhou, Q., Smith, J.B., and Grossman, M.H. (1995). Molecular cloning and expression of catrocollastatin, a snake-venom protein from Crotalus atrox (western diamondback rattlesnake) which inhibits platelet adhesion to collagen. *Biochemistry Journal* 307, 411-417.